

NASA CONTRACTOR  
REPORT



NASA CR-20

0061255



LOAN COPY: RETURN TO  
AFWL (DOUL)  
KIRTLAND AFB, N. M.

STUDY OF CRITICAL DEFECTS  
IN ABLATIVE HEAT SHIELD SYSTEMS  
FOR THE SPACE SHUTTLE

by R. L. Thompson, W. D. Rummel, and W. E. Driver

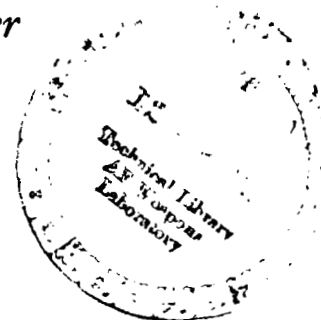
Prepared by

MARTIN MARIETTA CORPORATION

DENVER DIVISION

Denver, Colo. 80201

for Langley Research Center



NATIONAL AERONAUTICS AND SPACE ADMINISTRATION • WASHINGTON, D. C. • APRIL 1972



0061255

1. Report No. NASA CR-2010		2. Government Accession No.		3. Recipient's Catalog No.	
4. Title and Subtitle STUDY OF CRITICAL DEFECTS IN ABLATIVE HEAT SHIELD SYSTEMS FOR THE SPACE SHUTTLE				5. Report Date April 1972	
7. Author(s) R. L. Thompson, W. D. Rummel, and W. E. Driver				8. Performing Organization Report No. MCR 71-233	
9. Performing Organization Name and Address Martin Marietta Corporation Denver Division Denver, Colo. 80201				10. Work Unit No.	
12. Sponsoring Agency Name and Address National Aeronautics and Space Administration Washington, DC 20546				11. Contract or Grant No. NAS1-10289	
				13. Type of Report and Period Covered Contractor Report	
				14. Sponsoring Agency Code	
15. Supplementary Notes					
16. Abstract Results are presented from an investigation to determine the effects of fabrication-induced defects on the performance of an ablative heat shield material in a simulated space shuttle reentry environment. Non-destructive methods for detecting the defects were investigated. The material considered is a fiber-filled, honeycomb-reinforced, low-density elastomer. Results were obtained for density variations, voids, fiber bundles, crushed honeycomb, undercut honeycomb, unbonded areas, face sheet delaminations, and cure variations. The data indicate that, within reasonable tolerances, the fabrication defects investigated are not critical in terms of reentry performance of the heat shield.					
17. Key Words (Suggested by Author(s)) Space Shuttle, Heat shield, Ablators, Defects, Non-destructive evaluation				18. Distribution Statement Unclassified - Unlimited	
19. Security Classif. (of this report) Unclassified		20. Security Classif. (of this page) Unclassified		21. No. of Pages 144	
				22. Price* \$3.00	

\*For sale by the National Technical Information Service, Springfield, Virginia 22151

1. Space Shuttle.  
2. Ablative materials -- nondestructive testing  
3. Heat Shielding -- testing.

12 Apr 72



## CONTENTS

	Page
SUMMARY . . . . .	1
INTRODUCTION . . . . .	2
IDENTIFICATION AND CHARACTERIZATION OF POTENTIALLY CRITICAL DEFECTS . . . . .	3
DEFECT DETECTION INVESTIGATIONS . . . . .	22
THERMAL PROTECTION SYSTEM PERFORMANCE REQUIREMENTS . . . . .	35
MODELS AND INSTRUMENTATION . . . . .	47
TEST APPARATUS AND PROCEDURES . . . . .	64
TEST RESULTS AND DISCUSSION . . . . .	76
CONCLUSIONS . . . . .	128
RECOMMENDATIONS . . . . .	130
APPENDIX A CONVERSION OF U.S. CUSTOMARY UNITS TO SI UNITS . . . .	132
APPENDIX B FABRICATION OF LOW-DENSITY ELASTOMERIC HEAT SHIELD . .	134

### Figure

1 Ablative Panel Design . . . . .	5
2 Ablative Panel Life Sequence . . . . .	6
3 Potential Critical Defects . . . . .	8
4 Voids in Ablative Material . . . . .	11
5 Honeycomb Core Defects . . . . .	16
6 Defective Core Splice . . . . .	17
7 Broken Core, Panel #18 . . . . .	24
8 X-Radiograph of Panel #10b (Plan View) Showing Void and Core Splice . . . . .	26
9 X-Radiograph of Panel #22 (Side View) Showing High- Density Layer . . . . .	26
10 Multiform Fused Silica . . . . .	27
11 Nylon Phenolic Molding Compound, Chopped . . . . .	27
12 X-Radiograph, Panel #10 Showing Voids . . . . .	28
13 Neutrograph, Panel #10 Showing Voids . . . . .	28
14 Face Sheet-to-Core Unbond in Panel #30 . . . . .	30
15 Panel #5, 10 Minutes after Removal from Oven Controlled at 212°F (373 K), One Isotherm Only . . . . .	31
16 Panel #5, 13 Minutes after Removal from Oven Controlled at 212°F (373 K) . . . . .	31
17 Baseline Logistics Mission Profile, High Crossrange System . . . . .	38
18 Thermal Protection, High Crossrange Orbiter . . . . .	40
19 Aerodynamic Characteristics, High Crossrange System . . . .	41
20 Trajectory Parameters, High Crossrange System . . . . .	42

21	Void Specimen Design . . . . .	52
22	Ablative Test Specimen Showing Thermocouple Installation . . . . .	56
23	Large Honeycomb . . . . .	58
24	Altered Cure Billet 17 . . . . .	59
25	Relative Radiographic Density vs Packing Method . . . . .	60
26	Plasma Arc Test Specimen Design . . . . .	62
27	Tensile Specimen, Ablator in Honeycomb . . . . .	63
28	Tensile Specimen, Ablator . . . . .	63
29	Large Test Panel, Defect Locations . . . . .	65
30	Large Test Panels, Thermal Vacuum Test Instrumentation . . . . .	66
31	Ablative Panel Thermocouple Locations . . . . .	67
32	High Crossrange Mark I Delta Orbiter, Nominal Entry Trajectory . . . . .	68
33	Steady-State Calorimeter . . . . .	70
34	Tensile Test Setup with Optron Optical Extensometer . . . . .	72
35	Sound Spectrum Used in Acoustic Tests . . . . .	74
36	Acoustic Test Setup with Ablative Panel Mounted . . . . .	75
37	Temperature Conditioning Setup after Cold Cycle . . . . .	77
38	Experimental Heating Distribution Over Cylinder-Wedge . . . . .	78
39	Effect of Bond Coat on Peak Back Surface Temperature Rise . . . . .	82
40	Effect of Bulk Density Variations on Peak Back Surface Temperature Rise . . . . .	83
41	Effect of Density Distribution on Peak Back Surface Temperature Rise . . . . .	84
42	Effect of Voids on Peak Back Surface Temperature Rise . . . . .	85
43	Effect of Core Size on Peak Back Surface Temperature Rise . . . . .	86
44	Effect of Cure Cycle on Peak Back Surface Temperature Rise . . . . .	87
45	Average Surface Temperature . . . . .	88
46	Effect of Density on Backface Temperature Rise . . . . .	89
47	Effect of Unit Weight on Backface Temperature Rise . . . . .	91
48	Effect of Void Location on Backface Temperature Rise . . . . .	92
49	Bond Coat Effects on Temperature Profile, High-Flux End of Heating . . . . .	93
50	Density Uniformity Effects on Temperature Profile, High-Flux End of Heating . . . . .	94
51	Void Effects on Temperature Profile, High-Flux . . . . .	95
52	Control Temperature Profile, High-Flux End of Heating . . . . .	96
53	High Void Temperature Profile, High-Flux End of Heating . . . . .	97
54	Control Temperature Profile, Low-Flux End of Heating . . . . .	98
55	Effect of Density Distribution on Weight Loss . . . . .	100
56	Data Scatter, Low Flux . . . . .	101
57	Data Scatter, High Flux . . . . .	102

58	Charred Plasma Arc Specimens, Nominal Density . . . . .	104
59	Charred Plasma Arc Specimens, Backface Void . . . . .	105
60	Charred Plasma Arc Specimens, Large Honeycomb . . . . .	106
61	Typical Char Surface and Cross Section, 2X Magnification . . . . .	107
62	Ablation Depth vs Density . . . . .	108
63	Tensile Strength Ambient Temperature . . . . .	110
64	Tensile Elongation Ambient Temperature . . . . .	111
65	Tensile Modulus Ambient Temperature . . . . .	112
66	Effect of Core Coating on Tensile Strength . . . . .	113
67	Effect of Core Coating on Elongation . . . . .	114
68	Effect of Core Coating on Tensile Modulus . . . . .	115
69	Tensile Specimens, Bond Coat Study . . . . .	116
70	Effect of Density on Tensile Properties . . . . .	118
71	Effect of Honeycomb on Tensile Strength . . . . .	119
72	Effect of Honeycomb on Elongation . . . . .	120
73	Tensile Specimens, No Core . . . . .	121
74	Panels after Removal from Cold Soak . . . . .	123
75	Ablative Surface after Cold Soak; Core Frosted . . . . .	123
76	Defective Panel after Plasma Arc Test . . . . .	125
77	Summary of Peak Temperature Measurements . . . . .	126
78	Control Panel Showing Area of Shock Interaction . . . . .	127

# Table

I	Relative Microwave Values vs Density and Thickness . . .	32
II	Shore "A" Durometer Hardness . . . . .	32
III	Shuttle Mission Characteristics . . . . .	37
IV	Events Sequence, Space Shuttle Mission Phase, High Crossrange System . . . . .	39
V	Plasma Arc Specimen Data . . . . .	49
VI	Tensile Specimen Data . . . . .	50
VII	Billet Fabrication Data . . . . .	54
VIII	Plasma Arc Test Inputs . . . . .	80
IX	Summary of Plasma Arc Test Data . . . . .	81

# STUDY OF CRITICAL DEFECTS IN ABLATIVE HEAT SHIELD SYSTEMS FOR THE SPACE SHUTTLE

By R. L. Thompson, W. D. Rummel, W. E. Driver  
Martin Marietta Corporation

## SUMMARY

The potential use of ablative materials for Space Shuttles requires development of low-cost fabrication processes. These fabrication costs could be substantially reduced if the acceptability of certain noncritical defects in the ablative heat shield could be demonstrated.

An experimental program was conducted to investigate methods for detecting defects and to identify fabrication defects critical to the performance of the heat shield during the Shuttle reentry environment. A NASA-Langley ablator, MG-36, served as a baseline material for this study. This material consists of an open-face honeycomb bonded to a fiberglass subsheet and filled with a low-density silicone ablative material. The ablative filler consists of a silicone resin, glass fibers, and phenolic microspheres. Defects were introduced by altering the fabrication process and by using simulated models to produce fabrication variances and physical flaws. Thermal tests of material specimens were conducted in a plasma arc facility.

Results were obtained on bulk density variations between panels and density gradients, voids, core damage, ablator bonding to the core, unbonds between the core and the face sheet, delaminations of the face sheet, high-density (metal) inclusions, fiber bundles, undercut core, and cure variations between panels. The responses of these specimens were compared with the responses of specimens prepared in accordance with a baseline process. The results show certain trends in back surface temperature and, although final designation as to criticality depends on vehicle design criteria and requirements, certain general requirements have been set forth for evaluation of study results. Bulk density variations, density gradients, localized core crushing, and cure variations were all found to be noncritical with respect to material thermal performance. Large voids that resulted in a 20% density reduction significantly affected back surface temperature. However, there was no catastrophic failure such as loss of ablator from the honeycomb cells even when the material was charred past the void areas. The selection and application of a resin bond coating to the honeycomb core for bonding the filler was found to affect both the bond strength and the insulative capability of the material. No evidence was found to indicate that small, high-density (metal) inclusions or occasional fiber bundles had any effect on material behavior.

## INTRODUCTION

Ablative materials have been used extensively on past manned and unmanned reentry vehicles to provide thermal protection during reentry. The design evaluation of ablative heat shield systems depends on knowing certain basic or critical properties of the material. Often these properties are based on small controlled sample tests from which engineering design data are obtained. These data are typically generated from samples that are nearly free of physical flaws and fabrication variances. Thus, designs have been established based on ideal performance, and system reliability has been assured through elaborate manufacturing and quality control procedures that would insure nearly defect-free panels. Since previous investigations have considered fabrication defects only during hardware verification phases, very little experimental data are available concerning the sensitivity of critical material properties to defects.

The approach above has produced costly heat shields and, in reviewing the flight performance of such programs as Apollo, PRIME, etc, the question has been raised as to the necessity of a "defect-free" design. The possible cost savings from a simplified process for the application of ablators to vehicles the size of the proposed Space Shuttle makes it very desirable to further investigate the effects of these material variations on performance. This study was conducted to determine these effects before fabrication processes are established so the processes may be directed toward low-cost methods and the need for process control and quality inspection may be minimized.

The basic objectives of this program were to determine, through a comprehensive test program considering all phases of the Space Shuttle flight environments, the (1) effects on ablative panel performance of the defects that commonly occur during panel fabrication, (2) methods for inspection and certification of ablative heat shields, and (3) consequence of accepting noncritical defects on heat shield panel fabrication cost.

The program was planned as a six-task effort of which the present contract, NAS1-10289, covered only the first three tasks. By task, the specific objectives are to:

Task I - Identify and characterize potentially critical defects, survey inspection techniques and evaluate those most suitable for locating and identifying defects in the heat shield, and develop methods for inducing the appropriate defects into test specimens of the baseline heat shield system;

Task II - Plan Tasks III thru VI and conduct NDT inspection of GFP ablative panels;

Task III - Investigate the effects of various fabrication-induced defects on the ablator performance in the simulated Shuttle reentry environment.

During Task III, the following variances were investigated with respect to thermal performance:

- 1) Bond coat effects;



- 2) Bulk density variations;
- 3) Density gradients;
- 4) Void locations;
- 5) Core reinforcement effectiveness;
- 6) Cure cycle variations.

Tensile property tests were conducted to determine the effects of bond coating, density, honeycomb core, cure cycle, and fibers on filler bond strength and the ultimate strain and elastic modulus of the ablative material.

A secondary objective of this study phase was to perform exploratory environmental exposure tests to obtain a basis for the execution of Task IV work, during which nonentry environments will be considered. With this objective in mind, two 8x16x2-inch (20.3x40.6x5.1-cm) panels were fabricated and exposed to simulated pre-reentry environments prior to reentry thermal testing. One of these panels contained the following defects: crushed core, undercut core, no bond coat, fiber bundles, high-density area, low-density area, and metal inclusions. In addition, a core-to-face sheet unbond and face sheet delamination were incorporated at two of the four attachment points.

This report presents the results of Tasks I, II, and III of this study. Two systems of units are used for defining physical quantities, the U.S. Customary System and the International System of Units. Mr. W. D. Brewer, Langley Research Center, was technical representative for the project.

## IDENTIFICATION AND CHARACTERIZATION OF POTENTIALLY CRITICAL DEFECTS

### Discussion of Critical Defects

The thermal protection system for the Space Shuttle must be designed to meet certain performance requirements. In the case of an ablative system, the performance requirements are identified as follows:

- 1) A thermal insulation capability to protect the structure to a given temperature;
- 2) A structural capability to insure retention of the ablative layer;
- 3) Retention of the char layer;
- 4) Compatibility with other onboard systems and with the payload and/or space stations.

The above requirements define a set of critical properties for the ablative system. These properties must be established, together with the selected material and design, so the performance requirements are met. For the material and the design (ref fig. 1) considered in this program, the basic critical properties have been identified as:

- 1) Thermal properties;
- 2) Ablative layer mechanical properties;
- 3) Char layer integrity;
- 4) Surface erosion resistance;
- 5) Chemical composition and stability;
- 6) Ablative layer bond to subpanel, e.g., face sheet, support panel, basic structure;
- 7) Panel dimensions;
- 8) Subpanel mechanical properties.

A critical defect is defined as a perturbation of the ablative system that affects the above critical properties to the extent that the system does not meet the basic performance requirements. For example, out-of-tolerance microspheres could cause the ablative mixture to be dry. This, in turn, could cause the ultimate strain to be low, resulting in cracks during the orbital phase of the mission and ultimately in loss of the char during entry. By the above definition, the critical property involved is the ultimate strain of the ablative layer and the critical defect is the presence of out-of-tolerance microspheres.

The concept of a critical defect is further exemplified in figure 2, which shows the sequence of events for the life of the ablative panels. Except for defects that are introduced by mishandling, all defects will be introduced before completion of the panel assembly. Furthermore, assuming the raw materials meet specific acceptance criteria, the majority of defects will be introduced during the subcomponent fabrication (ablative material mixing, face sheet bonding) or during panel fabrication (filling, curing, and machining). Since the basic defects are created and should be detected and controlled in the subcomponent and panel fabrication phase, this phase will be the focal point of this program.

In reviewing the performance requirements, the insulation capability is the salient requirement since the sole purpose of the ablative heat shield system is to protect the structure. The structural and the char layer retention requirements really support the insulation performance requirement. They are defined as basic performance requirements because they are essential and provide a basis for defining the properties that dictate the structural and the char layer integrity of the ablative system.

- Note:
1. The heat shield consisted of a full-depth, phenolic-glass honeycomb filled with an elastomer ablator and bonded to a fiberglass backface sheet
  2. The panel thickness 2.0 in. (5.08 cm) was nominally compatible with thermal protection requirements for the bottom forward area of the Shuttle vehicle

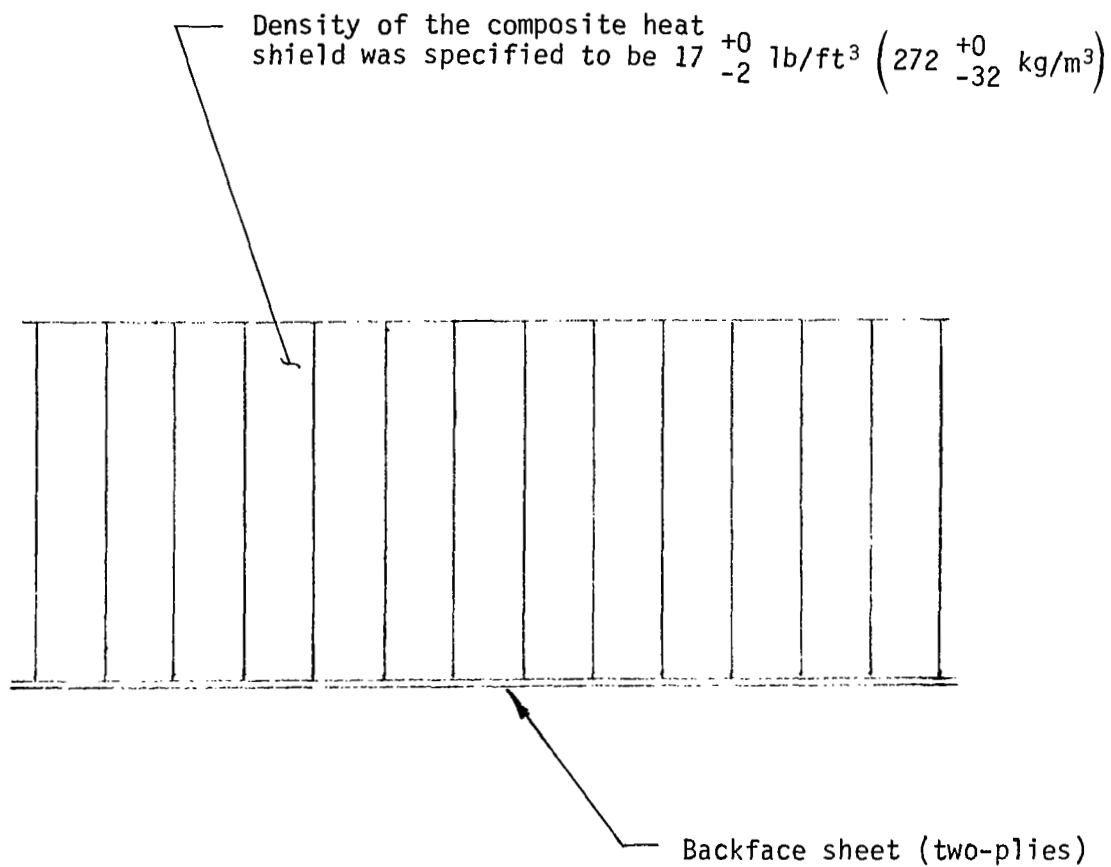


Figure 1.- Ablative Panel Design

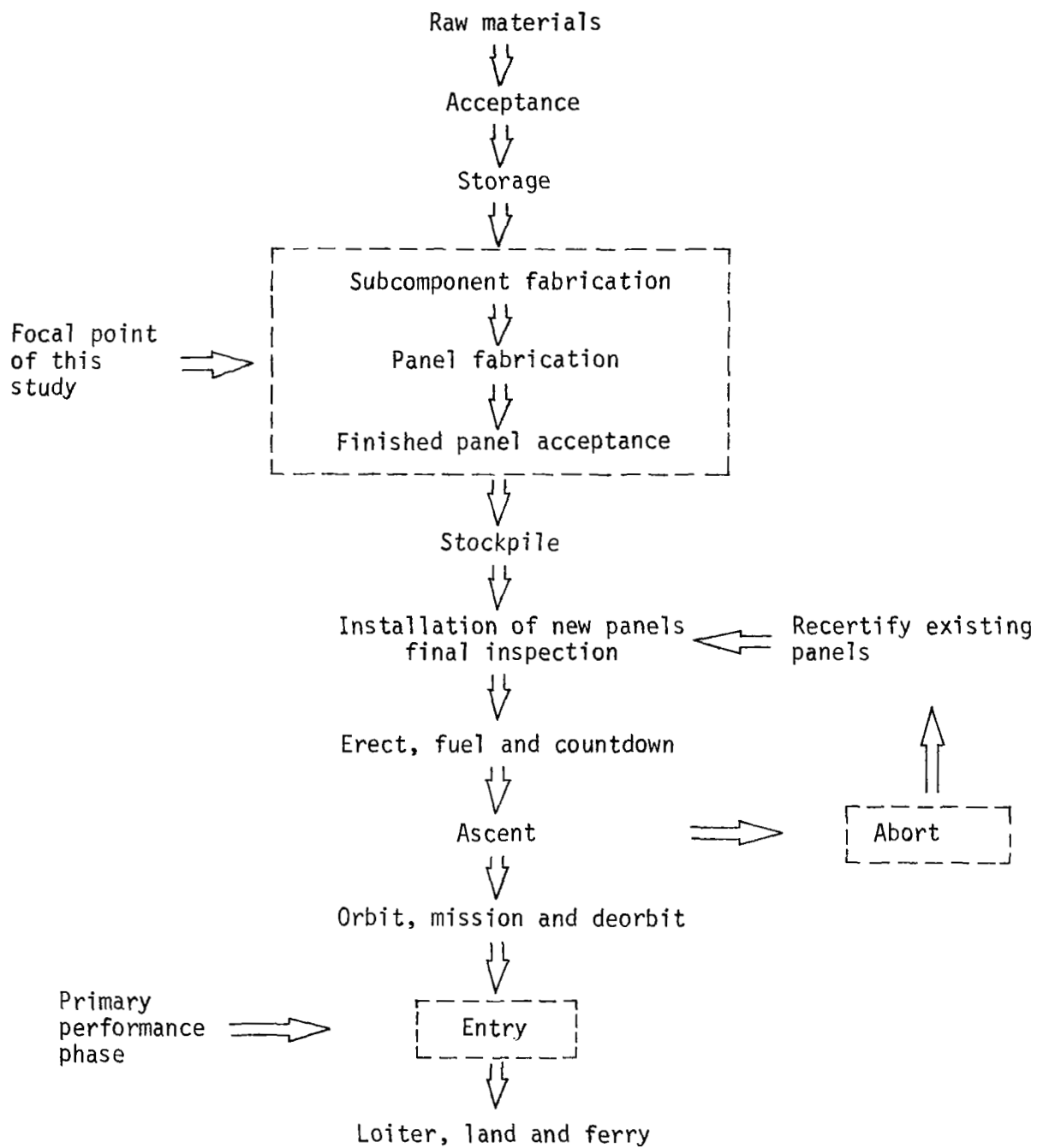


Figure 2.- Ablator Panel Life Sequence

The compatibility performance requirement is unique in that it defines failures of the ablative system in mission phases other than reentry. This requirement has been established on the premise that the presence of the ablative system will not cause failures of other systems. For example, an improperly cured panel could lead to excessive outgassing during the orbit phase that could damage optical systems on a payload or a space station. This then is a failure of the ablative system where the critical defect is an improperly cured panel.

A second type of compatibility failure is where the other system harms the ablative system. For example, the ablative material may be protected from damage by a particular fluid through the use of a protective coating. A break in the coating could allow the fluid to soak into the panel and cause loss of the char layer and inadequate thermal protection during entry. In this case, the break in the coating is the critical defect and the loss of the char layer is the performance failure.

### Defects Identified

Defects that have been identified as potentially critical are shown in figure 3, which also relates these defects in terms of their effects on critical properties. One of the most obvious conclusions drawn from this figure is that not only the thermal properties but also the mechanical and char integrity properties are important in assuring successful heat shield performance.

The basis for this compilation was a literature search and review of the fabrication process.

### Ablative Material Defects

The most important properties of the ablative material are its insulation characteristics, char stability, and resistance to surface erosion. In addition, the material provides added stiffness against bending and vibration or flutter-induced loads. The following defects have been identified as affecting these properties.

Cracks.— Cracks are defined as vertical discontinuities that can be contained within the filler of a given cell or run continuously across many adjacent cells.

Cause: Since the ablator material provides much of the basic stiffness for the reference design and for the large panels being considered for the Space Shuttle, 2x4-ft (0.67x1.22 m), cracking caused by unsupported handling becomes a very real possibility. Other causes would be residual stresses, cold soak strain, and thermal stresses during reentry.

Critical properties									
Potential critical defects	Ablative material	Thermal	Ablative layer mechanical	Char layer integrity	Surface erosion resistance	Chemical composition and stability	Ablative layer bond to subpanel	Dimensional	Subpanel mechanical
Cracks			•	•					
Delaminations			•	•					
Voids		•		•					
Unbonded to honeycomb		•	•	•					
Density		•		•	•				
Constituent integrity		•	•	•	•				
State of cure			•	•	•	•			
Homogeneity		•	•	•	•				
Formulation		•	•	•	•	•			
Foreign matter									
Inhibitors			•	•	•	•			
Inert to resin				•		•			
Moisture content				•		•			

Figure 3.- Potential Critical Defects

Critical properties									
Potential critical defects		Thermal	Ablative layer mechanical	Char layer Integrity	Surface erosion resistance	Chemical composition and stability	Ablative layer bond to subpanel	Dimensional	Subpanel mechanical
<u>Honeycomb</u>									
Crushed				•					
Broken ribbons			•	•					
Distorted cells			•	•					
Broken node bonds			•						
Splices		•	•						
Undercut				•					
Unbonded to substructure			•				•		
<u>Panel substructure</u>									
Resin content, mold cycle, etc									•
<u>Panel configuration</u>									
Thickness		•						•	
Width and length		•		•				•	•
Edge conditions		•		•				•	
Attachment alignment			•	•			•	•	•
Contour		•						•	

Figure 3.- Potential Critical Defects (cont)

Effect: Localized surface cracks that run out to the cell walls could lead to char loss if coupled with poor strength in the filler-to-core bond. Cracks running across cells could seriously reduce overall panel stiffness and, under flight-induced buffeting and vibration loads, the panel would be susceptible to crack propagation leading to excessive loading of the attachments and possible panel loss.

Delaminations.- Delaminations are defined as discontinuities approximately parallel to the ablative panel surface. They would normally be constrained by the cell walls and not be susceptible to propagation.

Cause: By our definition, delaminations occur in a plane normal to the applied pressure direction during filling and cure. Inhomogeneities in the filler can become stratified or layered under pressure and, at elevated temperatures, result in localized residual stresses after cure. These residual stresses are a possible source of delamination. However, a more likely source would be tension stresses developed during reentry tending to pull the char layer apart.

Effect: If these delaminations are present or develop during reentry, they will affect char strength and could result in char loss.

Voids.- Voids are defined as material discontinuities with ablative material not in contact across the discontinuity. Voids in honeycomb-filled ablative materials normally are found near the face sheet or in areas where core splices have been made. Their size, number and orientations are generally random (see fig. 4).

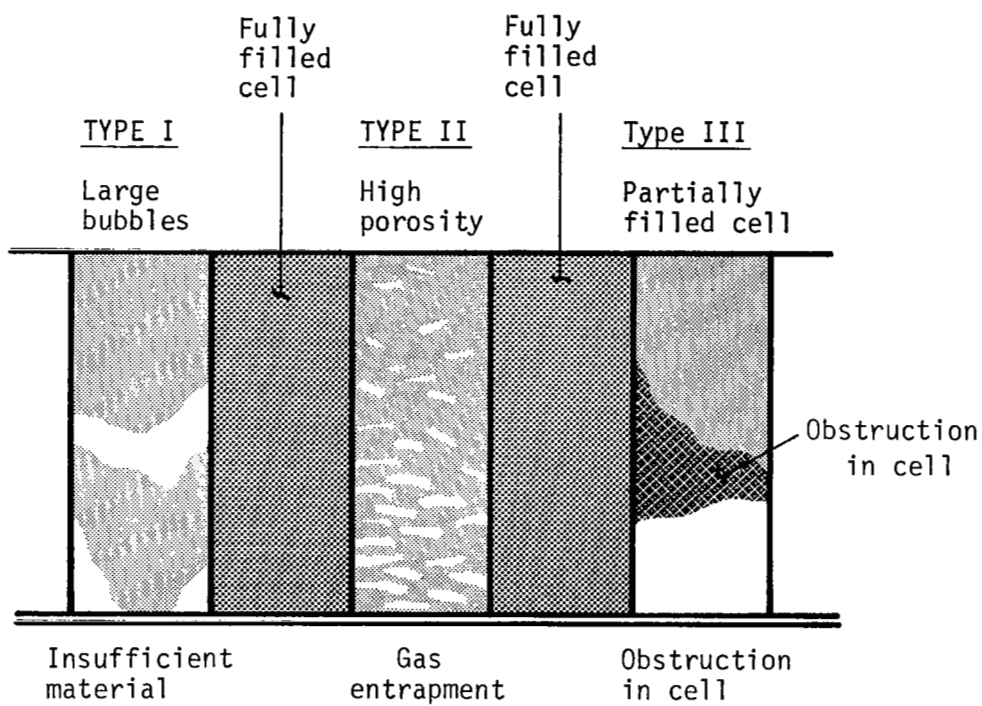
Cause: Voids are caused by lack of sufficient ablative material within a cell, entrapment of gases during fabrication, and obstructions in the cell passage. An example of an obstruction is surplus resin used for core splicing or core bond coating.

Effect: Voids can affect thermal performance in the following ways. Voids of Type I (large bubbles) are most detrimental when they occur near the surface and become exposed through surface recession. The increases in thickness required to maintain structure design temperatures was shown to be approximately equal to the void dimension in the direction of heat flow.\* Voids of Type II (high-porosity) in effect reduce material density and could cause increased surface recession and roughness. Depending on degree, this could affect surface heating and ultimately increase structure temperatures. Voids of Type III (partially filled cells) are of special concern because they result in completely vacant cells below the obstruction. Although the effect on structure temperature is unknown, it could be catastrophic depending on the number and size of these voids.

---

\* Carlson, D. L.: Test Report, Plasma Arc Tests for Acceptance Criteria of Body Heat Shield Materials. Martin Report CR-360, March 1966.





CAUSES:

Figure 4.- Voids in Ablative Material

Unbonds from honeycomb core.- Unbonds from the honeycomb core are defined as discontinuities at the interface between the honeycomb cell wall and the ablative filler. The unbonds can occur along one or more cell walls.

Cause: In many ablative-filled honeycomb structures, a bond between the filler and the core is achieved by pretreating the core often with an adhesive coating. Failure to perform this operation or failure to perform it properly can cause poor or weak bonds. Other causes of unbonds would be thermal expansion of the ablator out of the cells, and thermal shrinkage during cold soak.

Effect: Bond failure could result in loss of filler during vacuum cold soak and loss of char during reentry. In addition, a crack or unbond along one side of a cell wall will prevent the transmission of strain to the adjacent cell, thus affecting panel strength and stiffness.

Density.- Density is a very important material characteristic because of its effect on insulation and ablation properties. Density gradients can occur from the surface to the face sheet and density variations from cell to cell and panel to panel can be produced during fabrication.

Cause: Density gradients result when pressure applied to the filler material at the top of the cell is not uniformly transmitted to the bottom of the cell. The major causes of density variations from cell to cell are the localized use of impact force and its rather random application by fabrication personnel. Other less significant causes are the variation in filler density caused by such raw material variations as microsphere size and poor mixing of the material. The density gradient normal to the surface is a direct result of force transfer to the cell walls.\*

Effect: Density variations cause complications and uncertainties in defining reliable analytical models for performance predictions. Aerodynamic performance could be affected by a density variation from one cell to another because the density variations could produce low-density areas at the surface. During reentry this could produce nonuniform surface recession and would affect aerodynamic smoothness, possibly causing downstream flow separation.

Filler integrity.- The major functions of the fillers in the ablative material are to provide added strength to the elastomeric matrix and reduce the composite density. The following defects can affect these properties.

Broken fibers: One way that fibers reinforce the char layer is by bridging the low-density pyrolysis zone. For these fibers to be effective, their length must be greater than the pyrolysis zone width. Since silica fibers are extremely small and brittle, they are susceptible to breakage.

Cause: During processing these fibers can become broken and disintegrated because of their low physical strength.

---

\* Chandler, Huel H.: Low-Cost Ablative Heat Shields for Space Shuttles. NASA CR-111800, October 1970.

Effect: Broken fibers may not be of adequate length to bridge the pyrolysis zone and thus will reduce the material's ability to retain its char. In addition, the strength of the char to resist skin friction shear forces may be reduced.

Broken microspheres: Microspheres are used as a low-density filler in many ablative materials and, because they have low strength, they can be broken quite easily.

Cause: A certain percentage of microspheres are broken when received from the manufacturer. Many more can be broken during mixing (the percentage depending on the shearing action of the mixer and mixing time) and packing of the ablative filler into the core.

Effect: Variations in the percent of broken microspheres from one batch to another could significantly affect such material properties as density and conductivity.

State-of-cure.- The state-of-cure or crosslinking in elastomeric ablative materials is known to be affected by state variables of temperature, pressure, and cure time.

Cause: Variations in temperature can result from a lack of oven control. Cure pressure can be affected by leaks in the vacuum bag, variations in pump operation, and variations in atmospheric pressure. Cure time can be affected by variations in warmup time for different sized parts, failure of oven controls, or neglect by operator.

Effect: Cure temperature and pressure variations can affect the thermal and physical properties of the ablative material. These variations may result in cracks and panel warpage affecting such things as char retention, bond strength, ultimate strain capability, and loading on the attachments.

Inhomogeneity.- Inhomogeneity is an undesirable characteristic in many engineering materials because of its adverse effect on properties. Inhomogeneities alter the molecular structures and give rise to stress concentrations. The following inhomogeneities have been identified for the ablative material considered in this study.

Fiber bundles: Fibers are normally included in an ablative material to provide a measure of reinforcement of both the char surface and the pyrolysis zone. For this reinforcement to be uniform and fully effective, fiber dispersion must be uniform.

Cause: Several factors have been identified as possibly causing nonuniformity in fiber dispersion. A predominant cause is thought to be the lack of shearing action during mixing. Another cause that has been identified is the collection of fibers on the sides of the mixing bowls. This presents two problems. First, when fibers separate from the walls, they do not redisperse. Secondly, some fibers are lost and the actual percentage in the material is reduced.

Effect: The effect of fiber bundles or poor dispersion is to reduce their effectiveness in reinforcing the char and the char retention strength in the pyrolysis zone.

Microsphere agglomeration: Microsphere agglomerations are defined as groups of microspheres that are bound together by mechanical forces.

Cause: The basic causes of these agglomerations are absorbed moisture and the pressures occurring during storage that, after sufficient time, tend to compact the microspheres.

Effect: The effects on ablative material properties are obvious since each agglomerate represents a domain of essentially foreign material with different properties. In addition, surface voids can be caused by agglomerates at or near the surface. This would directly affect insulative properties and surface smoothness.

Resin ratio variations: The basic function of the resin system is to bind together the other constituents. Nonuniform distribution of the resin will produce resin-rich and resin-starved areas, thus producing variations in material strength, thermal expansion, and other properties.

Cause: Resin variations are caused by microsphere agglomerates, inadequate ablative material mixing, and from the resin coating applied to the core.

Effect: Resin-rich areas would have a much greater coefficient of expansion and produce high local stresses on temperature change. These stresses could open cracks during cold soak, cause shear failure of the filler bond with the core, and load the face sheet at the core bond in tension. Significant effects can also be expected in strain capability, elastic modulus, and conductivity.

Formulation variations.- Small variations in constituent percentages will likely have little or no effect on material properties, with perhaps the exception of the catalyst percentage.

Cause: The causes of formulation variations would most likely be errors in measurements, although, as cited earlier, fibers can become lost due to their tendency to collect on surfaces.

Effect: Changes in the catalyst percentage can affect the onset of cure, degree of cure, and the amount of reaction products remaining in the cured material. In all cases, detrimental effects on mechanical properties can be expected. The percentage of fibers can be expected to have some effect on char strength and retention.

Foreign matter.- Foreign matter is any unwanted matter that enters into the material by accident.

**Inhibitors:** Inhibitors are characterized by their neutralization of the catalyst, thus retarding or completely stopping cure.

**Cause:** These inhibitors can be introduced in many innocent ways, such as a faulty seal in a mixer allowing oil or grease to fall into the material batch.

**Effect:** Total cure prevention will depend in most cases on the percentage of inhibitors included. However, some variation in mechanical properties can be expected if inhibitors are included.

**Inerts:** Poor process control could result in introduction of inert materials. The most typical of these would be metals and wood that are commonly used as manufacturing aids. Particle sizes may vary considerably from microscopic to a size easily detected by radiographic inspection. In addition, salt compounds of the alkali metals such as sodium chloride and potassium chloride have been found in ablative materials.

**Cause:** These inerts can be introduced in several ways, including poor quality control, contaminated raw materials, and by equipment wear.

**Effect:** The microscopic particles that would likely result from wear of equipment are not of concern because they should not significantly affect any of the material properties or performance requirements. Although alkali metals will have little effect on performance properties, they could add to the problems of compatibility of the ablator with RF transmission during reentry.

**Moisture content.**— A significant characteristic of low-density materials is their affinity for absorbing moisture.

**Cause:** Two possible causes of moisture in the material are moisture contained in the raw materials, particularly the microspheres, and moisture absorbed by the ablative panel from the environment.

**Effect:** Moisture contained in the microspheres can cause the spheres to burst during vacuum cure and thus affect density. Moisture absorbed by the finished ablative panel can freeze in the launch and orbit environments and thus cause unwanted cracking and promote spallation during reentry.

### Honeycomb Core Defects

The function of the honeycomb core in the ablative material is to attach the ablative layer to the fiberglass face sheet; reinforce and attach the char layer to the virgin ablative layer; and control cracking in the char layer. The following defects associated with the honeycomb have been defined on the basis of potentially interfering with these three functions (the various honeycomb core defects are shown in figures 5 and 6).

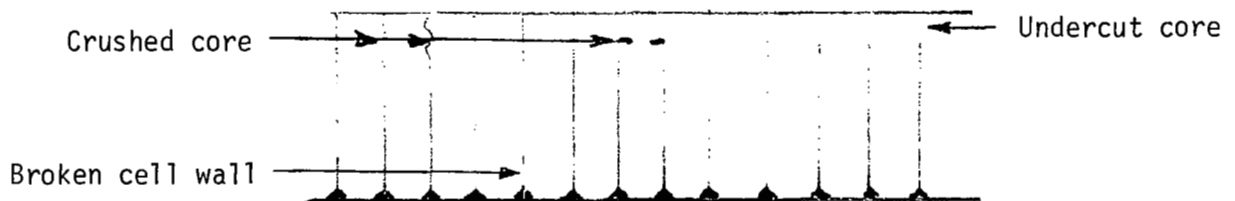
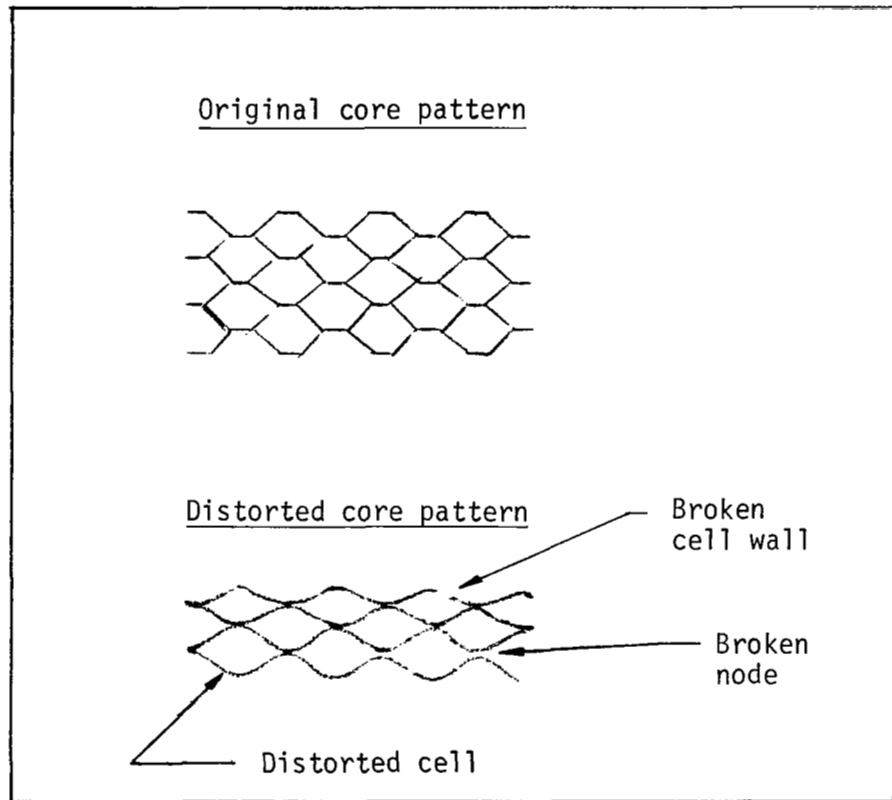


Figure 5.- Honeycomb Core Defects

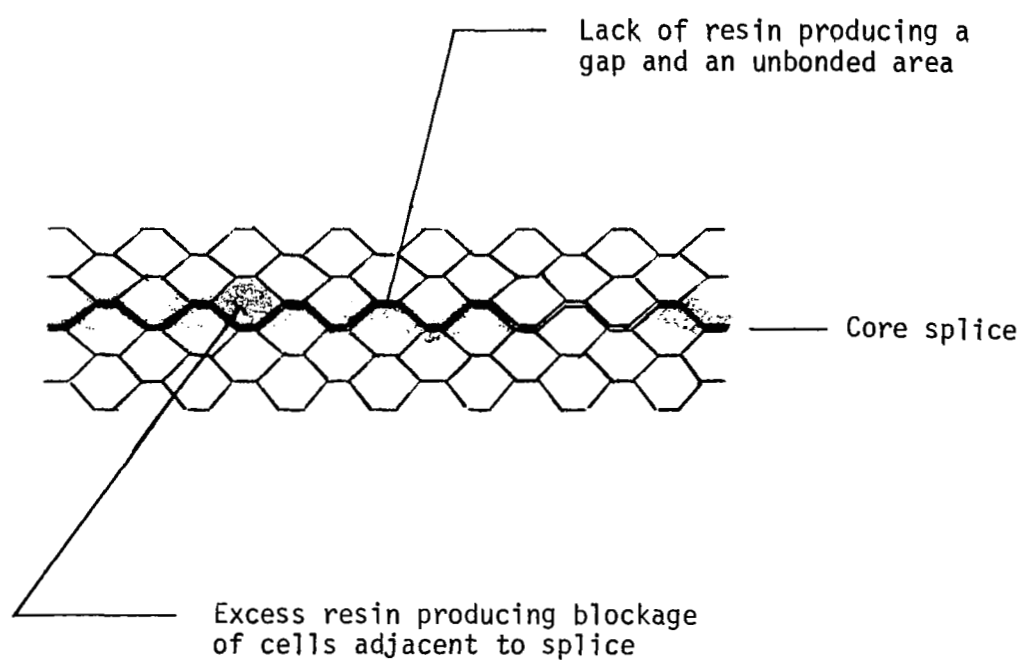


Figure 6.- Defective Core Splice

Crushed core.- Crushed core is defined as wrinkled core ribbons both internally and near the ablative panel surface.

Cause: This defect is caused by column loading of the core. It is expected to occur primarily as a result of impacting the ablative filler during the packing process. When the layer of ablative filler is driven completely into the honeycomb core and the top of the core is exposed during the impacting process, crushing of the core can be expected.

Effect: Crushed core results in a loss of its integrity and, therefore, a loss in its effectiveness to reinforce the char layer.

Distorted core.- This defect occurs when the cell shape is deformed from its original configuration. An example is where the cells have been distorted from a hexagon shape to a sine wave shape, or where the surface has been pushed sideways and tips the cell walls from the vertical.

Cause: Core distortions can be caused by abnormally high packing pressures or by lateral forces imposed by a vacuum bag.

Effect: Distorted core may imply that there are residual stresses in the ablator layer imposed between the distorted core and the ablative filler material. This could result in cracking when the surface is heated during reentry and possibly result in some char loss.

Broken core ribbons.- When the cell walls are torn either vertically or horizontally, the defect is defined as broken core ribbons. They can vary from a partial break in one cell wall to breaks extending over many cells.

Cause: These breaks or tears can be caused by excessive packing pressure, overflexing of the honeycomb, or lateral forces imposed by the vacuum bag.

Effect: Broken core ribbons can result in a weakened attachment of the ablative layer to the fiberglass face sheet, reduction in the reinforcement of the char layer, or excessively wide surface cracks in the region of the broken ribbons. The weakened attachment and wide cracks may cause failure either during cold soak or reentry.

Broken node bonds.- When the ribbon-to-ribbon bond has been separated making the cell walls discontinuous, the defect is described as a broken node bond. This defect is similar to vertically broken core ribbons.

Cause: These breaks can be caused by excessive packing pressure or overflexing of the honeycomb.

Effect: These breaks can result in excessively wide surface cracks either during cold soak or during reentry.

Undercut core.- This defect refers to a variation in core thickness so the core does not extend all the way to the outer surface of the ablative layer. Fabricating panels oversize and machining them to final thickness would alleviate the problem.



Cause: This defect would be caused by an undertolerance core and/or machining errors.

Effect: The most significant effect on end performance would be the lack of support in the filler at the panel surface. This could affect the char retention and the ability of the honeycomb to control surface cracks.

Defective core splices.- Splices that have excess resin or are not bonded are considered defective core splices. This is shown in figure 6.

Cause: Defective core splices can be caused by the application of an improper amount of resin at the bondline.

Effect: The result of an excessive amount of resin is to block adjacent cells and thus interfere with cell filling and packing operations, in addition to causing a local anomaly in the ablator layer. A deficient amount of resin will produce a poorly bonded or unbonded core splice that may result in an excessively wide crack when the panel is subjected to cold temperatures or heated during reentry.

### Face Sheet Defects

It is assumed that the Shuttle ablative panels will be directly attached to the metal structure. Although this will provide some support against pressure loads, inertia and thermal loads will produce large bending loads tending to warp and lift the panel away from the metal structure. Large tension loads will be produced at the attachments. The primary function of the face sheets will be to provide adequate bearing and shear strength at the attachment locations. The following defects have been identified as affecting these strength properties.

Delaminations.- Delaminations are physical separation of the two plies of cloth.

Cause: Delamination during fabrication can be caused by organic contaminants, resin-starved areas, and staged or cured resin areas.

Effect: The effects of delaminations on shear or bearing strength will depend on the relative location of the delamination with respect to the attachment points. A delamination at the attachment hole would result in greatly reduced face sheet stiffness because of a lack of interlaminar shear strength between the plies. This could readily result in attachment failure and lead to the more catastrophic failure of panel loss.

Spliced face sheets.- Spliced face sheets would be an overlapping of two adjacent pieces of cloth to form a larger sheet.

Cause: The reason for overlapping is simply the unavailability of a manufactured piece of the desired size.

Effect: The splice could result in local unbonds or poor bonds of the core because of the step introduced along its boundaries. The effect on performance would be to reduce the ablative material bond strength.

## Configuration Defects

This refers to variations in panel dimensions, general conditions of edges, and surfaces. The following defects associated with panel configuration are identified.

Thickness.-- This is defined as the ablative layer dimension required to limit the temperature of the structure to a specified design value.

Effect: Thickness is a most important dimension that must be controlled because of its effect on both structure temperature and vehicle weight. In addition to establishing manufacturing tolerances, when determining thickness acceptance criteria, we should consider the question of designing to a minimum or designing to a constant thickness.

Width and length.-- These dimensions control overall panel size.

Cause: Width and length dimensions can vary because of the difficulties in machining ablative materials and operator errors.

Effect: Overall panel dimensions must be maintained to assure mechanical mating with adjacent panels and to control gaps and joint sizes between panels. Of course, this problem can be minimized by the use of compatible sealer materials to fill these gaps and reduce heat leaks to the structure.

Attachments.-- Poor hole alignment and interface match will impose added loads at these attachment points and interfaces.

Hole alignment: This is defined as the location of attachment holes in the ablative panel with attachment anchor studs on the structure.

Cause: Manufacturing out-of-tolerances.

Effect: Improper mating with the attachment stud can cause prestraining of the entire panel. This would not normally be a problem if design tolerances are maintained. Also floating attachment points can be used to minimize mechanical and thermally induced strains.

Interface mismatch: This defines the distance between ablative panel face sheets and the support structure at the attachment.

Cause: Interface mismatch can be caused by warped panels and out-of-plane attachment locations.

Effect: Strains produced by forcing an interface match can result in high built-in bondline strains that could produce cracks during orbit and re-entry.

Edge conditions.— This refers to such defects at the panel edges as unfilled cells, and chipped, worn, and uneven edges and corners.

Cause: Since the specified panels do not contain edge members or reinforcement coatings, they are susceptible to damage during machining, handling, transportation, and installation.

Effect: Poor edges will result in heat leaks to the structure.

Surface smoothness.— The surface of a flight vehicle should be as smooth as possible to eliminate perturbations of the aerodynamic performance characteristics and heating. The following defects associated with surface smoothness have been identified.

Waviness: Waviness is defined as a random curvature of the surface.

Cause: This could be caused by contouring the ablator outer surface to the substructure. It could also result during reentry due to thermal strains causing bowing of the ablative panels.

Effect: Waviness in supersonic flow will produce antisymmetrical pressure distributions around the crests and troughs of the wall and increase the drag force.

Mismatch of edges: This refers to a step in the outer surface from one panel to the next.

Cause: Mismatched edges would result from a change in panel thickness or displacement of the attachment surface.

Effect: Two types of steps can occur -- a rise and a drop. In both cases, an attached shock could be produced in supersonic flow, increasing local heating by an order of magnitude.\*

Roughness: Roughness refers to a lack of surface smoothness or evenness.

---

\* Jones, Robert A.; and Hunt, James L.: Effects of Cavities, Protuberances, and Reaction-Control Jets on Heat Transfer to the Apollo Command Module. NASA TM X-1063, 1965.

Hunt, James L.; and Jones, Robert A.: Effects of Several Ramp-Fairing, Umbilical, and Pad Configurations on the Aerodynamic Heating to the Apollo Command Module at Mach 8. NASA TM X-1640, 1968.

Cause: Rough surfaces can be caused by accidental chipping, gouging, and tool marking during machining and transportation. Also, uneven expansion and recession between the ablator and core or from cell to cell can occur during reentry heating.

Effect: Roughness can affect the boundary layer and produce turbulence, separation, and vorticity that affect both heat transfer and flight performance.\*

## DEFECT DETECTION INVESTIGATIONS

Investigation of inspection methods was initiated by reviewing Space Shuttle requirements and environments, by reviewing the literature on ablative materials inspection, and by reviewing inspection methods used in programs involving similar materials and processes.<sup>†</sup> Emphasis was placed on nondestructive inspection methods for evaluation of defects. An experimental program was then initiated to evaluate:

- 1) The effects of process and material variables on various nondestructive evaluation techniques;
- 2) The relative defect detection sensitivities of various nondestructive evaluation techniques.

The defects evaluated were:

- 1) Unbond of honeycomb core to face sheet;
- 2) Unbond of ablator to core and face sheet;
- 3) Deformed core;
- 4) Face sheet delamination;
- 5) Density variations;
- 6) Homogeneity variations;

---

\* Pyle, Jon; and Montoya, Lawrence C.: Effects of Roughness of Simulated Ablative Material on Low-Speed Performance Characteristics of a Lifting-Body Vehicle. NASA TM X-1810, 1969.

<sup>†</sup>Thompson, R. L.; and Rummel, W. D.: Study of Critical Defects in Ablative Heat Shield Systems (Task I Summary). MCR-71-14. January 1971.

- 7) Voids;
- 8) Cracks;
- 9) Foreign inclusions;
- 10) Cure variations;
- 11) Variations in moisture content.

The nondestructive techniques evaluated were:

- 1) Visual;
- 2) X-radiography;
- 3) Neutron radiography;
- 4) Sonics/ultrasonics;
- 5) Thermal;
- 6) Microwave;
- 7) Holography;
- 8) Durometer hardness.

Forty-one 6x6x3-inch (15.2 x 15.2 x 7.6-cm) thick panels of the MG-36 material containing mechanical and material anomalies, as described in MCR-71-14,\* were evaluated by the various nondestructive test techniques to establish the relative detection sensitivities and interaction effects.

### Results of Test Panel Inspection

Visual inspection.- Visual inspection was useful as a process control tool in evaluating the honeycomb integrity and configuration prior to the face sheet bonding operation. After panel cure, honeycomb-to-face sheet unbonds could be observed quite readily due to the transparency of the face sheet material. However, a change in face sheet material or increased face sheet thickness could eliminate detection. On the ablator side, surface-connected mechanical defects such as voids, cracks, etc were detected. Crushed honeycomb was also observed by surface inspection (fig. 7). Color and uniformity variations due to mix, cure, and contamination were noted.

---

\**Ibid.*

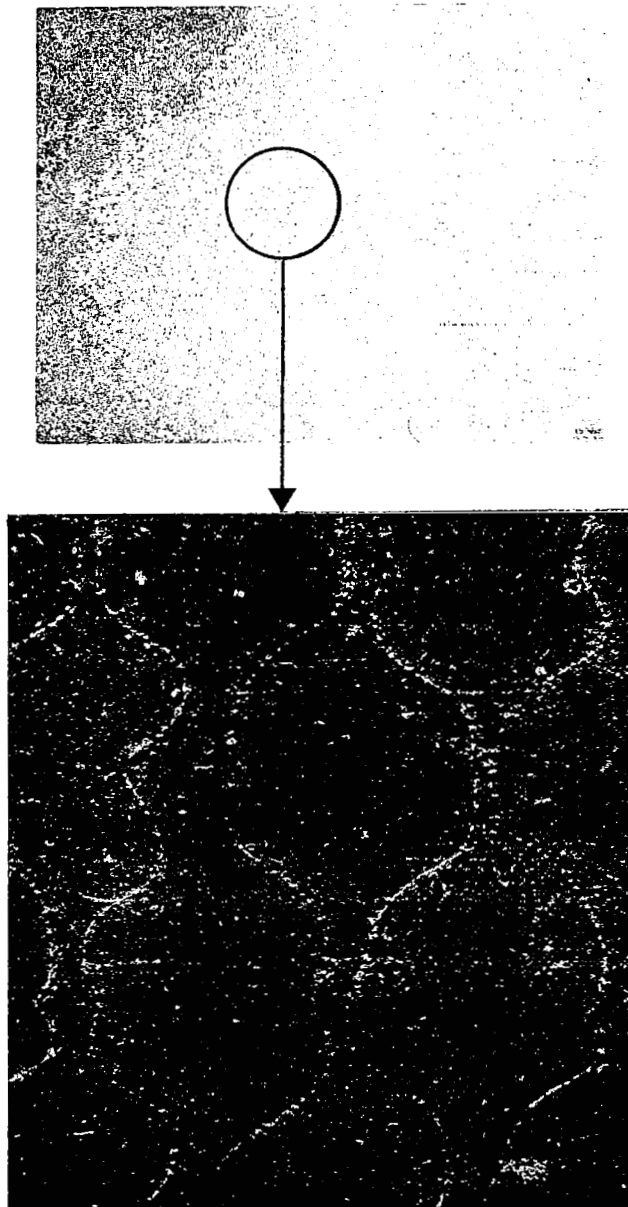


Figure 7.- Broken Core, Panel 18, 10X Magnification

X-radiographic inspection.- X-radiography was evaluated to determine its effectiveness in detecting internal soundness and in indirectly measuring bulk material variations. Anomalies detected were crushed honeycomb core, cracks, inclusions, voids, and density variations (fig. 8). Minor process variables such as uniformity of fiber distribution and agglomeration of phenolic microspheres were also noted. Crushed honeycomb 0.100-inch (0.254-cm) deep was detected. Metal inclusions as small as 0.005 inch (0.0127-cm) diameter and voids 1/8x1/4 inch (0.318x0.635 cm) were detected. Cracks through the full 3.0-inch (7.6-cm) thickness were detected. Density variations from the front to the back of panels were observed by radiography through the full 6.0 inches (15.25 cm) (side view section, fig. 9). Attempts were made to correlate the physical density of the material with the X-radiographic density using internal step wedges during exposure and scanning microdensitometer analysis of the radiographs. The fact that no significant correlation to physical density was obtained was attributed to variations in the silicone wet coating used to bond the ablative material to the honeycomb core and to slight variations in the radiographic technique. Suggested actions to minimize this problem were:

- 1) A change in process to minimize or eliminate the silicone bond coating;
- 2) Use of a penetrometer and an ablative material step wedge on all subsequent radiographs;
- 3) Optimization of the X-ray technique to attain maximum sensitivity.

The critical sensitivity of X-ray energy to two heat shield materials is illustrated in figures 10 and 11.

Since reading and analysis of X-radiographs constitutes a significant cost in use of X-radiography, a laboratory technique for enhancing such images was evaluated. A false-color real-time television imaging system was used to process both side and plan view radiographs for conformance to density requirements and for presence of voids. The technique shows promise for density analysis and is a significant aid in evaluating voids. Further work on image processing and automatic film readout is recommended.

Neutron radiographic inspection.- Neutron radiography was evaluated to determine the ability to measure internal soundness and to indirectly measure bulk material variations. Radiographs were made with two different reactor systems to attain maximum sensitivity and variation. Techniques were of particular interest for evaluation of panels if metallic face sheets were substituted for the fiberglass/epoxy face sheets. Overall sensitivity of the neutron radiographs was not as great as that obtained by X-radiography of the same panels even for those areas containing excessive silicone bond coating (fig. 12 and 13). Sensitivity to the silicone variations is attributed to the high gamma radiation in the neutron beam that produces a combined gamma and neutron radiograph. Additional effort to filter and collimate the neutron beam could greatly improve results but were beyond the scope of this program.

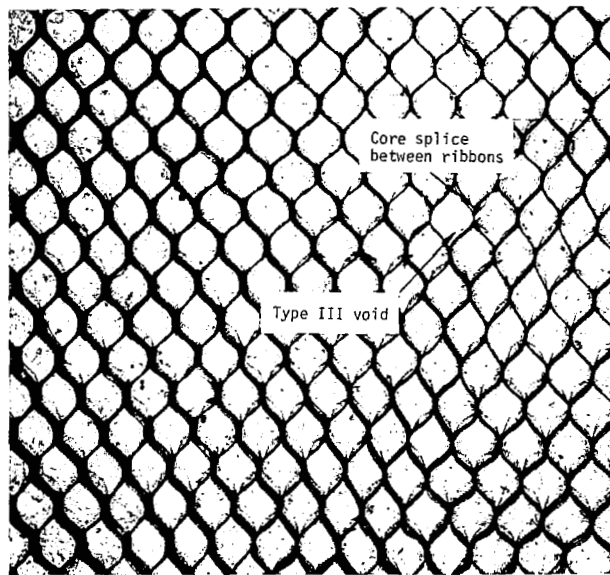


Figure 8.- X-Radiograph of Panel #10b (Plan View) Showing Void and Core Splice

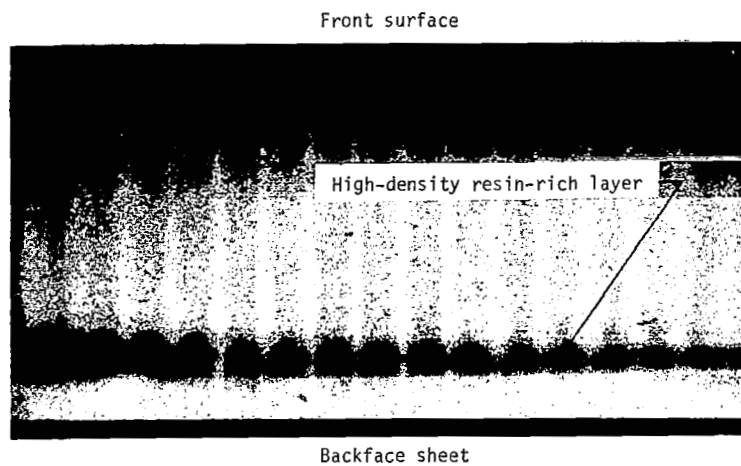


Figure 9.- X-Radiograph of Panel #22 (Side View) Showing High-Density Layer



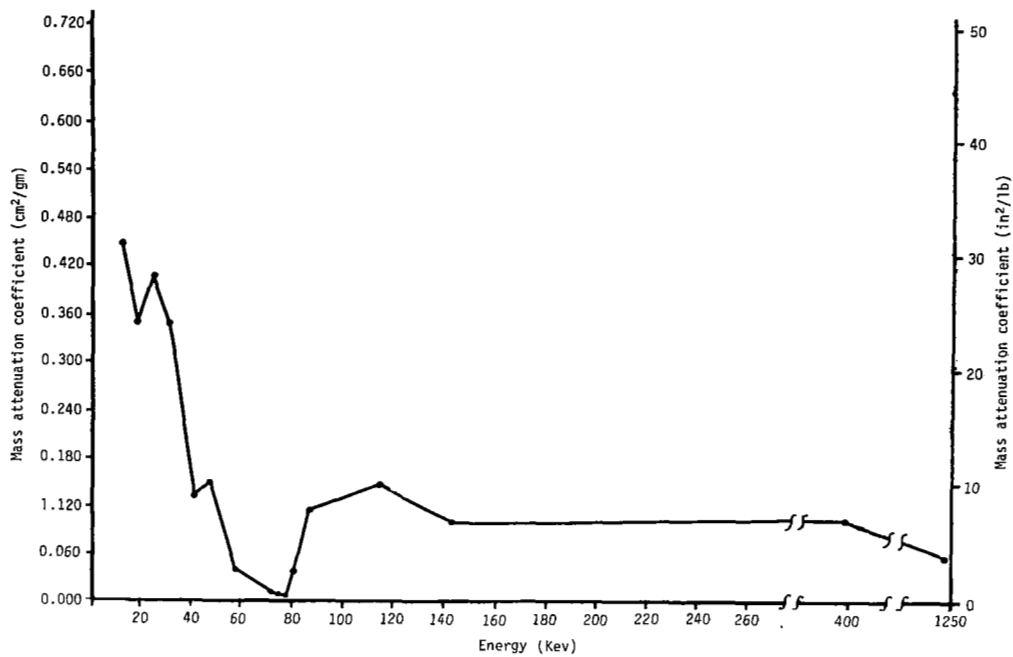


Figure 10.- Multiformal Fused Silica [126.3 lb/ft<sup>3</sup> (2025 kg/m<sup>3</sup>)]

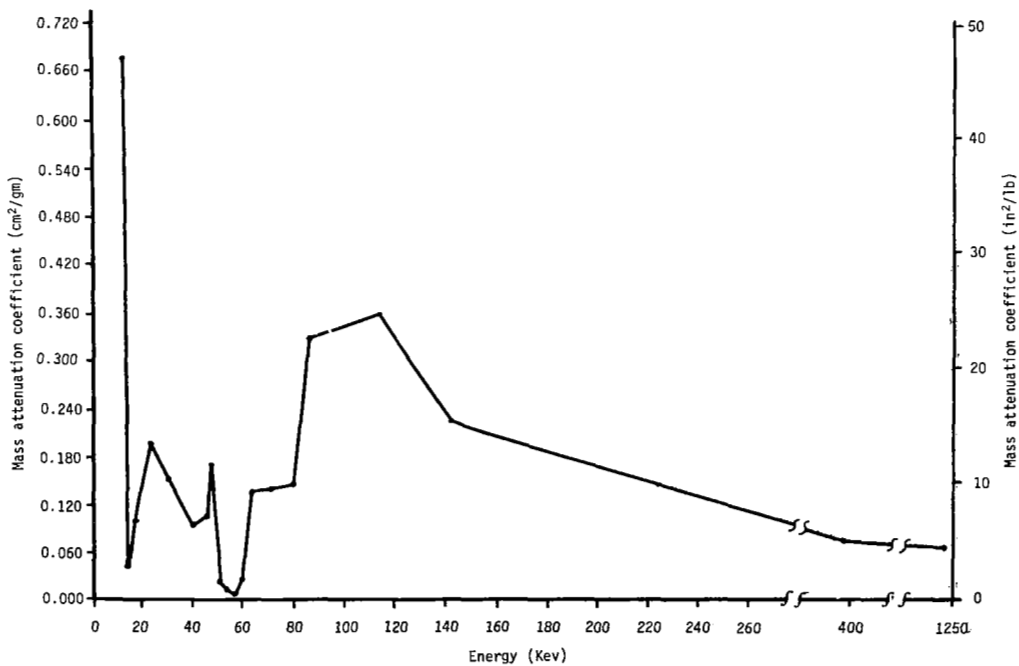


Figure 11.- Nylon Phenolic Molding Compound, Chopped  
[72.8 lb/ft<sup>3</sup> (1165 kg/m<sup>3</sup>)]

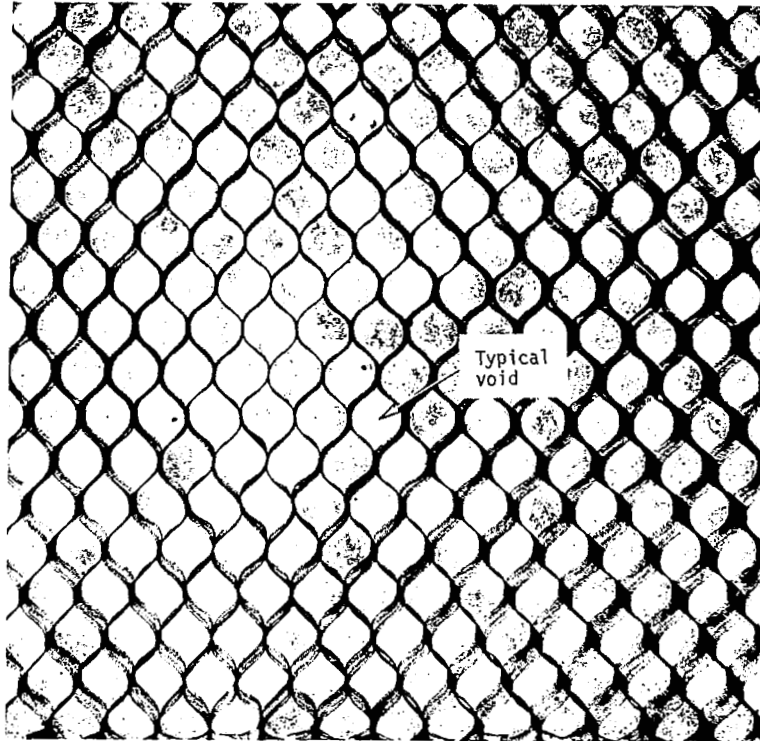


Figure 12.- X-Radiograph, Panel #10 Showing Voids

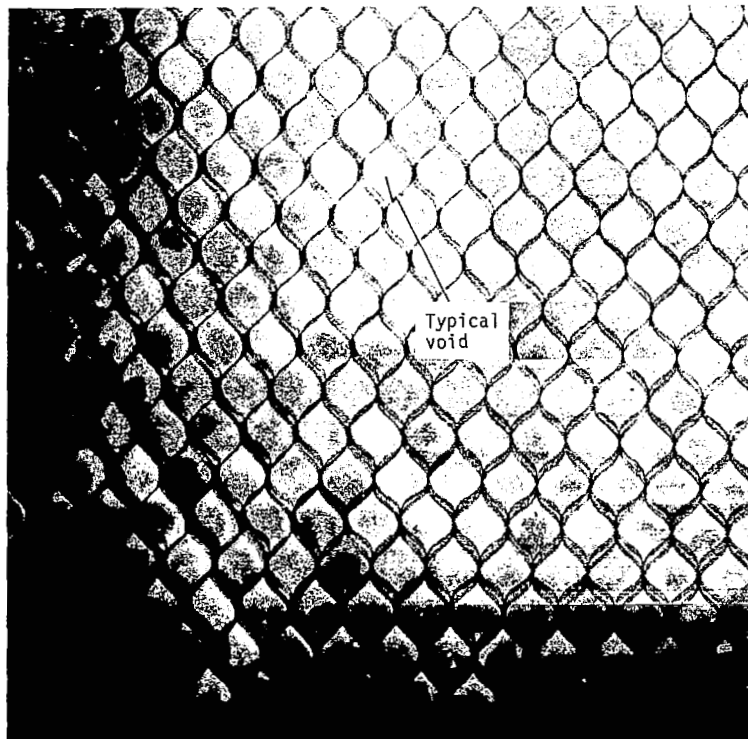


Figure 13.- Neutrograph, Panel #10 Showing Voids

Sonic/ultrasonic inspection.- Immersion ultrasonic inspection utilizing both pulse-echo and through-transmission techniques was evaluated for detection of honeycomb core-to-face sheet unbonds. Through-transmission techniques were discarded because of high material attenuation. Pulse-echo techniques were successful in detecting small unbonds but the method was difficult because of the thinness and waviness of the face sheet. The immersion technique was discarded because of problems in encapsulating the panel to eliminate water absorption.

Unbonds were readily visible by variation in face sheet color and could be verified by coin tapping (fig. 14). Efforts in evaluating test panels with sonic or ultrasonic techniques were discontinued. Additional work was recommended for detection of unbonds from the ablative side using a resonator technique.

Thermal inspection.- Thermal inspection was evaluated using an AGA Thermovision infrared scanning system. The infrared scanner technique was selected rather than liquid crystal and thermophosphor techniques because of its sensitivity and noncontact. Controlled heating and cooling, as well as pulsed techniques, were evaluated for sensitivity to anomalies. These methods exhibited sensitivity to internal density variations (fig. 15 and 16) but not to unbonds. The technique could be a useful supplement to X-radiography for gross inspection and should be considered for field application.

Microwave inspection.- All panels were subjected to microwave inspection to detect mechanical anomalies and to evaluate the effects of material variations on microwave energy. This method's inherent sensitivity to both material and mechanical variations makes it promising for low-cost production inspection but makes analysis difficult unless all material parameters can be accounted for. Table I illustrates the relative sensitivity of a microwave technique to variation in thickness and density parameters. To improve analysis, additional parameters such as resin content, cure, moisture content, etc must be known (constant or measured). The technique shows promise for control of processing operations but must be better characterized for field application.

Holographic inspection.- Holographic inspection, or more specifically, holographic interferometry, was evaluated as a laboratory technique for panel inspection. No positive results were obtained because of difficulties in holding and stressing the panels using laboratory fixtures. The technique does, however, offer great promise for production processing of panels when adequate tooling is provided. Further evaluation of this technique is recommended for low-cost inspection on a production-line basis.

Durometer hardness measurement.- Durometer (indentation) hardness measurements were made on all panels to evaluate detection of density and cure variations. The data are shown in table II. Even though this technique cannot be used to measure a single independent material processing parameter unless other parameters are known, it does provide a simple and economical tool for verifying uniformity within a panel and with respect to other panels. Therefore, it is recommended as a measure of process uniformity. The Shore "A" durometer hardness unit is not ideally suited for measurement of soft ablative materials and alternative designs are recommended for production and field application.

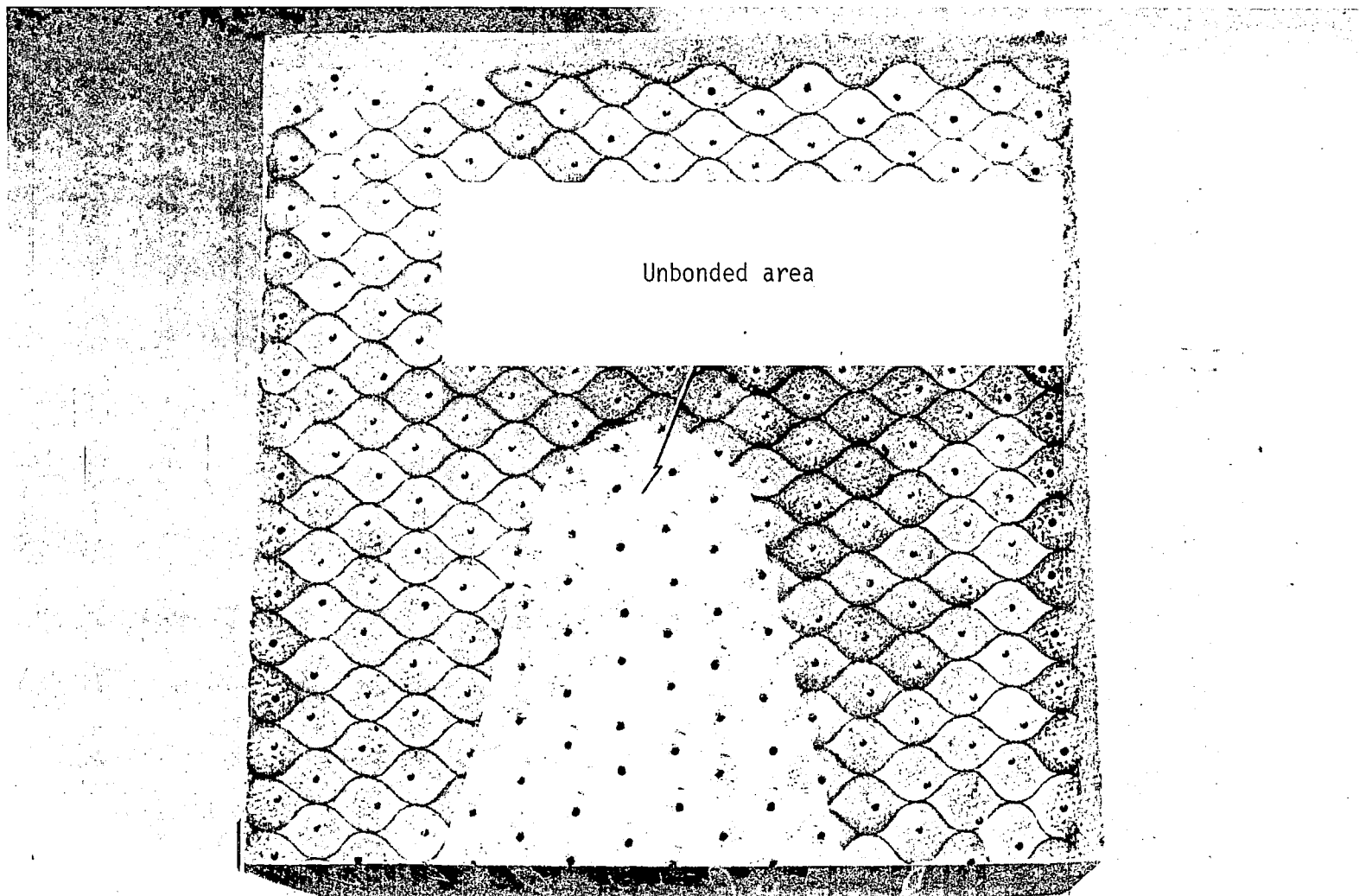


Figure 14.- Face Sheet-to-Core Unbond in Panel #30

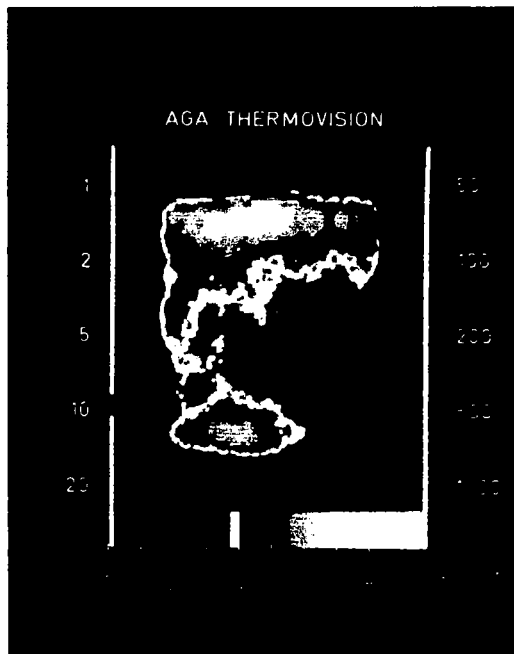


Figure 15.- Panel #5, 10 Minutes after Removal from Oven Controlled at 212°F (373K), One Isotherm Only

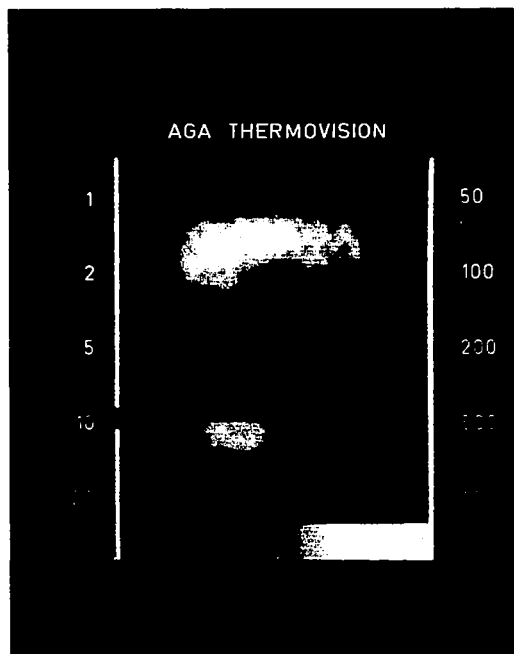


Figure 16.- Panel #5, 13 Minutes after Removal from Oven Controlled at 212°F (373K)

TABLE I.- RELATIVE MICROWAVE VALUES VS DENSITY AND THICKNESS

Sample	Density, lb/ft <sup>3</sup> (kg/m <sup>3</sup> )		Thickness, in. (cm)		Meter	Amplitude	Phase
5	14.2	(227.5)	2.959	(7.516)	78.2	38.5	37.31
5A	17.6	(282.0)	2.815	(7.150)	74.6	32.8	31.91
5B	16.7	(267.5)	3.008	(7.640)	32.0	55.8	33.81
6	11.8	(189.0)	2.996	(7.610)	82.8	33.4	36.77
6A	16.1	(258.0)	2.910	(7.390)	61.2	38.3	37.48
6B	16.6	(266.0)	3.010	(7.645)	21.0	52.6	34.08
7	15.7	(251.5)	2.909	(7.389)	58.0	39.1	36.17
7A	17.8	(285.0)	2.975	(7.557)	21.6	50.6	32.16
7B	18.5	(296.5)	3.030	(7.696)	12.2	36.9	31.98

TABLE II.- SHORE "A" DUROMETER HARDNESS

Sample	Description	Density, lb/ft <sup>3</sup>	(kg/m <sup>3</sup> )	Durometer Average Value (Shore A)
A. Average durometer value vs density of selected NDT samples				
6	Low density	11.8	(189.0)	35.8
5	Low density	14.2	(227.5)	64.4
7	Density control	15.2	(243.5)	44.4
6a	Density control	16.1	(258.0)	62.6
6b	Density control	16.6	(266.0)	64.4
5b	Density control	16.7	(267.5)	66.8
5a	High density	17.6	(282.0)	76.4
7a	High density	17.8	(285.0)	73.4
7b	High density	18.5	(296.5)	70.0
B. Average durometer value vs grease contamination in selected NDT ablative samples				
5b	Control	16.7	(267.5)	66.8
16	One gram of grease contamination	17.0	(272.5)	70.8
17	Two gram of grease contamination	16.5	(264.5)	64.2
C. Average durometer values vs percent catalyst in selected NDT ablative samples				
18	6% catalyst	18.8	(301.0)	66.4
7a	10% catalyst (control)	17.8	(285.0)	73.4
19	14% catalyst	17.3	(277.0)	77.6
D. Average durometer value vs cure temperature of selected NDT ablative samples				
20	225°F (381K) cure	18.0	(288.5)	69.8
7a	250°F (395K) cure (control)	17.8	(285.0)	73.4
21	275°F (408K) cure	17.9	(287.0)	78.4
E. Average durometer value vs cure time of selected NDT ablative samples				
22	12-hr cure	17.2	(275.5)	72.2
5b	16-hr cure (control)	16.7	(267.5)	66.8
23	20-hr cure	17.0	(272.5)	72.2
F. Average durometer value vs vacuum for selected NDT ablative samples				
24	24 in. of Hg (81 kN/m <sup>2</sup> ) (control)	16.2	(259.5)	66.8
25	12 in. of Hg (40.5 kN/m <sup>2</sup> )	16.2	(259.5)	68.4
G. Average durometer value vs moisture for selected NDT ablative sample				
24	Control	16.2	(259.5)	66.8
26	Moisture	17.0	(272.5)	69.4

Conclusions and recommendations from the panel study.- Results of the panel study showed that visual, X-radiographic, and indentation hardness inspections were immediately applicable to ablative panel evaluation. Further, neutron radiography, holography, infrared microwave, and sonic evaluations showed promise for inspection if some tooling and developmental efforts were applied. Visual, X-radiograph, and indentation hardness techniques were judged to be adequate for evaluation of prototype government-furnished panels and for the test sample evaluation proposed in the succeeding program tasks.

## Evaluation of Government-Furnished Heat Shield Panels

Panel description.- Five government-furnished heat shield panels [approximately 24 ft<sup>2</sup> (2.2 m<sup>2</sup>)] were evaluated by nondestructive test techniques and the results were confirmed by dissection of selected panel areas. These panels were fabricated by four different companies and are representative of the low-density elastomeric compositions. Four of the panels were flat, 24x24x2 inches (61x61x5.1 cm), and one panel was 24x48x2 inches (61x122x2 cm) with a 24-inch (61-m) radius of curvature in the 24-inch (61-m) direction. All panels were honeycomb-reinforced and were backed by a nonmetallic face sheet.

The purpose of this inspection phase was to assess the problems in, and effects of, applying state-of-the-art nondestructive techniques to full-scale panels and to evaluate the qualities of panels produced by different processes and different vendors. Visual, X-radiographic, and durometer hardness were used as the primary techniques, with infrared and coin-tap inspections as the secondary techniques.

Results of inspection.- The four flat panels showed similar characteristics, with minor variations due to processing differences. X-radiographs of panels fabricated with a phenolic resin wet coat on the honeycomb core were easier to read and analyze than those fabricated with a silicone resin wet coat on the core. The differences are attributed to the high relative X-ray absorption of the silicone resin material that masks bulk density variations in the ablative material. This factor contributed to a process change for subsequent engineering samples produced in Task III. Although variations in packing uniformity and core damage through the panel thickness were noted in varying processes, they are minor and should not significantly affect performance. On dissection, some variation in honeycomb-to-face sheet and ablator-to-face sheet adhesion was noted on two of the panels. Considerable variation in durometer hardness was found between panels and on the back of a section of each panel with the face sheet removed.

Inspection of the curved panel revealed problems in both X-radiographic inspection and in producing a curved panel. Because parallax problems were greater in X-radiographic inspection of the curved panel than in inspection of flat panels alternative techniques were developed. The flat panels were inspected using a conventional X-ray tube and a 7-foot (2.14 m) target/film distance. Target/film distance is the distance from the X-ray source, i.e., the target of the X-ray tube, to the X-ray film. A rod anode X-ray tube tilted 17° from normal and a 20-inch (51-cm) target/film distance was used to inspect the curved panel. Voids,

cracks, and honeycomb crushing were revealed in the curved panel. On dissection, voids and density variations near the face sheet were confirmed. In addition, the face sheet was poorly bonded to the honeycomb and ablative material.

No face sheet-to-core unbonds were detected on any of the panels by visual or coin-tap techniques.

Infrared inspection revealed the presence and the position of core splices in all panels but did not reveal small void areas in the curved panel.

Process analysis.- In analyzing the various fabrication processes from the standpoint of inspection ease, the following observations were made:

- 1) The BRU-LE panels fabricated by closed die molding techniques had the most uniform material density. The numerous inclusions found in this panel may not affect thermal performance but could be eliminated by better process control. Evidence of broken core in this panel indicates that the process parameters have not been optimized. Poor face sheet adhesion of this panel indicates that the single-step bond process needs to be further investigated;
- 2) The MAR-LE panel varied in radiographic density, but appeared uniform on dissection. A change in the bond coating material is indicated to minimize inspection problems;
- 3) The FAN-LE panel showed areas of varying radiographic density indicative of voids. Side view radiographs revealed a less dense band of material near the face sheet indicating nonuniformity in packing. Hardness measurements of the ablator with the face sheet removed indicated good uniformity but lower values than the panel face. The lower hardness values also indicate low-density material near the face sheet;
- 4) The NAR-LE panel was least uniform in radiographic density, in ablative material adhesion, and in face sheet adhesion. A change in process is indicated to correct these variations;
- 5) The NAR-LE curved panel exhibited voids, density variations, poor face sheet adhesion, and poor ablator adhesion. A change in process is also indicated for fabrication of these panels.

### Quality Assurance and Inspection of Task III Test Specimens

During fabrication of Task III test specimens, normal quality assurance measures were applied to attain specimen uniformity. This included assurance of raw material quality; fabrication process conformance; and nondestructive inspection of specimen billets, uninstrumented specimens, and final-instrumented plasma arc specimens. Nondestructive inspection consisted of visual inspection for general condition, X-radiography for internal condition, and homogeneity and durometer hardness for cure uniformity. The fabrication process was changed to eliminate



silicone wet coating and to substitute a phenolic bond coating. This change, in combination with greater familiarity with the MG-36 material, resulted in uniformity of X-radiographic density and in uniformity through the material thickness. Fibrous materials were evident on the surface of all specimens and small metallic inclusions were noted in most specimens. Hardness variations were as predicted for each sample variation (i.e., low for contaminated samples, nominal values for normal densities and processing and high for higher density samples) and further verified the sensitivity of this technique. Overall specimen uniformity was better than any panels inspected during Task I or II.

All instrumented plasma arc specimens were X-radiographed to precisely measure thermocouple locations. After test, all samples were again radiographed to determine thermocouple position and depth of char. The X-ray data were correlated with results obtained by specimen dissection.

## THERMAL PROTECTION SYSTEM PERFORMANCE REQUIREMENTS

A considerable variety of missions are envisioned for a workhorse Space Shuttle system, each having its own particular set of environments. Of the two stages, the orbiter vehicle will experience the more intense and diversified inputs. This vehicle must integrate the basic characteristics of four spacecraft -- launcher, orbiter, entry body, and subsonic airplane.

Key baseline system requirements\* that will influence the study of the effects of defects in ablator panels are:

- 1) Reusable orbiter;
- 2) Low- and high-crossrange version;
- 3) Seven-day mission duration;
- 4) Built-in go-around capability;
- 5) Capable of ferry flights;
- 6) Intact abort;
- 7) Ten-year lifetime, 100 missions;
- 8) Survivability against radiation;
- 9) Fail-operational and fail-safe redundancy requirements;
- 10) Compatible with payloads.

---

\* Space Shuttle Program, Phase B, System Study Data Book. McDonnell-Douglas/Martin Marietta Report MDC E0189, Volume I - Part I, October 19, 1970.

The design reference mission selected is logistics resupply of a space station; the insertion orbit is 50 x 100 n. mi. (92.6 x 185.2 km), while the reference orbit is 270 n. mi. (500.0 km) and circular at 55° inclination. Additional details are presented in table III, which also lists other potential missions of interest.

The time scale for the baseline mission is presented in figure 17 and the events sequence is correspondingly listed in table IV.

Major emphasis was placed on the delta shaped high-crossrange orbiter illustrated in figure 18. Aerodynamic and trajectory parameters are summarized in figures 19 and 20.

Defects produced during TPS fabrication can manifest themselves during events other than entry. Dormant types of critical defects can germinate during the following phases:

- 1) Launch site storage;
- 2) Installation on vehicle;
- 3) Prelaunch chilldown near cryogenic fuels;
- 4) Contact with oils, vapors, etc;
- 5) Ascent,
  - a) Heating,
  - b) Acoustics,
  - c) Vibration,
  - d) Max q,
  - e) Separation;
- 6) Orbit,
  - a) Cold soak,
  - b) Radiation,
  - c) Solar heat cycles,
  - d) Mission inputs,
  - e) Deorbiting.

TABLE III.- SHUTTLE MISSION CHARACTERISTICS

Missions Orbital characteristics	Space station/ base logistics support	Placement & retrieval of satellites	Delivery of propulsive stages & payloads	Delivery of propellants	Satellite service & maintenance	Short duration orbital mission
Altitude, n.mi. (km)	200 to 300 (370.4 to 555.6)	100 to 800 (185.2 to 1481.6)	100 to 200 (185.2 to 370.4)	200 to 300 (370.4 to 555.6)	100 to 800 (185.2 to 1481.6)	100 to 300 (185.2 to 555.6)
Inclination, deg	28.5 to 90	28.5 to sun syn- chronous	28.5 to 55	28.5 to 55	28.5 to sun syn- chronous	28.5 to 90
On-orbit $\Delta V$ , 1000 fps (1000 mps)	1 thru 2 (0.305 thru 0.610)	1 thru 5 (0.305 thru 1.524)	1 thru 1.5 (0.305 thru 0.457)	1 thru 2 (0.305 thru 0.610)	1 thru 5 (0.305 thru 1.524)	1 thru 2 (0.305 thru 0.610)
On-orbit stay time, days	7	7	7	7	7-15	7-30
Crew	2	2	2	2	2	2
Passengers	rotate 50 men/quarter	2	2	2	4	12
Discretionary payload						
Weight, 1000 lb (1000 kg)	70/quarter (31.8/quarter) <sup>c</sup>	--	--	--	--	--
Volume 1000 ft <sup>3</sup> , (1000m <sup>3</sup> )	--	5 thru 10 (0.412 thru 0.184)	10 (0.284)	10 (0.284)	5 thru 10 (0.142 thru 0.284)	4 thru 6 (0.153 thru 0.170)
Critical di- mension dia- meter, ft. (m)	10 thru 15 (3.1 to 4.6)	15 (4.6)	15 (4.6)	15 (4.6)	15 (4.6)	15 (4.6)
<sup>c</sup> Includes passengers.						

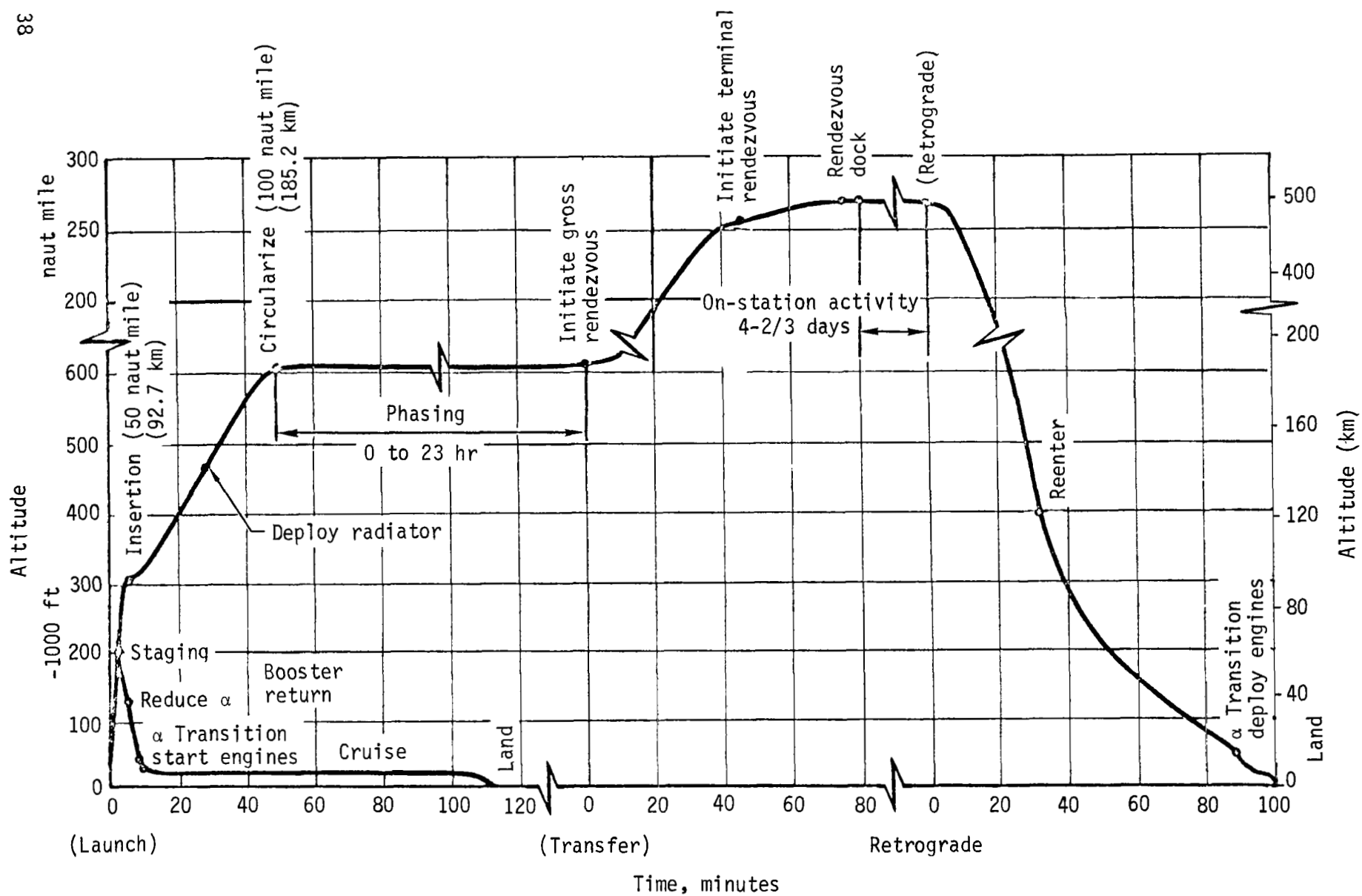


Figure 17.- Baseline Logistics Mission Profile, High Crossrange System

TABLE IV EVENTS SEQUENCE SPACE SHUTTLE MISSION PHASES, HIGH-CROSSRANGE SYSTEM (Logistics Mission)

Phase	Duration		Boundary	
	Booster	Orbiter	Booster	Orbiter
Ascent	201 s	436 s	Tower clearance thru stage separation	Tower clearance to 50 x 100 n. mi. (92.7 x 185.2 km) orbit insertion
On-orbit	--	6 days 20 hr	--	50 x 100 n. mi. (92.7 x 185.2 km) orbit insert to position for retrograde
Descent	108 min	74 min	Stage separation thru air-breathing engine shutdown	Retrograde burn thru air-breathing engine shutdown
Ferry	--	--	Postflight operations thru vehicle deservice after ferry flight	
Postflight <sup>α</sup>	.85 days (14 hr)		Engine shutdown thru vehicle deservice	
Maintenance <sup>α</sup>	3.4 days (54 hr)		Transport to maintenance area to maintenance cycle completion	
Payload installation <sup>α</sup>	0.25 days (4 hr)		--	May occur after maintenance cycle, during prelaunch (prior to erection), and/or during launch countdown
<sup>α</sup> Elapsed time based on two 8-hr shifts per day, 20th unit through maintenance.				

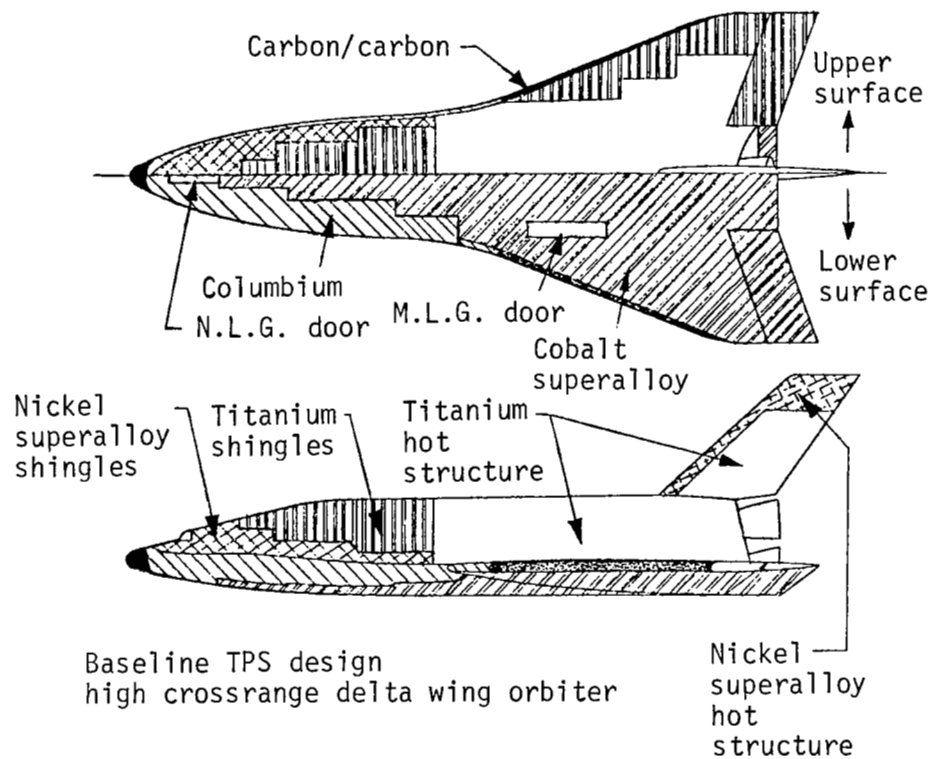
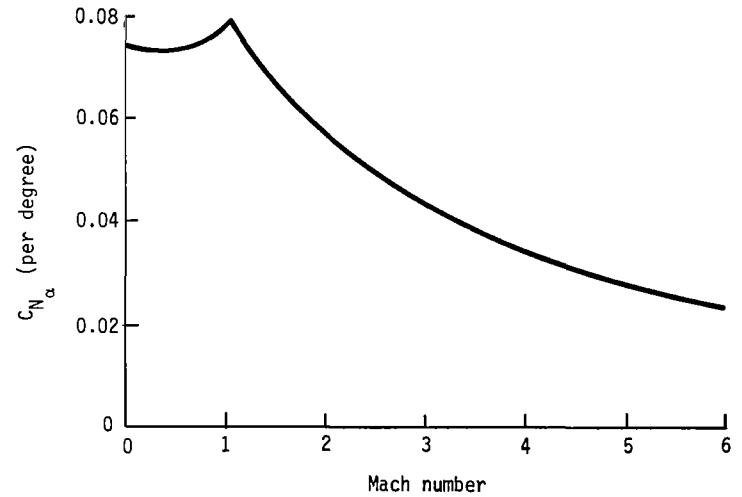
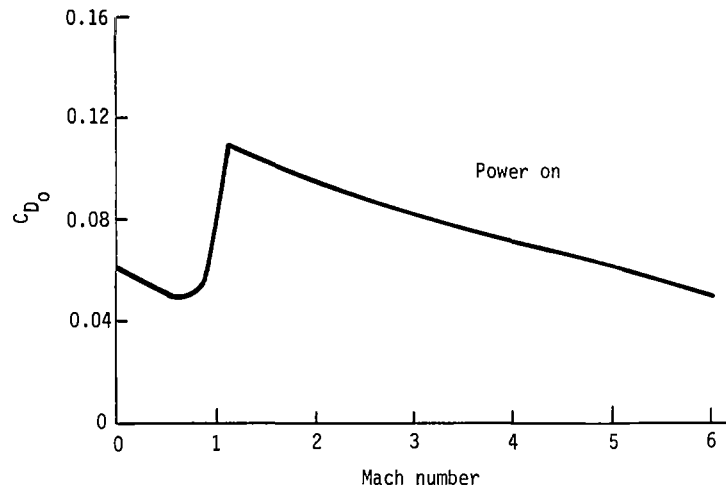


Figure 18.- Thermal Protection, High-Crossrange Orbiter

# LAUNCH ARRANGEMENT CHARACTERISTICS



Subsonic  
 $S_{ref} = 5,935 \text{ ft}^2 \text{ (} 552 \text{ m}^2 \text{)}$   
 $L = 157.5 \text{ ft (} 48 \text{ m)}$   
 $X_{cg} = 67\% L_{body}$

## DELTA ORBITER CHARACTERISTICS

Hypersonic  
Mach = 20; Altitude = 200,000 ft (61,000 m)  
 $S_w = 5,935 \text{ ft}^2 \text{ (} 552 \text{ m}^2 \text{)}$   
 $X_{cg} = 66\% L_{body}$

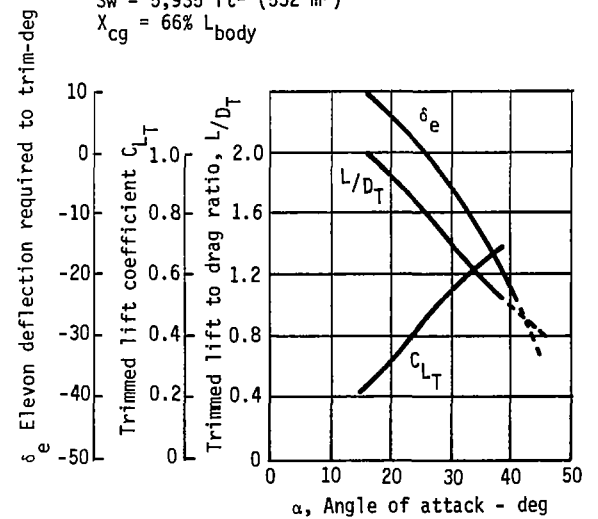
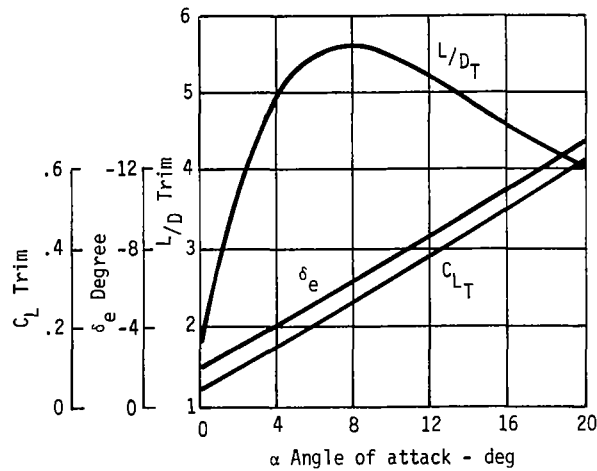
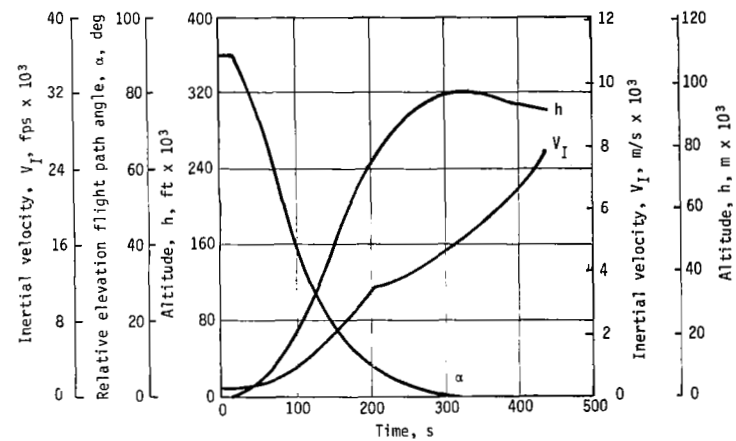
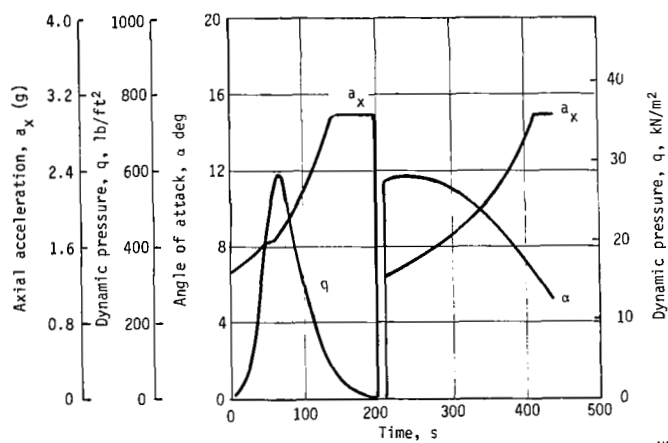


Figure 19.- Aerodynamic Characteristics, High-Crossrange System

## NOMINAL ASCENT TRAJECTORY



## NOMINAL ENTRY TRAJECTORY

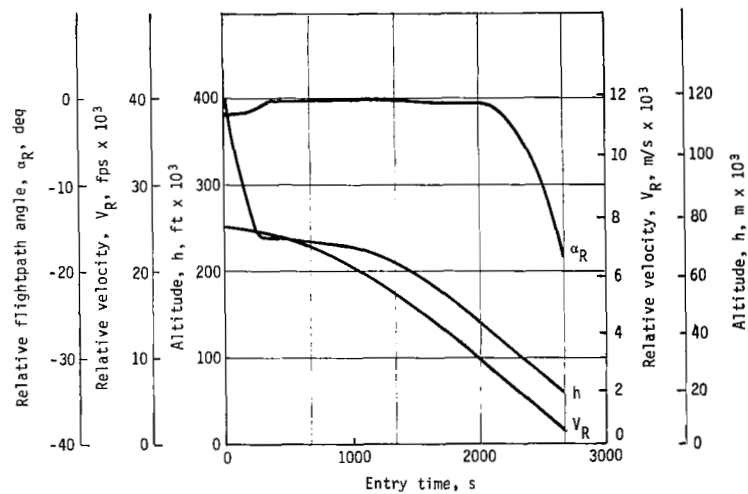
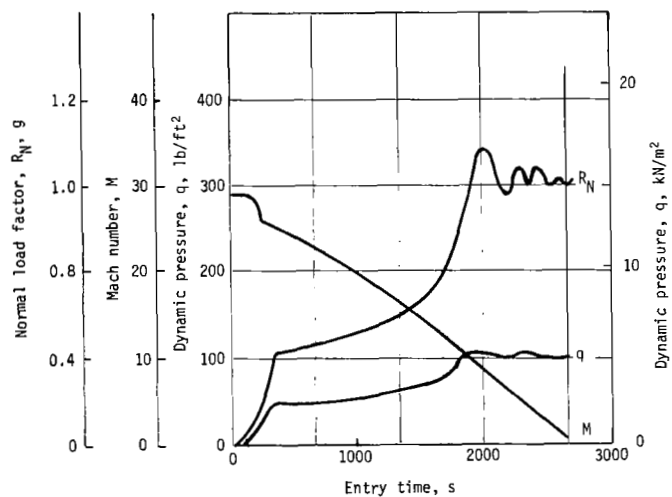


Figure 20.- Trajectory Parameters, High-Crossrange System



The Shuttle missions will impose significant performance requirements on the heat shield system for the nonentry phases in addition to those specifically concerned with the entry phase. These will be dictated primarily from compatibility requirements imposed by other subsystems of the Shuttle and the overall missions. The following compatibility requirements are apparent at this time.

- 1) Aero system,
  - a) Surface smoothness,
  - b) Contour,
  - c) Particle erosion;
- 2) Mechanical systems,
  - a) Operation of doors and other mechanisms,
  - b) Hydraulic fluids,
  - c) Lubricants;
- 3) Communications system,
  - a) Boundary layer contamination,
  - b) Ground plane effect;
- 4) Propulsion system,
  - a) Fuels,
  - b) Oxidizer (lox);
- 5) Thermal control system,
  - a) Emissivity and absorptivity,
  - b) Outgassing contamination;
- 6) Payload and space station compatibility, including outgassing contamination.

These Shuttle missions and environments dictate certain performance requirements that an ablative thermal protection system must satisfy to ensure success and crew safety during Space Shuttle orbital missions. These requirements in turn define the critical material properties outlined here. The correlation of test and analytical results with induced fabrication defects is keyed to these critical properties.

The salient parameter in thermal performance is backface temperature excursions that could induce overheating in the supporting structure. The baseline ablator configuration was examined and it was assumed that this composite panel is attached to primary vehicle structure (aluminum) at discrete points. The gap between the face sheet and primary structure is considered essentially zero. The design nominal back surface temperature is 300°F (422K). At this time, information concerning the Shuttle design is not sufficient to establish actual values for some of the requirements outlined.

The performance requirements are divided into the categories of thermal, structural, char layer integrity, and compatibility with other systems and the mission. Although degradation in any of these classes because of critical defects can precipitate difficulties in all the categories, they are discussed independently in the following sections.

## Thermal Criteria

The critical thermal properties of the ablative panels to ensure that the design structure temperatures are not exceeded are:

- 1) Thermal conductivity;
- 2) Specific heat;
- 3) Density;
- 4) Emissivity;
- 5) Degradation kinetics;
- 6) Degradation products;
- 7) Heat of reactions;
- 8) Surface recession kinetics.

A broadbrush evaluation of these properties is obtained from the insulation efficiency parameter. This basic parameter provides a "partial" evaluation of these critical thermal properties; however, for the criteria to be complete, structure temperature excursions must also be considered. For example, study

results show that the efficiency of a 15 to 17 lb/ft<sup>3</sup> (240 to 272 kg/m<sup>3</sup>) material was the same, yet structure temperatures differed by 40°F (277K). Thus, the important evaluation in this case is structure temperature and, for a design temperature overshoot of 75°F (42K) [25%\* of the 300°F (422K) design value], the effect of a local 2 lb/ft<sup>3</sup> (32 kg/m<sup>3</sup>) decrease in density would be noncritical. However, consider the case where a density decrease is coupled with crushed core, which resulted in char loss. In this case, the temperature overshoot could easily become critical.

Because the combinations of defects are numerous and in reality some defects might be "allowed" through design compromises, the present study has taken the simplified approach that a given defect is classified as critical only if it alone exceeds the overshoot tolerance. Thus, to determine the criticality of the various defects investigated, backface temperature response and thermal efficiency were compared with defect-free control specimens.

### Structural Criteria

The requirements for structural performance of the material are designed to assure confidence that ablator panels with passable defects possess adequate strength to perform the following functions:

- 1) Transmit flight loads to the primary structure;
- 2) Accommodate thermal and pressure-induced loads without excessive cracking;
- 3) Provide adequate overall panel stiffness to limit load-induced strain in the char layer to an acceptable level;
- 4) Maintain adequate strength between the filler and cell walls to prevent loss of filler;
- 5) Prohibit attachment point failures that would jeopardize panel retention;
- 6) Withstand the launch noise (159 dB) environments;
- 7) Possess sufficient mechanical properties ( $E$ ,  $\alpha$ ,  $\epsilon_{ult}$ ) to ensure no cracking at temperatures of -150°F (173K) during orbit.

---

\* A tolerance of 25% is allowed based on the design criteria developed for the PRIME program.

## Char Layer Integrity

Efficient performance of the ablative thermal protection system depends on the char layer. Performance of the char layer depends on a variety of factors. For this reason integrity of the char layer is included as a system performance requirement. Char layer integrity is defined as retention of the char layer by maintaining its attachment to the virgin ablative material layer; the restriction of spallation of large particles of char; and chemical stability of the char constituents during the heated periods to preclude sudden melting or collapsing of the char layer. Char integrity must be maintained for the following conditions:

- 1) Heating rate, 15 to 55 Btu/ft<sup>2</sup>-s (0.17 to 0.625 MW/m<sup>2</sup>);
- 2) Local pressure, 0.005 atm (507 N/m<sup>2</sup>);
- 3) Heat transfer coefficient, 0.005 to 0.006 lb/ft<sup>2</sup>-s (0.0098 to 0.0294 kg/m<sup>2</sup>-s);
- 4) Enthalpy, 3000 to 12 000 Btu/lb (6.98 to 27.9 MJ/kg);
- 5) Viscous shear, ~ 2 psf (95.8 N/m<sup>2</sup>);
- 6) Local pressure gradients (undefined);
- 7) Substructure-induced strain (1.0%);
- 8) Prior environment exposure (undefined);
- 9) Pulse requirements for the above items (undefined).

## Compatibility

The ablative thermal protection system must be compatible with other systems, the payload, and the overall mission. The following items have been identified as compatibility requirements for which specific levels must be defined:

- 1) Vacuum outgassing during orbit,
  - a) Rate,
  - b) Level,
  - c) Products;
- 2) Surface smoothness;

- 3) Particle erosion,
  - a) During nonentry phases,
  - b) During entry;
- 4) Melt flow during entry;
- 5) Outgassing products during entry;
- 6) Emissivity and absorptivity during nonentry phases;
- 7) Onboard fluids,
  - a) Lox,
  - b) Hydraulic,
  - c) Lubricants,
  - d) Fuels;
- 8) Dielectric constant.

## MODELS AND INSTRUMENTATION

Sixty-nine standardized plasma arc "splash" models, two 16x8x2-inch (40.6x20.3x5.08 cm) ablative panels, and 95 tensile coupons were tested during this investigation. The "splash" specimen design was verified during a screening test phase in which planned specimen instrumentation was also evaluated. In addition, it was agreed during Task II discussions with the Langley Technical Monitor that the following two items would also be incorporated in this screening phase. First, the processing times and char bond strength of a core bond coat of Dow Corning 182 silicone resin and the Monsanto SC1008 phenolic resin would be compared. Based on the results, a study baseline bond coat would be selected. Secondly, an evaluation would be made of Hitco F100 A-25 fibers as a substitute for the contract-specified microquartz fibers discontinued by Johns Manville. Other specific objectives at the preliminary screening tests were to:

- 1) Evaluate material response and the need for wrapping specimen sides to prevent material loss at the edges;
- 2) Qualitatively evaluate the effects of edge radius on heating uniformity and specimen performance;
- 3) Determine the optimum model diameter with respect to side heating and surface heating uniformity;

- 4) Verify the placement of thermocouples within the test specimens for determination of surface temperature and temperature distribution;
- 5) Evaluate the reliability and accuracy of back surface thermocouples.

Fifteen specimens were fabricated and tested for this purpose.

Concurrent with these screening tests, an in-house study was conducted to evaluate such potential processing improvements as ablative filler mixing, fiber dispersion, and core loading.\* The data from both these efforts were incorporated in material fabrication and specimen design procedures.

### Defects Investigated

From the compilation of the potentially critical defects identified in the previous section, the following "defects" were selected for investigation during the reentry phase of the Space Shuttle mission.

Density.- During Task I, variations in density seemed to have a very definite effect on filler bond strength. This effect was especially noticeable when the honeycomb core was pretreated with the DC-1200 silicone primer. The adhesion between the filler and the honeycomb was related to the density variation from surface to face sheet.

The density variation models made using the impact filling method included nominally packed models with a bulk density of 16 lb/ft<sup>3</sup> (256 kg/m<sup>3</sup>) and over-packed and underpacked models with bulk densities of 16 to 18 lb/ft<sup>3</sup> (272 to 288 kg/m<sup>3</sup>) and 14 to 15 lb/ft<sup>3</sup> (224 to 250 kg/m<sup>3</sup>). Results were obtained concerning the effect of (1) bulk density variations and density gradients through the material on thermal efficiency, char depth, and char integrity, and (2) the effect of bulk density variations on char-to-core bond strength.

Filler bond to H.C..- It was found during Task I that resin bond coating of the core before packing was necessary to obtain a good bond of filler to core. It was noted that "excess" resin is carried down the cell by the wiping action of the filler. This excess resin is concentrated near the face sheet and is undesirable because of its effect on material properties and homogeneity and because it increases the difficulty in interpreting NDT inspection results. The test models identified in tables V and VI are intended to provide data on the effects of bond coating on thermal performance, char retention strength, and filler bond strength.

Voids.- Voids are a common defect in honeycomb ablators that can occur if packing is improperly performed. Although the most common occurrence will be near the face sheet, they can occur in depth throughout the thickness. Thus, large voids (25% of cell volume) in all cells were located at various depths within the

---

\* Chandler, Huel H.: Earth Entry Ablative Heat Shield. R-70-48669-008, June 1971.

TABLE V.- PLASMA ARC SPECIMEN DATA

Model no.	Billet no.	Material Variation	Model size				Density		Nominal test heat flux	
			Thickness		Diameter		lb/ft <sup>3</sup>	kg/m <sup>3</sup>	Btu/ft <sup>2</sup> -s	MW/m <sup>2</sup>
			in.	cm	in.	cm				
19S-1	19	Uniform density	2	5.08	4.984	12.66	16.3	261.1	23	0.261
19S-2	19	Uniform density	2.062	5.24	5.0	12.70	16.3	261.1	23	0.261
19S-3	19	Uniform density	2	5.08	5.0	12.70	16.3	261.1	23	0.261
19S-4	19	Uniform density	2	5.08	5.016	12.74	16.3	261.1	55	0.624
19S-5	19	Uniform density	2	5.08	5.016	12.74	16.3	261.1	55	0.624
19S-6	19	Uniform density	2	5.08	4.984	12.66	16.3	261.1	55	0.624
4B-1	4	Phenolic bond coating	2	5.08	5.0	12.70	16.4	270.7	23	0.261
4B-2	4	Phenolic bond coating	2	5.08	4.984	12.66	16.4	270.7	23	0.261
4B-3	4	Phenolic bond coating	2	5.08	5.016	12.74	16.4	270.7	23	0.261
4B-4	4	Phenolic bond coating	2	5.08	5.0	12.70	16.4	270.7	55	0.624
4B-5	4	Phenolic bond coating	2	5.08	5.016	12.74	16.4	270.7	55	0.624
4B-6	4	Phenolic bond coating	2	5.08	4.984	12.66	16.4	270.7	55	0.624
5B-7	5	Silicone bond coating	2	5.08	5.0	12.70	16.1	257.9	23	0.261
5B-8	5	Silicone bond coating	-	-	-	-	-	-	-	-
5B-9	5	Silicone bond coating	2	5.08	5.0	12.70	16.1	257.9	23	0.261
5B-10	5	Silicone bond coating	2	5.08	5.0	12.70	16.1	257.9	55	0.624
5B-11	5	Silicone bond coating	2	5.08	5.0	12.70	16.1	257.9	55	0.624
5B-12	5	Silicone bond coating	2	5.08	5.0	12.70	16.1	257.9	55	0.624
6B-13	6	No bond coating	2	5.08	4.969	12.62	16.2	259.5	23	0.261
6B-14	6	No bond coating	2	5.08	4.969	12.62	16.2	259.5	23	0.261
6B-15	6	No bond coating	2	5.08	4.984	12.62	16.2	259.5	23	0.261
6B-16	6	No bond coating	2	5.08	4.969	12.62	16.2	259.5	55	0.624
6B-17	6	No bond coating	2	5.08	4.969	12.62	16.2	259.5	55	0.624
6B-18	6	No bond coating	2	5.08	4.984	12.66	16.2	259.5	55	0.624
10D-1	10	High density	2	5.08	5.0	12.70	17.3	277.1	23	0.261
10D-2	10	High density	2	5.08	4.922	12.50	17.3	277.1	23	0.261
10D-3	10	High density	2	5.08	5.0	12.70	17.3	277.1	23	0.261
10D-4	10	High density	2	5.08	5.0	12.70	17.3	277.1	55	0.624
10D-5	10	High density	2	5.08	5.0	12.70	17.3	277.1	55	0.624
10D-6	10	High density	2.062	5.24	4.969	12.62	17.3	277.1	55	0.624
11D-7	11	Control density	2	5.08	5.0	12.70	16.1	257.9	23	0.261
11D-8	11	Control density	2	5.08	4.953	12.58	16.1	257.9	23	0.261
11D-9	11	Control density	2	5.08	4.969	12.62	16.2	257.9	23	0.261
11D-10	11	Control density	2	5.08	5.0	12.70	16.1	257.9	55	0.624
11D-11	11	Control density	2	5.08	4.984	12.66	16.1	257.9	55	0.624
11D-12	11	Control density	2	5.08	4.984	12.66	16.1	257.9	55	0.624
12D-13	12	Low density	2	5.08	4.984	12.66	15.0	240.3	23	0.261
12D-14	12	Low density	2	5.08	5.0	12.70	15.0	240.3	23	0.261
12D-15	12	Low density	2	5.08	5.0	12.70	15.0	240.3	23	0.261
12D-16	12	Low density	2	5.08	5.0	12.70	15.0	240.3	55	0.624
12D-17	12	Low density	2	5.08	5.016	12.74	15.0	240.3	55	0.624
12D-18	12	Low density	2.062	5.24	5.016	12.74	15.0	240.3	55	0.624
1V-1	1	Voids location A	2	5.08	5.016	12.74	15.8	253.1	23	0.261
1V-2	1	Voids location A	2	5.08	5.016	12.74	15.8	253.1	23	0.261
1V-3	1	Voids location A	2	5.08	5.016	12.74	15.8	253.1	23	0.261
2V-10	2	Voids location A	2	5.08	5.016	12.74	16.4	262.7	55	0.624
2V-11	2	Voids location A	2	5.08	5.016	12.74	16.4	262.7	55	0.624
2V-12	2	Voids location A	2	5.08	5.0	12.70	16.4	262.7	55	0.624
1V-4	1	Voids location B	2	5.08	5.0	12.70	15.8	253.1	23	0.261
1V-5	1	Voids location B	2	5.08	5.0	12.70	15.8	253.1	23	0.261
1V-6	1	Voids location B	2	5.08	5.016	12.74	15.8	253.1	23	0.261
2V-13	2	Voids location B	2	5.08	5.016	12.74	16.4	262.7	55	0.624
2V-14	2	Voids location B	2	5.08	5.016	12.74	16.4	262.7	55	0.624
2V-15	2	Voids location B	2	5.08	5.016	12.74	16.4	262.7	55	0.624
1V-7	1	Voids location C	2	5.08	5.016	12.74	15.8	253.1	23	0.261
1V-8	1	Voids location C	2	5.08	5.0	12.70	15.8	253.1	23	0.261
1V-9	1	Voids location C	2	5.08	5.0	12.70	15.8	253.1	23	0.261
2V-16	2	Voids location C	2	5.08	5.016	12.74	16.4	262.7	55	0.624
2V-17	2	Voids location C	2	5.08	5.016	12.74	16.4	262.7	55	0.624
2V-18	2	Voids location C	2	5.08	5.0	12.70	16.4	262.7	55	0.624
15H-1	15	3/4-in. (1.91 cm) core	2	5.08	5.0	12.70	17.0	272.3	23	0.261
15H-2	15	3/4-in. (1.91 cm) core	2	5.08	5.0	12.70	17.0	272.3	23	0.261
15H-3	15	3/4-in. (1.91 cm) core	2	5.08	4.953	12.58	17.0	272.3	23	0.261
15H-4	15	1-1/8-in. (2.85 cm) core	2	5.08	4.984	12.66	17.0	272.3	23	0.261
15H-5	15	1-1/8-in. (2.85 cm) core	2	5.08	5.0	12.70	17.0	272.3	23	0.261
15H-6	15	1-1/8-in. (2.85 cm) core	2	5.08	5.0	12.70	17.0	272.3	23	0.261
16C-1	16	Altered cure	1.938	4.92	5.0	12.70	16.5	264.3	23	0.261
16C-2	16	Altered cure	2	5.08	5.0	12.70	16.5	264.3	23	0.261
16C-3	16	Altered cure	2	5.08	5.016	12.74	16.5	264.3	23	0.261

Note: For void location see Figure VII-1.

TABLE VI.- TENSILE SPECIMEN DATA

Model no.	Billet no.	Material variation	Density		Test temperature	
			lb/ft <sup>3</sup>	kg/m <sup>3</sup>	°F	K
B101-B105	7	Phenolic bond coating	16.3	261.0	76	298
B106-B110	7	Phenolic bond coating	16.3	261.0	-150	172
B111-B115	7	Phenolic bond coating	16.3	261.0	300	422
B116-B120	8	Silicone bond coating	16.2	259.5	76	298
B121-B125	8	Silicone bond coating	16.2	259.5	-150	172
B126-B130	8	Silicone bond coating	16.2	259.5	300	422
B131-B135	9	No bond coating	16.5	264.2	76	298
B136-B140	9	No bond coating	16.5	264.0	-150	172
B141-B145	9	No bond coating	16.5	264.0	300	422
D101-D105	13	High density	14.8	237.0	76	298
D106-D110	14	Low density	17.2	275.0	76	298
C106-C105	17	Altered cure	16.3	261.0	76	298
F101-F105	18	No fibers	15.3	245.0	76	298
S101-S105	20	Control	15.9	254.5	76	298
S106-S110	20	Control	15.9	254.5	-150	172
S111-S115	20	Control	15.9	254.5	300	422
S116-S120	21	No core	14.2	227.0	76	298
S121-S125	21	No core	14.2	227.0	-150	172
S126-S130	21	No core	14.2	227.0	300	422



specimen, as shown in figure 21, to evaluate their effect on char stability and thermal efficiency.

Crushed core.- A major defect associated with the impact filling operations was core crushing. This was caused by both accidental impacting of the core while filling, and by the highly localized application of pressures that split node bonds and cell walls. An evaluation was conducted to determine the degree of char support provided by the core.

Formulation.- The fibers were omitted as a constituent to determine the effect of fibers on the filler-to-honeycomb bond strength.

State-of-cure.- The cure cycle is known to affect mechanical properties and may affect both the degree of bonding with the core and the thermal properties. As an alternative to the Martin Marietta process, a lower temperature longer time cure similar to the Langley process was investigated to determine the effect of cure cycle variations on char strength and thermal performance. The investigation included studies to determine:

- 1) The effect of undercut core on char layer retention;
- 2) The effect of broken or missing cell walls on char retention;
- 3) The effect of large fiber bundles on char integrity;
- 4) The effect of local unbonds around an attachment point on ablative layer attachment strength;
- 5) The effect of local delaminations around an attachment point on ablative layer bond strength.

These defects were selected based on their frequency of occurrence during fabrication, and their anticipated effects on critical properties as defined in Task I.

## Process

The baseline process incorporated information from recently concluded NASA low-cost ablative heat shield fabrication studies and in-house efforts to reduce fabrication costs. The material specifications and fabrication processes are described in the following subsections.

Material specification.- All materials used were certified for compliance with manufacturers' published properties. The following materials were used:

- 1) Silicone resin (Sylgard 182, Dow-Corning);
- 2) Curing agent (Sylgard 182, Dow-Corning);
- 3) Refrasil glass fibers (F100 A-25, Hitco);

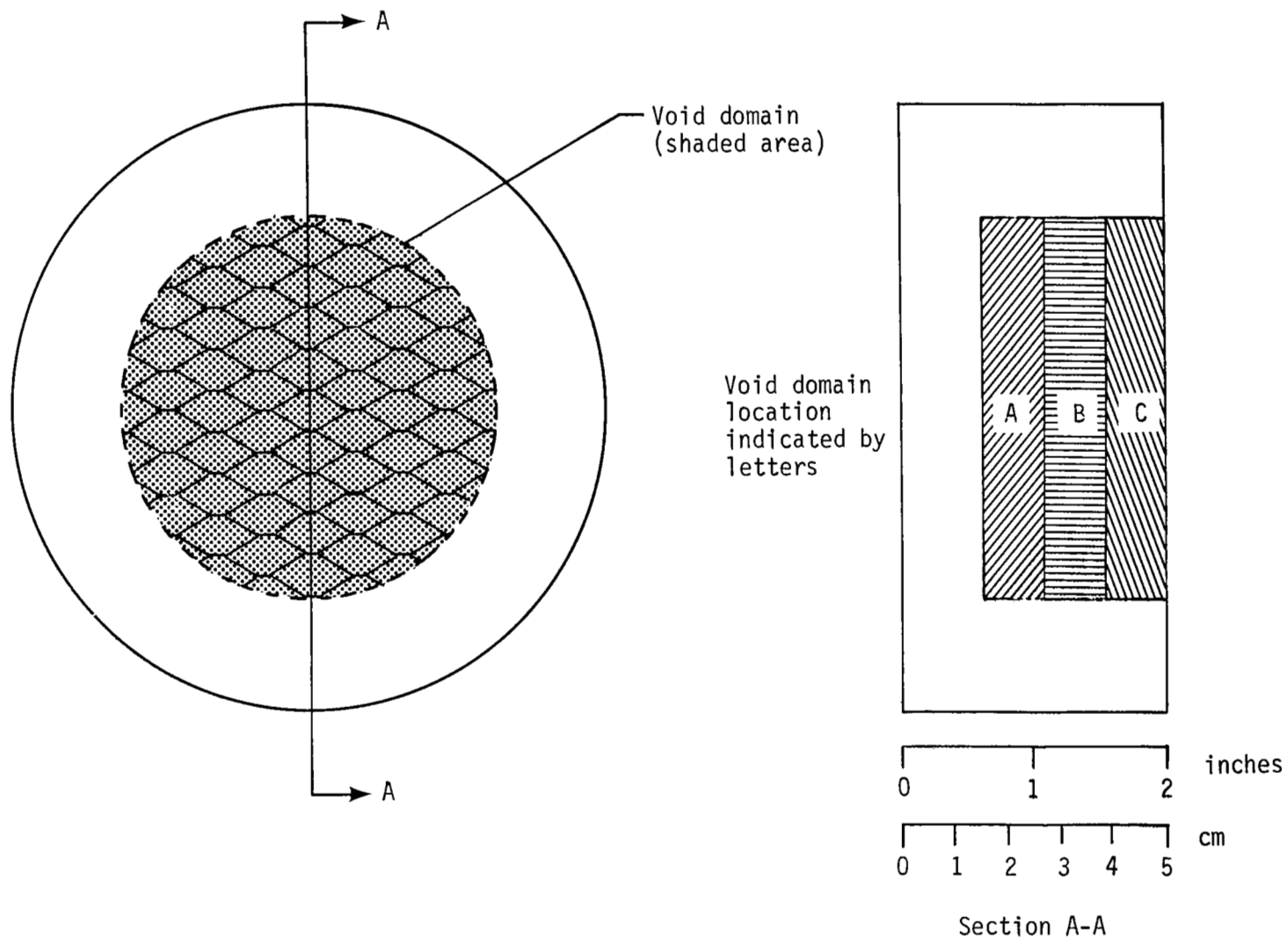


Figure 21.- Void Specimen Design

- 4) Phenolic Microballoons (BJO-0930, Union Carbide);
- 5) Glass-phenolic honeycomb (HRP 3/8-GF11-2.2, Hexcel Products Co.);
- 6) Epoxy glass prepreg cloth (181 glass fabric, Coast Manufacturing and Supply Division of Hexcel Products Co.);
- 7) Phenolic resin (SC1008, Monsanto).

The following formulation was used:

- 1) Silicone resin, 22.8% (by weight);
- 2) Silicone curing agent, 2.2%;
- 3) Refrasil fibers, 4.0%;
- 4) Phenolic Microballoons, 71.0%.

The nominal density of the ablative material MG-36 is  $17 \begin{smallmatrix} +0 \\ -2 \end{smallmatrix} \text{ lb/ft}^3$  ( $272 \begin{smallmatrix} +0 \\ -32 \end{smallmatrix} \text{ kg/m}^3$ ).

#### Fabrication process.-

Core and face sheet preparation: The glass/phenolic honeycomb was cut to the desired billet size and then vapor-degreased. The honeycomb to be used for the plasma arc specimens defined in table VII, with the exception of billets 1, 2, 3 and 19, was then bonded to a 2-ply glass/epoxy 181 backup sheet. This was accomplished by laying up two layers of prepreg cloth, crossplied at 90°, then primary bonding to the honeycomb using a vacuum bag. Relief holes with a 0.063-inch (0.16-cm) diameter were drilled through the laminate face into each honeycomb cell.

The glass face sheet was not bonded to the honeycomb for billets 1, 2, 3, and 19 because of the techniques employed to create voids and uniform density. Likewise, face sheets were not bonded to the honeycomb of the tensile specimen billets defined in table VII.

Core bond coat: The baseline process used the Monsanto SC1008 phenolic resin. The adhesive coat was applied to the honeycomb and face sheet by dip coating. The dip solution contained 50% ethyl alcohol. The excess resin was removed by inverting the assembly "face sheet up" and allowing it to drain on absorbent towels for 10 minutes. The core/face sheet assembly was then placed in an air circulating oven and B-staged at 120°F (322K) for 2 hours.

Mixing: Phenolic microsphere agglomerates were removed using a No. 30 grid sieve after which the fines were vacuum-dried 24 hours at 150° ± 10°F (356 ± 5.5K). Sylgard 182 resin and catalyst were weighed and mixed. Refrasil glass fibers were then weighed and mixed in a small planetary mixer with the Sylgard resin until satisfactory dispersion was obtained. The microspheres were then added and mixed 45 minutes.

TABLE VII.- BILLET FABRICATION DATA

Billet	Billet size		Honeycomb bond coat	Type of test	No. of Specimens
	in.xin.xin.	cmxcmxcm			
1	18x16x2	45.7x40.6x5.1	Phenolic	Plasma arc	9
2	18x16x2	45.7x40.6x5.1	Phenolic	Plasma arc	9
3	18x16x2	45.7x40.6x5.1	Phenolic	Plasma arc	-
4	16x12x2	40.6x30.5x5.1	Phenolic	Plasma arc	6
5	16x12x2	40.6x30.5x5.1	Silicone	Plasma arc	6
6	16x12x2	40.6x30.5x5.1	None	Plasma arc	6
7	16x16x1	40.6x40.6x2.5	Phenolic	Tensile	15
8	16x16x1	40.6x40.6x2.5	Silicone	Tensile	15
9	16x16x1	40.6x40.6x2.5	None	Tensile	15
10	16x12x2	40.6x30.5x5.1	Phenolic	Plasma arc	6
11	16x12x2	40.6x30.5x5.1	Phenolic	Plasma arc	6
12	16x12x2	40.6x30.5x5.1	Phenolic	Plasma arc	6
13	16x16x1	40.6x40.6x2.5	Phenolic	Tensile	5
14	16x16x1	40.6x40.6x2.5	Phenolic	Tensile	5
15	16x12x2	40.6x30.5x5.1	Phenolic	Plasma arc	6
16	16x6x2	40.6x15.3x5.1	Phenolic	Plasma arc	3
17	10x10x1	25.4x25.4x2.5	Phenolic	Tensile	5
18	10x10x1	25.4x25.4x2.5	Phenolic	Tensile	5
19	16x12x2	40.6x30.5x5.1	Phenolic	Plasma arc	6
20	16x16x1	40.6x40.6x2.5	Phenolic	Tensile	15
21	16x16x1	40.6x40.6x2.5	No core	Tensile	15
1A	16x8x2	40.6x20.3x5.1	Phenolic	Environmental	1
1B	16x8x2	20.6x20.3x5.1	Phenolic	Environmental	1

Density control and panel uniformity: The procedure used to control billet densities was to calculate the required amount of material based on mold volume and the desired panel density. The mold thickness was increased by 0.5 inch (1.27 cm) to provide a head or cushion of ablative material above the core to minimize localized surface distortion and damage to core bonds and walls. The core and face sheet assembly was weighed and subtracted from the total panel weight to give the ablative material weight. A thin sheet of plastic film was placed over the core and a picture frame placed over this assembly. Then 40% of the total ablative weight was placed in the frame and spread evenly over the panel. The film was removed, relasing the mixture into the core. The material was pressed into the core by hand. The process was repeated using 20% of the total ablative weight. This represented about all of the material that could be pressed by hand into the core. The two steps were found necessary to prevent cross movements of the ablative material when pressing by hand. The remaining 40% was loaded into the picture frame and spread evenly and the assembly vacuum bagged and evacuated. This remaining material was then impacted into the core to a final head height of 0.5 inch (1.27 cm) above the core.

A third step was added to verify panel uniformity by placing the packed panel in an autoclave and slowly pressurizing to 50 psi (344.5 kN/m<sup>2</sup>). If any cells were not completely filled, the material would move into these areas leaving a depression in the excess material placed on top of the panels. When this occurred, the bag was opened and the material smoothed out and the operation repeated.

Material cure: The assembly was cured at  $250 \pm 10^{\circ}\text{F}$  ( $394 \pm 5.5\text{K}$ ) for  $16 \pm 0.5$  hours under vacuum bag pressure.

## Material Billets

Billet size and fabrication was planned so all specimens of a given type for a given defect could be cut from a single billet. In total, 21 material billets were fabricated, ranging from 18x16x2 inches (45.8x40.6x5.1 cm) to 10x10x1 inches (25.4x25.4x2.54 cm).

Table VII identifies these billets, their size, the defects contained, and the identification of specimens cut from each billet. The following number-letter coding system was used to identify specimens and their included defects. The first digit or digits designated the material billet from which the specimen was obtained. A letter was then used to identify the defect simulated:

D - Density (bulk) variations;

B - Bond coat;

V - Voids;

H - Honeycomb cell size;

C - Cure cycle variation;

F - Fibers omitted;

S - Standard with uniform density.

The remaining digits then identified the individual test specimens within each of the above defect categories studied. Accordingly, density specimens were numbered 10D-1 to 10D-6, 11D-7 to 11D-12, 12D-13 to 12D-18 for the 18 specimens tested to evaluate the impact of bulk density change on thermal insulation.

Void billets.- The face sheet was omitted from billets 1, 2, and 3 because voids were simulated by removing cell material from the back surface side of each specimen. This was done by using a 0.375-inch (0.953 cm) drill. The diameter was selected to remove all cell material without damaging the core. The material remaining in the corner fillet was not removed because it was much easier to back-fill with circular rods of ablative material than to match variations in cell shape. Void location was controlled by setting up stops on a drill press. Ablative material rods were cut to the required length and pressed into the individual cells by hand. Figure 21 showed the void pattern, which approximated a 3.0-inch (7.65-m) diameter void domain. After placement of voids, face sheets were bonded to each specimen and instrumented as shown in figure 22.

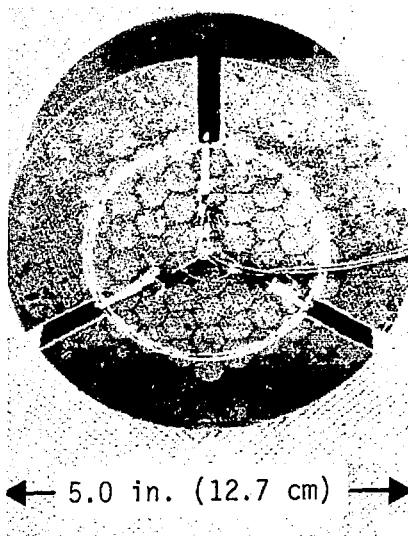


Figure 22.- Ablative Test Specimen Showing Thermocouple Installation

Bond coat billets.- Six billets numbered 4 through 9 were fabricated to investigate bond coat effects. All billets were packed for a nominal density of 16 lb/ft<sup>3</sup> (256 kg/m<sup>3</sup>). The bond coat was applied by dip-coating billets 4 and 7 in a 50/50 solution of SC1008 phenolic resin and ethyl alcohol. Billets 5 and 8 were sprayed with a 50/50 solution of DC-182 silicone resin and heptane; and billets 6 and 9 did not receive any precoat or primer. Billets 4, 5, and 6 were machined into 18 plasma arc specimens and 45 tensile coupons were obtained from billets 7, 8, and 9.

Bulk density variation billets.- The density billets 10 through 14 were obtained by varying the ablative loaded into the defined mold volume. A nominal density range of 14.5 to 17.5 lb/ft<sup>3</sup> (232 to 280 kg/m<sup>3</sup>) was attempted, with actual densities running 14.8 to 17.3 lb/ft<sup>3</sup> (237 to 277 kg/m<sup>3</sup>).

Honeycomb core size billet.- The effect of honeycomb core size on char retention was simulated by removing segments of core ribbons from billet 15 as shown in figure 23. In this way, cell size was enlarged from 0.375 inch (0.952 cm) to 0.75 inch (1.9 cm) and 1.125 inch (2.85 cm).

Cure cycle variation billets.- Billets 16 and 17 were cured according to the cure cycle described here. The part was encapsulated in a vacuum bag at 24 inches of Hg (81 kN/m<sup>2</sup>) and the oven controls were set to operate the oven at 160°F (344K) for 16 hours. The part was held at the reduced pressure level for one hour after the oven temperature had reached its operating level. The pressure within the molding chamber was then allowed to return to atmospheric pressure for the remainder of the cure cycle.

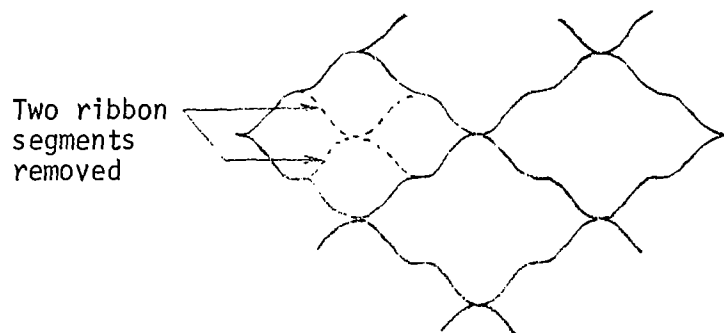
The billets were then postcured at 212°F (373K) for eight hours. Upon completion of the cure cycle, the panels were allowed to cool to approximately 100°F (311K) prior to removal from the oven. At the completion of cure, the mold assembly was opened and the material above the honeycomb was found to have delaminated at the core interface, as shown in figure 24. This delamination could have occurred at the time vacuum was removed and was not considered sufficient cause for panel rejection.

Billets with fibers omitted.- Fibers were removed from the formulation for the layup of billet 18. Thus the formulation became:

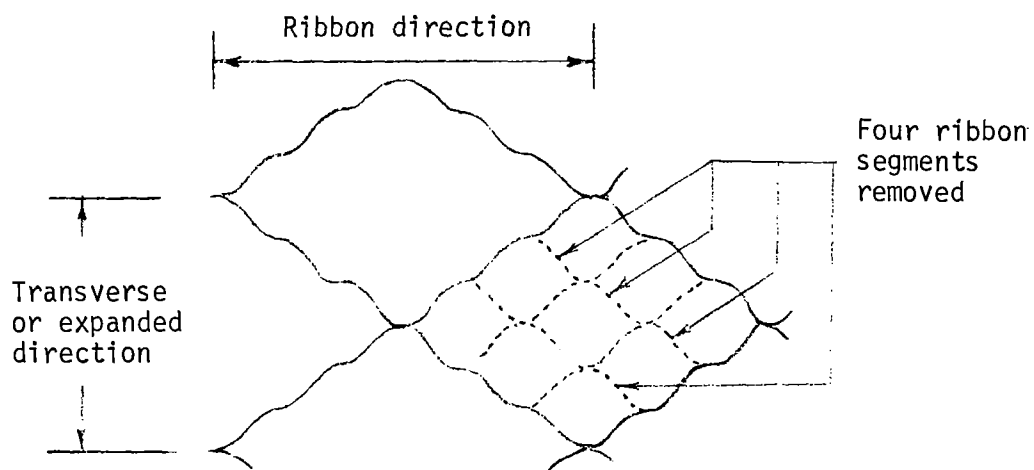
- 1) Sylgard 182 resin, 23.7% (by weight);
- 2) Sylgard 182 curing agent, 2.3%;
- 3) Phenolic microspheres, 74.0%.

Standard billet with uniform density.- Billet 19 was prepared without a face sheet and the ablative material was loaded into the core from both sides. This was accomplished by first loading as before, including bagging and vibrating the assembly. However, the ablative material was not fully compacted from this side. Instead it was compacted to a depth above the core of 0.75 inch (1.9 cm) and then the excess material was carefully removed into a container and the billet was inverted. This was done by sandwiching it between two mold plates and rotating the assembly 180°. The original mold base was then removed and the ablative material respread over the original bottom surface. This procedure produced a uniform density through the billet as shown in figure 25.

Billets 20 and 21 were prepared for tensile specimens with and without honeycomb core.



3/4-in. (1.91-cm) honeycomb



1-1/8-in. (2.86-cm) honeycomb

Figure 23.- Large Honeycomb



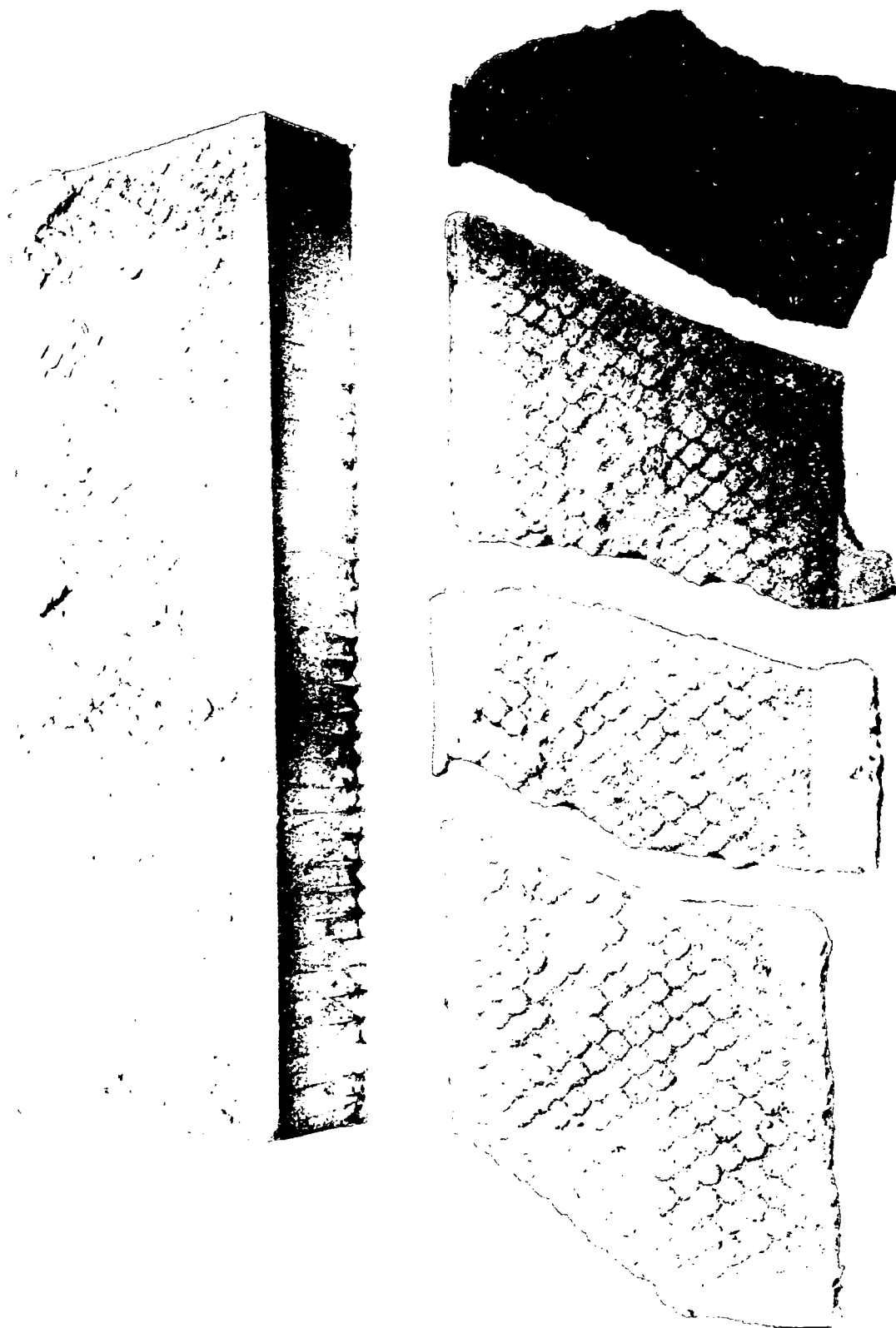


Figure 24.- Altered-Cure Billet 17

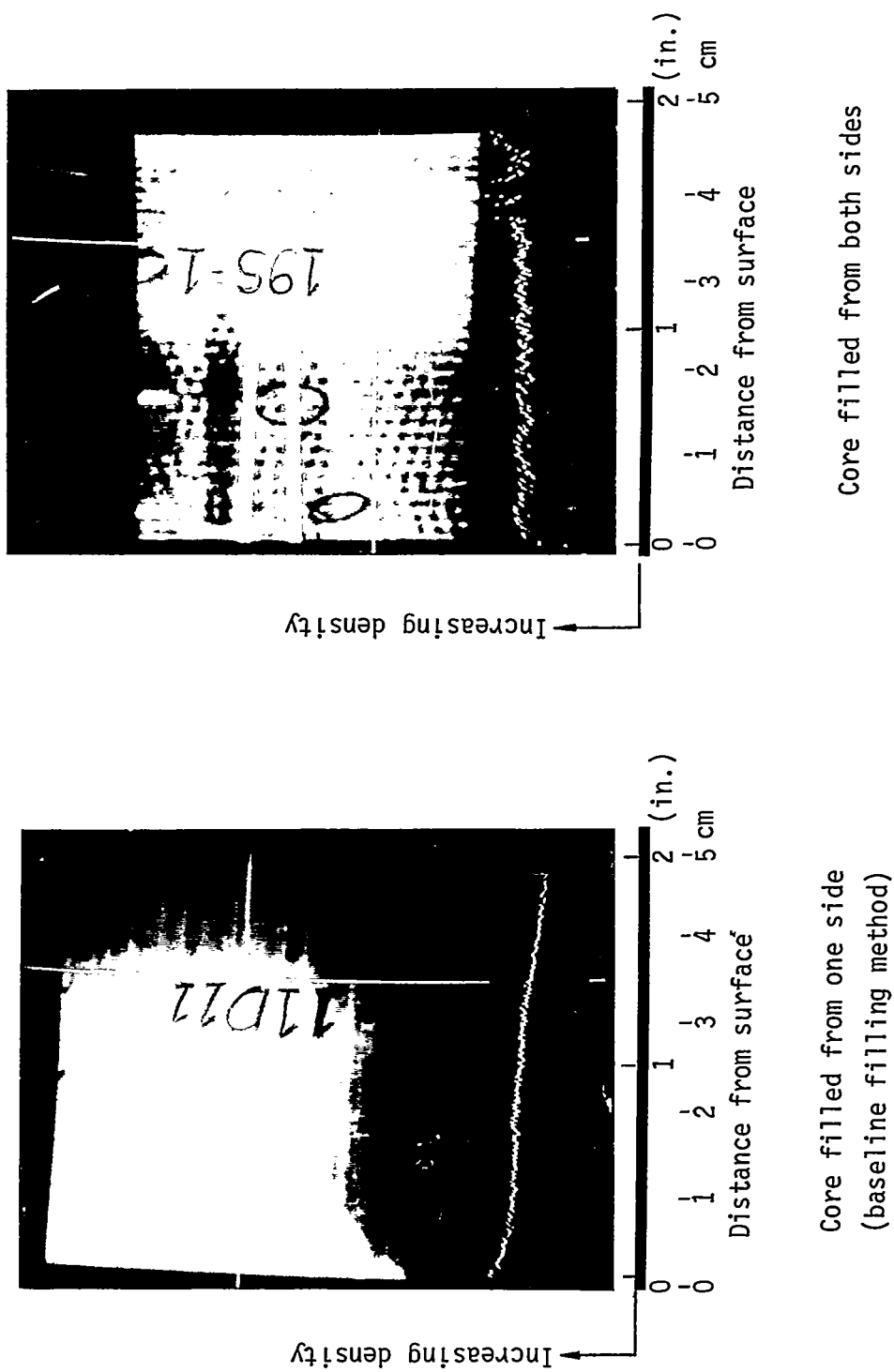


Figure 25.- Relative Radiographic Density vs Packing Method

## Test Specimens

Test specimens of each defect studied were obtained from a single billet. These billets were sized according to the number of specimens required for each defect studied. This approach not only conserved fabrication time, but also minimized data scatter due to slight variations in density, cure, and process variables.

Plasma arc splash specimens.— Data for individual specimens are tabulated in table VI. The screening tests indicated side heating to be a major problem with specimen diameters of 4.0 inches (10.15 cm) at the proposed conditions and test times. As a result, several model diameters were tested during this phase and the decision to test 5.0-inch (12.7 cm) diameter models was made based on side heating considerations. It was also learned during these early tests that thermal chemical recession of the char was not a problem, even at a heating rate of 60 Btu/ft<sup>2</sup>-s (0.68 MW/m<sup>2</sup>). Hence the selection of a recession-compatible material to use for wrapping specimen edges was not a factor. The use of two layers of resin-soaked glass cloth No. 181 provided adequate filler support at specimen edges. The specimen design shown in figure 26 resulted from these design studies.

The MG-36 ablative material specimens were machined from large billets in the form of 5.0-inch (10.15-m) diameter, 2.0-inch (5.08-cm) thick flat-faced cylinders. The specimens were instrumented with thermocouples to monitor the internal temperature. Thermocouple wire was 30-gage chromel-alumel and was covered with double-hole alumina tubing to electrically insulate the thermocouple leads from the ablative material char layer. All alumina tubing junctions were covered with Al<sub>2</sub>O<sub>3</sub> paste. Thermocouples were run out parallel to the heated surface to minimize the conduction error. The thermocouples were installed by machining slots in the specimen sides 1.0-inch (2.54-cm) deep by 0.25-inch (0.635-cm) wide from the back surface to the desired thermocouple depth. The placement pattern was in 60° intervals around the specimen center. Figure 22 shows the installation of thermocouples in specimen 2V-18.

A cut in the face sheet was made to isolate the center 3.0-inch (7.62-cm) instrumented core from such edge effects as contact with the base holder, etc. A thermocouple was attached to a copper disc that was bonded to the specimen back surface to obtain an average temperature measurement. This disc was 0.5 inch (1.27 cm) in diameter by 0.031-inch (0.079-cm) thick and was bonded at the center of the face sheet. A mounting ring of asbestos phenolic was bonded to the back surface of each specimen. An aluminum holder was mechanically fastened to the mounting ring for positioning the specimen on the inserter arm. Sixty-eight specimens were tested; one was damaged during fabrication. Twenty-three specimens contained four thermocouples each.

Tensile.— Tensile test specimens were fabricated to evaluate several parameters. Test specimens with honeycomb core were fabricated in accordance with figure 27. Billet number 21, which had no core, was machined as shown in figure 28.

Black and white optical targets were bonded onto each specimen for Optron tracking. These were bonded with Dow Corning 732 silicone to give a 2.0-inch (5.08-m) gage length.

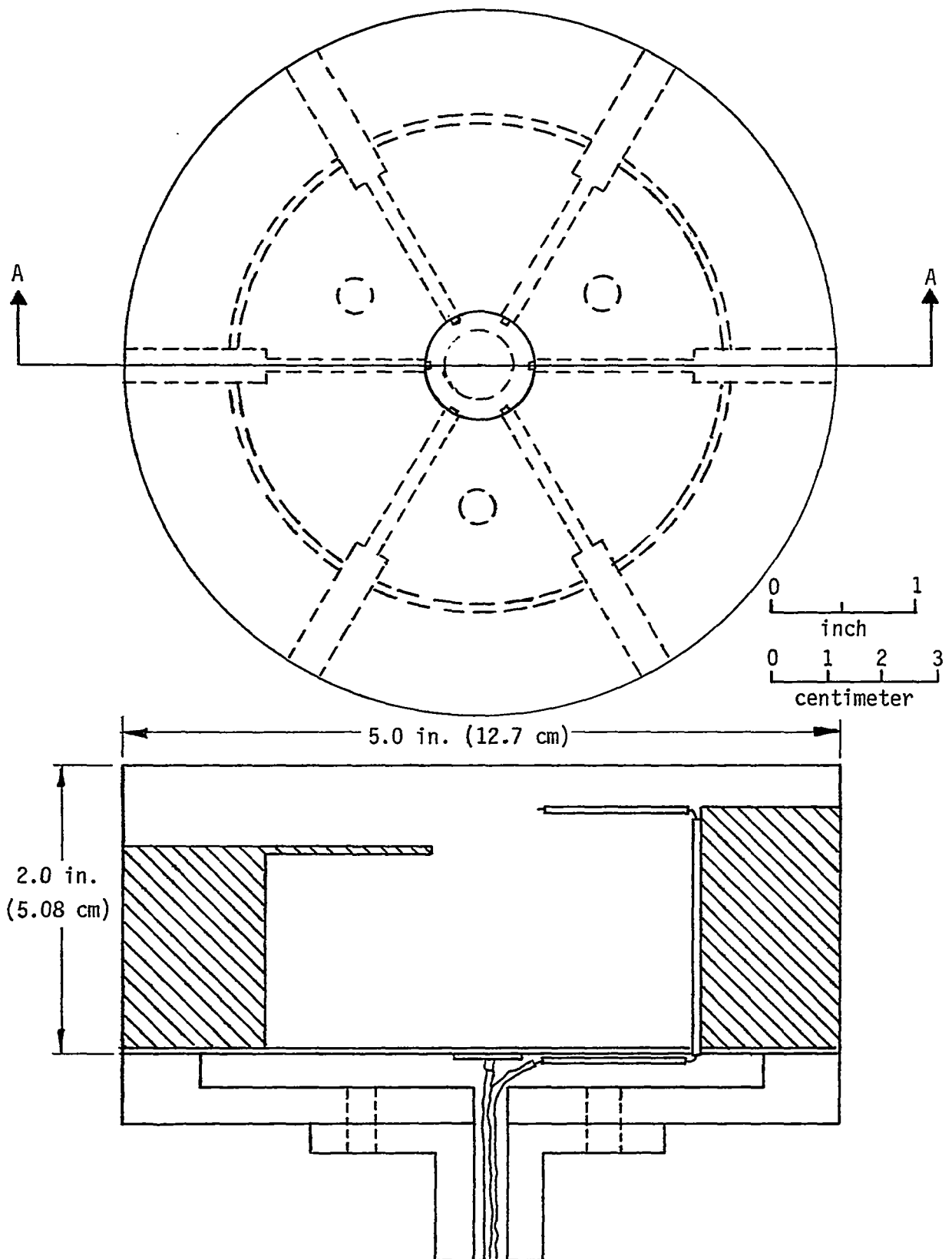


Figure 26.- Plasma Arc Test Specimen Design

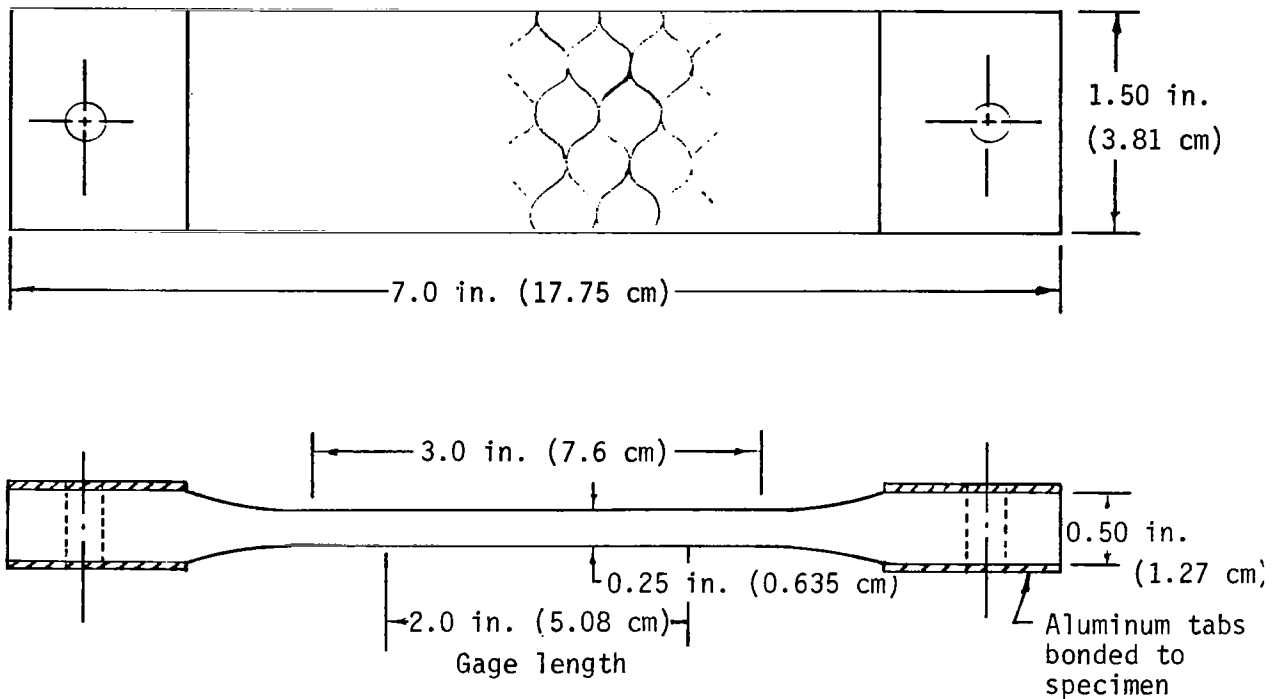


Figure 27.- Tensile Specimen, Ablator in Honeycomb

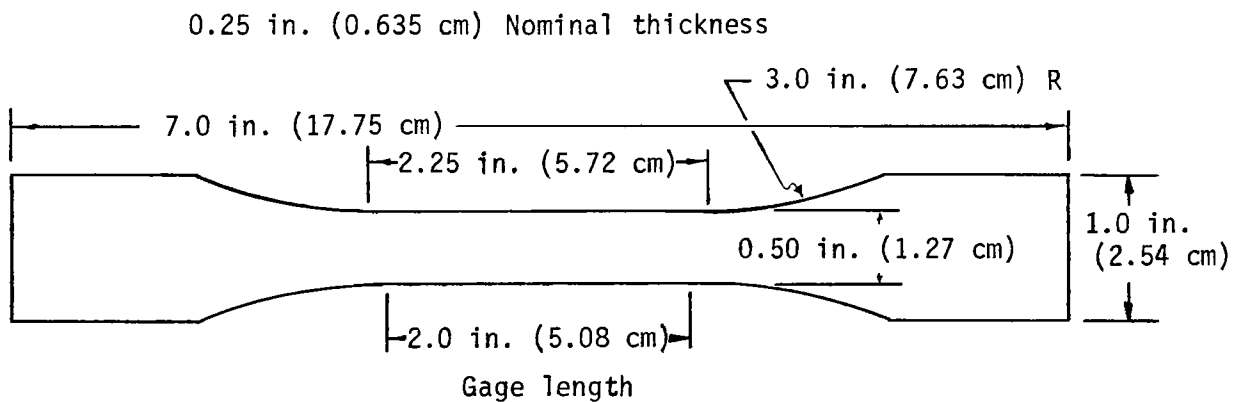


Figure 28.- Tensile Specimen, Ablator

Ablative panels.— Two 8x16x2-inch (20.3x40.6x5.08-cm) flat panels were fabricated to evaluate the effect of several environments. One panel had built-in defects as shown in figure 29. The second panel served as a control. Each panel contained four attachment points located near the corners. Attachment stud diameter was 0.25 inch (0.635 cm) and access was through removable ablator plugs that were 0.75 inch (1.91 cm) in diameter.

Thermocouples were installed on the front and back surface for the hot and cold soak exposure testing. Figure 30 shows the locations of these thermocouples.

The ablative test required reinstrumentation with 30-gage chromel-alumel thermocouples located  $\frac{1}{4}$  and 1 inch (0.635 and 2.54 cm) from the front face and at the back face. Thermocouple locations are shown in figure 31.

## TEST APPARATUS AND PROCEDURES

Three basic tests were selected to evaluate the MG-36 ablative material's performance under expected Space Shuttle environmental conditions during reentry. These tests -- plasma arc ablation performance, tensile property, and large panel environmental response -- were intended to provide quantitative data on the ablative layers' insulation properties, char layer integrity, ultimate strain, elastic modulus, and the overall thermal/mechanical performance of the ablative layer, the glass face sheets, and the attachment points.

### Plasma Arc Tests (Ablation Performance Tests)

Facility description.— Testing was conducted in the 1-megawatt Plasma Arc facility test chamber utilizing an F-5000 Thermal Dynamic arc heater and a 6-inch (15.25-cm) diameter supersonic nozzle. The full facility operating capabilities are defined in SR-1631-71-8.\* This test facility simulates hypervelocity heating during reentry by flowing a compressed gas mixture simulating air through an electric discharge. The gas undergoes a large thermal energy increase and is then expanded through a supersonic nozzle to a Mach number of approximately 3. All ablation performance tests during these investigations were performed by exposing material specimens to this thermal environment.

Test conditions and procedure.— The selection of plasma arc test conditions for these studies was based on a Mark I high-crossrange 1500-nautical-mile Delta wing orbiter.<sup>†</sup> A plot of trajectory parameters is shown in figure 32. Heating rate values are for a 1-foot nose radius and the total heat to the stagnation

---

\* Schmidt, G. J.: Plasma Arc Laboratory. SR-1631-71-8, July 1971.

<sup>†</sup> Andresen, T. L.: Phase B Thermal Environment Predictions for the Fixed Wing, the Mark I Delta, and the Composite Orbiters. McDonnell-Douglas Astronautics Company-East, Design Note No. O-East-Thermo-4, August 1970.

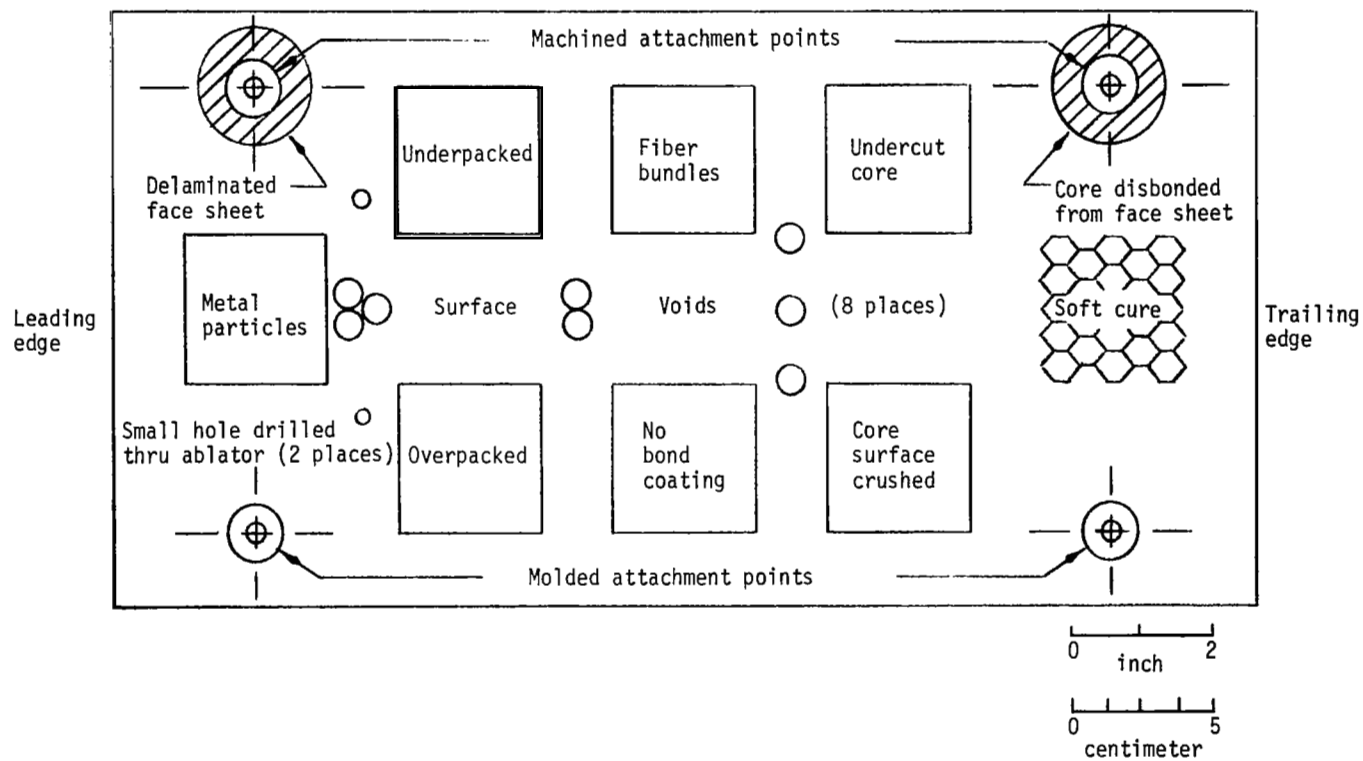


Figure 29.- Large Test Panel, Defect Locations

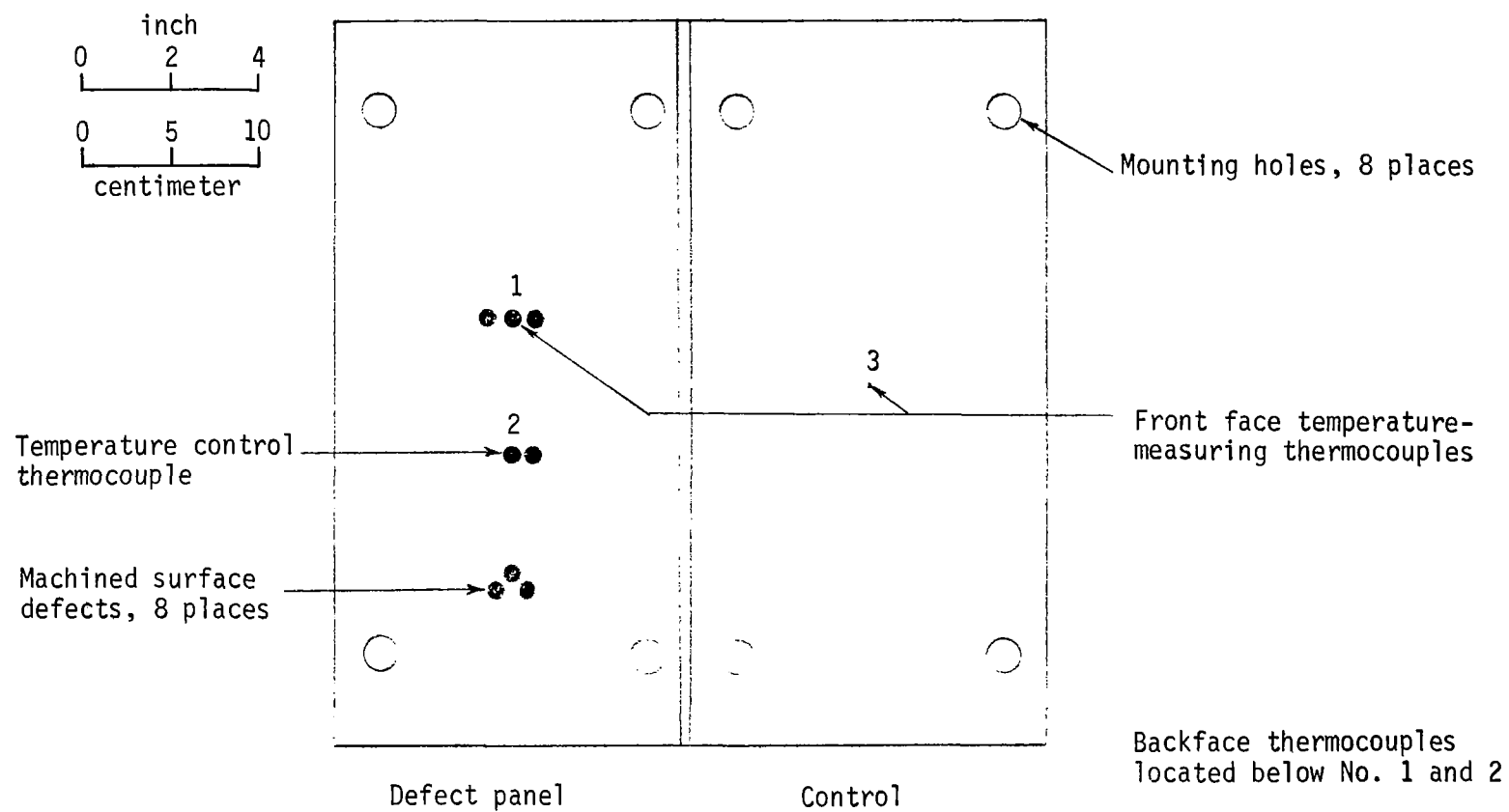
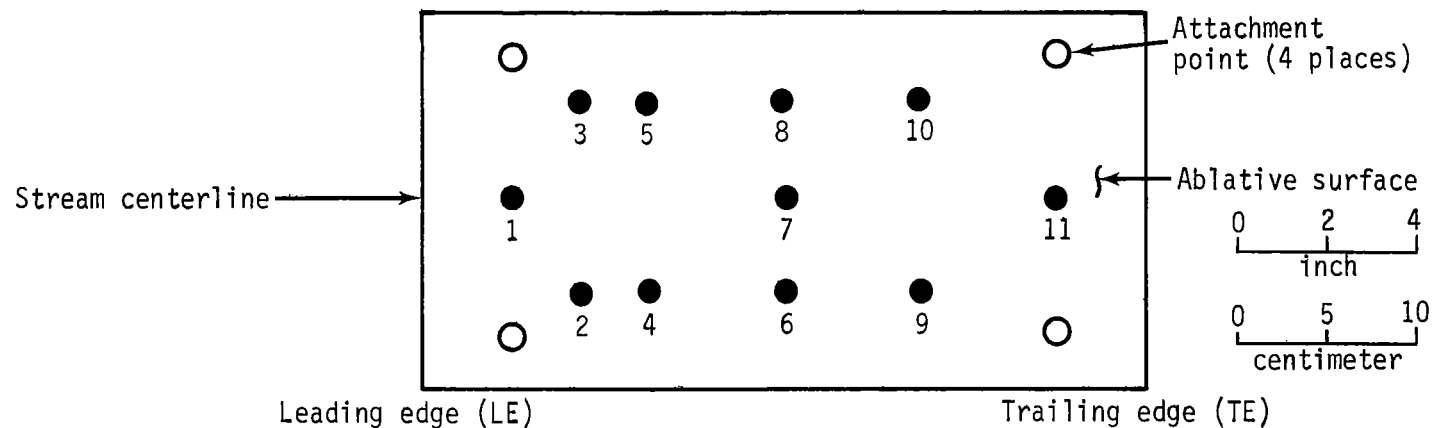


Figure 30.- Large Test Panels, Thermal Vacuum Test Instrumentation





Location no.	Thermocouple no.	Distance from LE		Distance from $\phi$		Distance from ablative surface	
		in.	cm	in.	cm	in.	cm
1	1	2.0	5.07	0	0	2.0	5.07
2	22	3.5	8.89	2.0	5.07	2.0	5.07
3	23	3.5	8.89	2.0	5.07	2.0	5.07
4	10, 11, 2	5.0	12.70	2.0	5.07	0.25, 1.0, 2.0	0.635, 2.54, 5.07
5	12, 13, 3	5.0	12.70	2.0	5.07	0.25, 1.0, 2.0	0.635, 2.54, 5.07
6	14, 15, 4	8.0	20.30	2.0	5.07	0.25, 1.0, 2.0	0.635, 2.54, 5.07
7	5	8.0	20.30	0	0	2.0	5.07
8	16, 17, 6	8.0	20.30	2.0	5.07	0.25, 1.0, 2.0	0.635, 2.54, 5.07
9	18, 19, 7	11.0	27.95	2.0	5.07	0.25, 1.0, 2.0	0.635, 2.54, 5.07
10	20, 21, 8	11.0	27.95	2.0	5.07	0.25, 1.0, 2.0	0.635, 2.54, 5.07
11	9	14.0	35.55	0	0	2.0	5.07

Figure 31.- Ablative Panel Thermocouple Locations

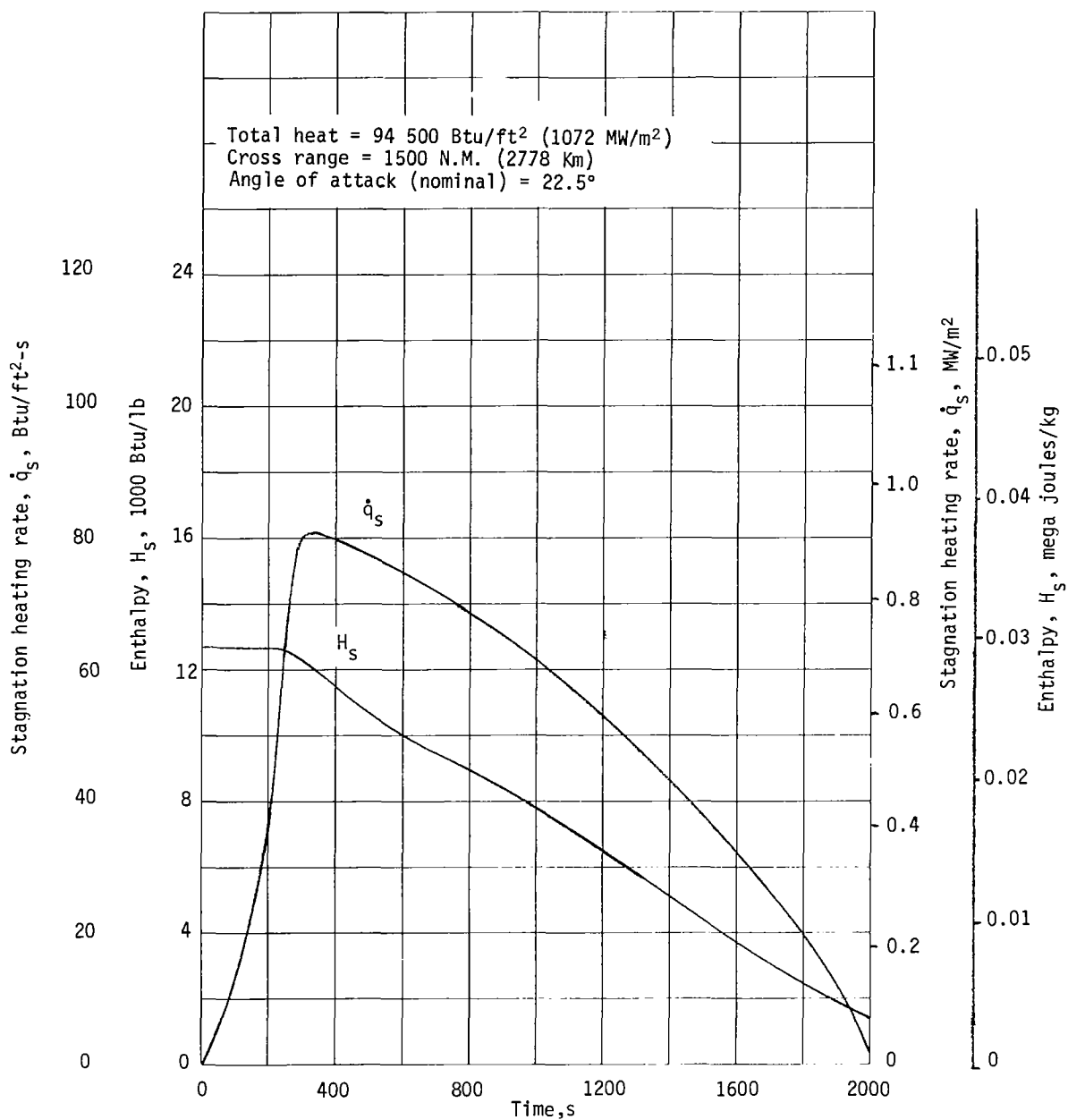


Figure 32.- High Crossrange Mark I Delta Orbiter, Nominal Entry Trajectory

point for this trajectory is approximately 95 000 Btu/ft<sup>2</sup> (1078 MJ/m<sup>2</sup>) for a nominal entry angle of 22.5°. Based on these trajectory values, two test conditions were selected that are representative of heating along the bottom forward (X/L = 0.10) centerline and shoulder areas of the Space Shuttle orbiter.

The two test streams calibrated had enthalpies of 3800 Btu/lb (8.846 MJ/kg) and 6000 Btu/lb (14.9 MJ/kg) at stagnation pressures of 0.0055 atmospheres (55.7 N/m<sup>2</sup>) and 0.0088 atmospheres (89.2 N/m<sup>2</sup>). Measured heating rates of 23 Btu/ft<sup>2</sup>-s (0.261 MW/m<sup>2</sup>) and 55 Btu/ft<sup>2</sup>-s (0.625 MW/m<sup>2</sup>) were determined using a Thermogage Asymptotic Calorimeter mounted in a water-cooled copper holder with the same size and shape as the test specimens to preclude size and shape correction factors. These measurements were determined after the arc jet had been run for a sufficient time to stabilize and several runs were made to determine repeatability from one operation to the next. The calibration body contained four sensing elements located various distances from the model centerline to provide radial distribution over the specimen face. The location of these elements and the measurements made are shown in figure 33 and table VI. Test point stability was checked by taking calorimeter measurements before and after each test series. The total enthalpy was determined from a heat balance test performed on the arc heater-plenum-nozzle system. The pressure at the model's stagnation point (static and dynamic) was measured with the facility pitot probe and surveys across the test stream were made and recorded for each test condition. Nominal values of these test parameters were repeatable within ±5%.

Many of the defects were expected to have a minor effect on the insulation performance of the material, and subtle specimen differences and or test point fluctuations were expected to mask the effect of the incorporated defects. Because of this concern, the following test rationale was adopted. Since at the low heating condition, it was assumed that the test point was "constant," all three replicas of each material variation were run in consecutive order.\* This allowed the data scatter due to potential specimen differences to be determined. At the high test point, the specimens were assumed "constant" and the data scatter due to potential test condition variations between torch operations was evaluated by mixing the specimens of each defect group, i.e., specimens 4B-5, 5B-10, and 6B-18 were run in consecutive order.

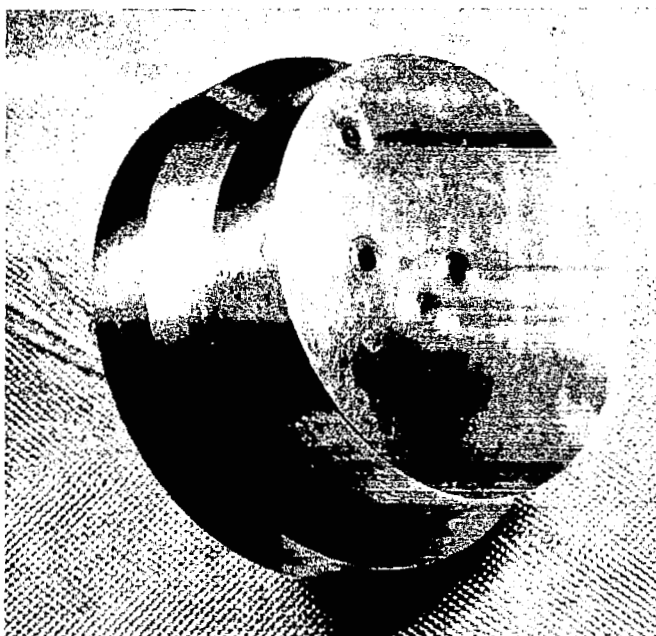
## Tensile Tests

Tensile tests were performed to evaluate strength, elongation, and modulus at three temperatures. The equipment and test conditions were:

- 1) Test machine - Instron universal testing machine;
- 2) Test speed - 0.1 in./minute (0.254 cm/min);

---

\* Since the facility has three positioning arms, three specimens can be tested, one after the other, during one torch operation.



Heat Flux Sensor  
(Typical 4 Places)

Sensor No.	Distance from Stagnation Point	
	in.	cm
1	0	0
2	0.7	1.78
3	1.3	3.31
4	1.9	4.83

Figure 33.- Steady-State Calorimeter

- 3) Temperature conditioning - Custom Scientific environmental chamber,
  - a) Hot + 300°F (422K) - Conditioning box on Instron with electrical heaters,
  - b) Cold - 150°F (172K) - Conditioning box on Instron with liquid N<sub>2</sub> cooling;
- 4) Temperature sensor - thermocouple;
- 5) Extensometer - Optron optical extensometer viewing through window of conditioning box;
- 6) Stress-strain recording - Instron head travel and Optron output recorded on XY recorder.

Figure 34 shows the test setup. Soak time was 10 minutes after reaching the test temperature. Elongation measurements were made within a 2-inch-gage section using the Optron optical system. Test temperatures were -150°F (172K), 75°F (297K), and 300°F (422K). A tolerance of ±10°F (5.6K) was allowed. The test chamber was purged with dry gas (nitrogen or air) at the -150°F (172K) temperature conditions.

### Large Panel Tests

Two large ablative panels were tested to evaluate the overall TPS response to a sequence of Space Shuttle environments. The following defects were included in one of the panels to obtain a relative performance evaluation:

- 1) Filler and core-to-face sheet bonding;
- 2) Attachment strength as affected by local core unbonds and face sheet delaminations;
- 3) Simultaneous evaluation of density, core bond coating, crushed and undercut core, metal inclusions, cure hardness, and fiber bundles.

These panels were exposed to the following environments:

- 1) Acoustic;
- 2) Hot soak under vacuum;
- 3) Cold soak under vacuum;
- 4) Reentry heating.

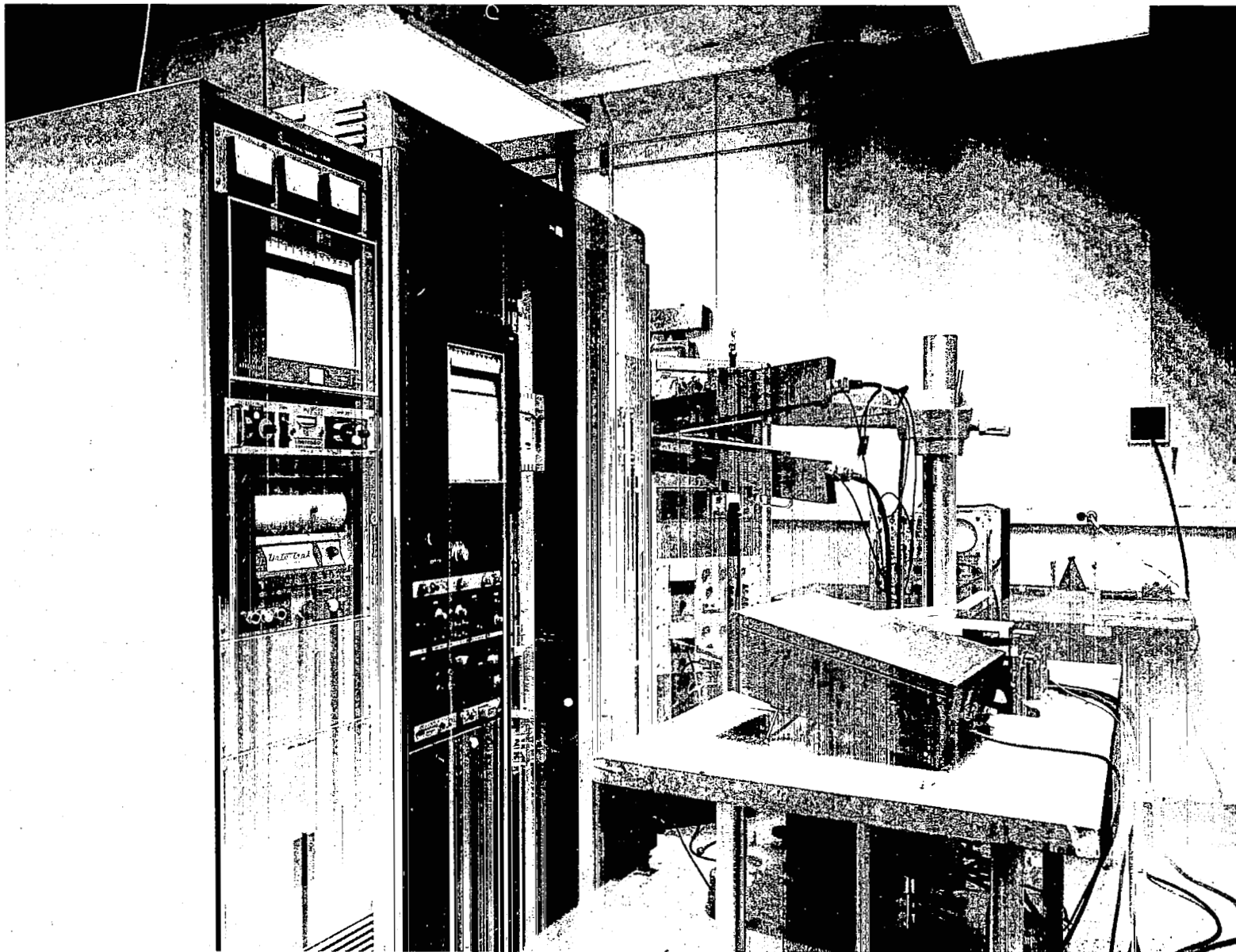


Figure 34.- Tensile Test Setup with Optron Optical Extensometer

These environmental exposures thus provided a basic overall evaluation of the MG-36 ablator's ability to survive the hostile environments of launch noise, orbit temperatures and vacuum, and reentry heating. In addition, the tests provided a relative comparison of the effect of defects on the ablative layers' performance.

Acoustic test.— Acoustic vibration tests were conducted to simulate liftoff and transonic flight. Tests were performed using a siren powered by two Allison jet engines. The acoustic spectrum was calibrated using a pine block dummy panel. Four different impeller speeds were used to simulate the spectrum that would be encountered at booster liftoff (fig. 35).

The 8x16x2-inch (20.3x40.6x5.08-cm) ablative panel was mounted on an 8x16x1-inch (20.3x40.6x2.54-cm) aluminum plate that was essentially rigid. This was suspended on elastic cord in front of the horn with the ablative panel facing into the horn (fig. 36). The energy level was changed by adjusting the pressure to give the following conditions.

	Overall noise level, db	Duration, s
Booster liftoff	156	15
Transonic flight	159	50

Both panels were tested simultaneously to these environments.

Hot vacuum test.— The test panel and a control panel were simultaneously subjected to vacuum and heat. Both panels were mounted on a 0.5-inch (1.27-cm) aluminum plate. Thermocouples were installed as shown in figure 30.

The purpose of the hot vacuum condition was to obtain a precursory evaluation of material offgassing characteristics and aging effects during orbit exposure and to thermally strain the ablative-to-face sheet bondline.

A 4-ft (1.2-m) diameter x 8-ft (2.4-m) vacuum chamber was used. Vacuum was maintained by a combination of pumps. A mechanical roughing pump with a rotor lobe blower was used to the 20- to 50-micron range. Cryopumping reduced this vacuum to  $1 \times 10^{-4}$  torr ( $1.3 \times 10^{-3}$  N/m<sup>2</sup>) where an ion pump could be turned on. Operating pressure was attained using the ion pump, with an additional pumping capacity from a titanium filament sublimator. Pressure was measured with a hot cathode ionization tube.

A quartz lamp was employed to heat the panels on the front face to induce thermal strains in the ablator and at the attachments. One thermocouple was used to control the front face temperature at 300°F (422K). A shroud surrounding the panels was maintained at -40°F (233K) with a heat exchanger system. A low shroud temperature was desired to reduce the load on the pumping system caused by background offgassing. This test condition was maintained for 72 consecutive hours.

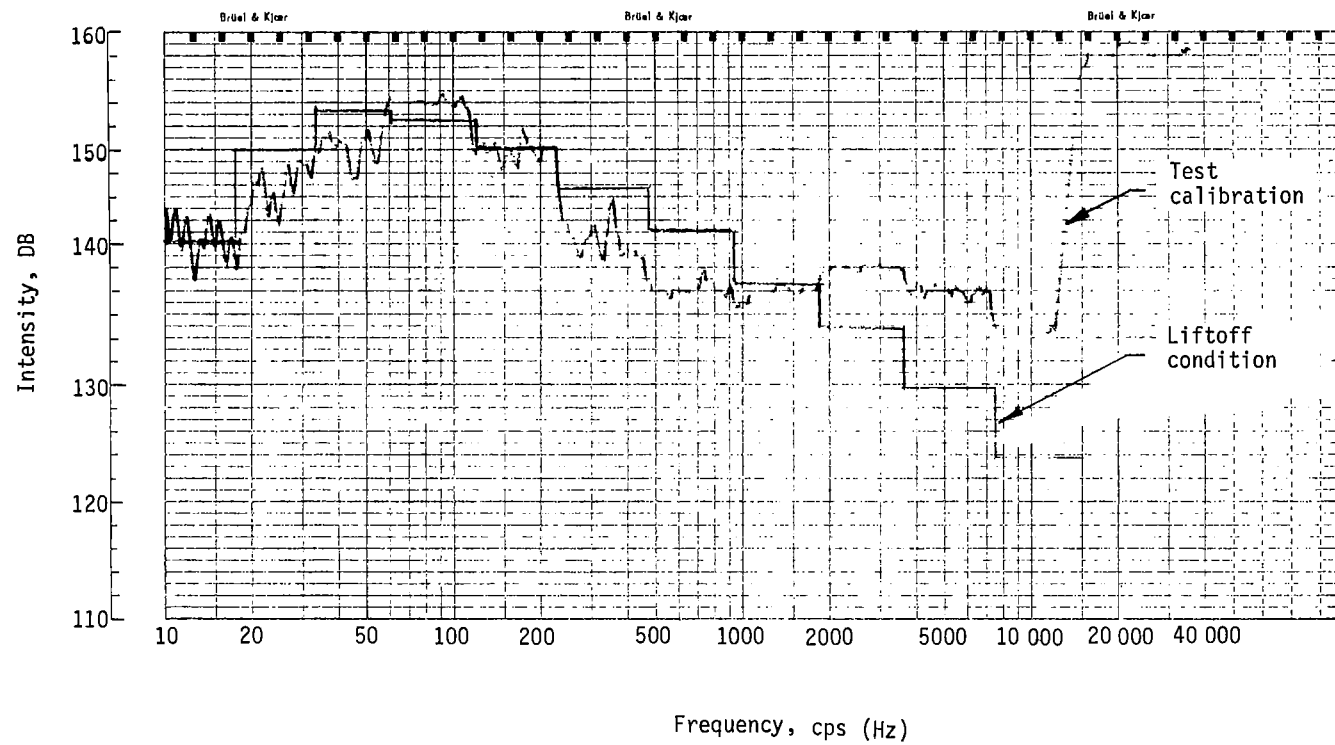


Figure 35.- Sound Spectrum Used in Acoustic Tests



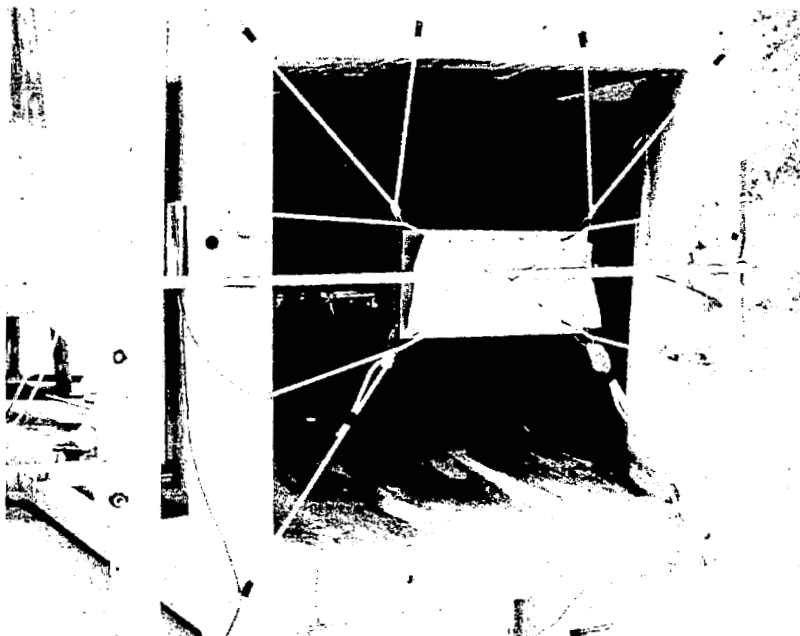


Figure 36.- Acoustic Test Setup with Ablative Panel Mounted

Cold vacuum test.— The purpose of the cold vacuum test was to strain the ablative filler bond to the honeycomb core and the ablative layer bond to the face sheet. This was accomplished using the same test setup and followed the hot vacuum testing (fig. 37).

The shroud inside the vacuum chamber was cooled with liquid nitrogen to a temperature of  $-320^{\circ}\text{F}$  ( $78\text{K}$ ). Infrared heaters were used on both sides of the samples to maintain the sample temperature at  $-150^{\circ}\text{F}$  ( $172\text{K}$ ) and the test duration was for 48 consecutive hours.

Ablation test.— Reentry heating was simulated in the Martin Marietta Plasma Arc facility utilizing a 10.0-inch (25.4-cm) diameter nozzle with the panel positioned at a  $20^{\circ}$  angle to the test stream. The panel was rigidly attached to the model holder at the four attachment points. This holder was designed with a water-cooled leading edge machined to a 1.25-inch (3.18-cm) radius. The blunting of the leading edge was found to enhance flow uniformity and improve heating distribution as shown in figure 38. This test condition was calibrated using a thin skin calorimeter body made of 0.063-inch (0.16-cm) Inconel X-750 sheet. Heating rates were calculated from the response of thermocouples that were spot-welded to the Inconel skin using the basic calorimeter equation

$$\dot{q}_{cw} = t \rho C_p \frac{dT}{dt}$$

where

$\dot{q}_{cw}$ , cold wall heat flux,  $\text{Btu/ft}^2\text{-s}$  or  $\text{MW/m}^2$ ,

$t$ , shell thickness, ft or m,

$\rho$ , density of calorimeter material,  $\text{lb/ft}^3$  or  $\text{kg/m}^3$ ,

$C_p$ , metal specific heat,  $\text{Btu/lb-}^{\circ}\text{F}$  or  $\text{J/kg-K}$ ,

$\frac{dT}{dt}$ , rise rate of back surface temperature,  $^{\circ}\text{F/s}$  or  $\text{K/s}$ .

The maximum skin temperature was limited to  $800^{\circ}\text{F}$  ( $700\text{K}$ ) so radiation losses, well below  $1.0 \text{ Btu/ft}^2\text{-s}$  ( $11.3 \text{ kW/m}^2$ ), could be neglected. Values of  $\rho$  and  $C_p$  were obtained from ASD-TDR-63-741.\*

## TEST RESULTS AND DISCUSSION

Data obtained from 68 plasma arc splash specimens, 95 tensile coupons, and two large ablative panels tested during Task III are presented.

---

\* Aerospace Structural Materials Handbook. ASD-TDR-63-741, Vol 2 including supplement of March 1965, Air Force Materials Laboratory, Wright-Patterson Air Force Base, Ohio.

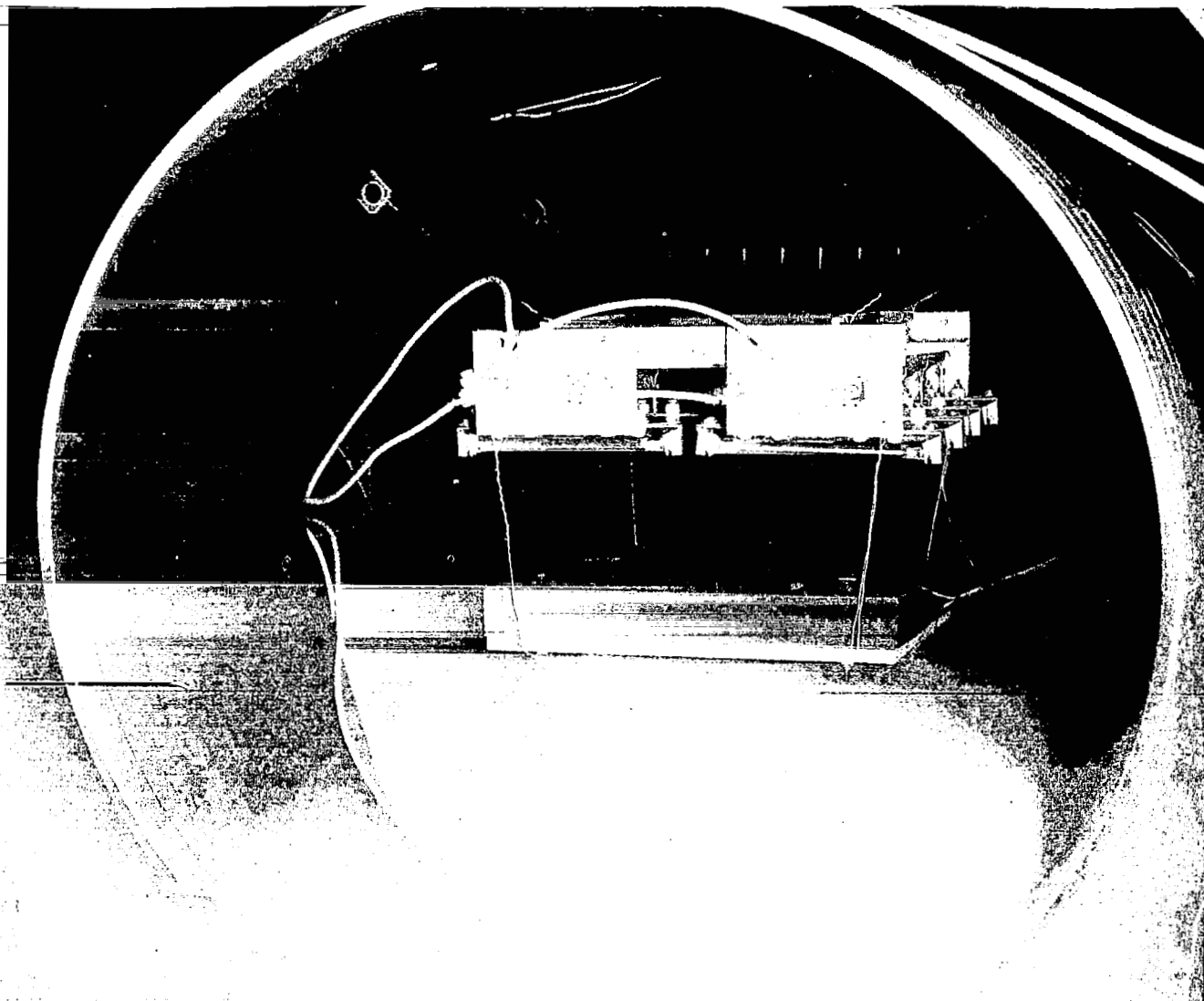


Figure 37.- Temperature Conditioning Setup after Cold Cycle

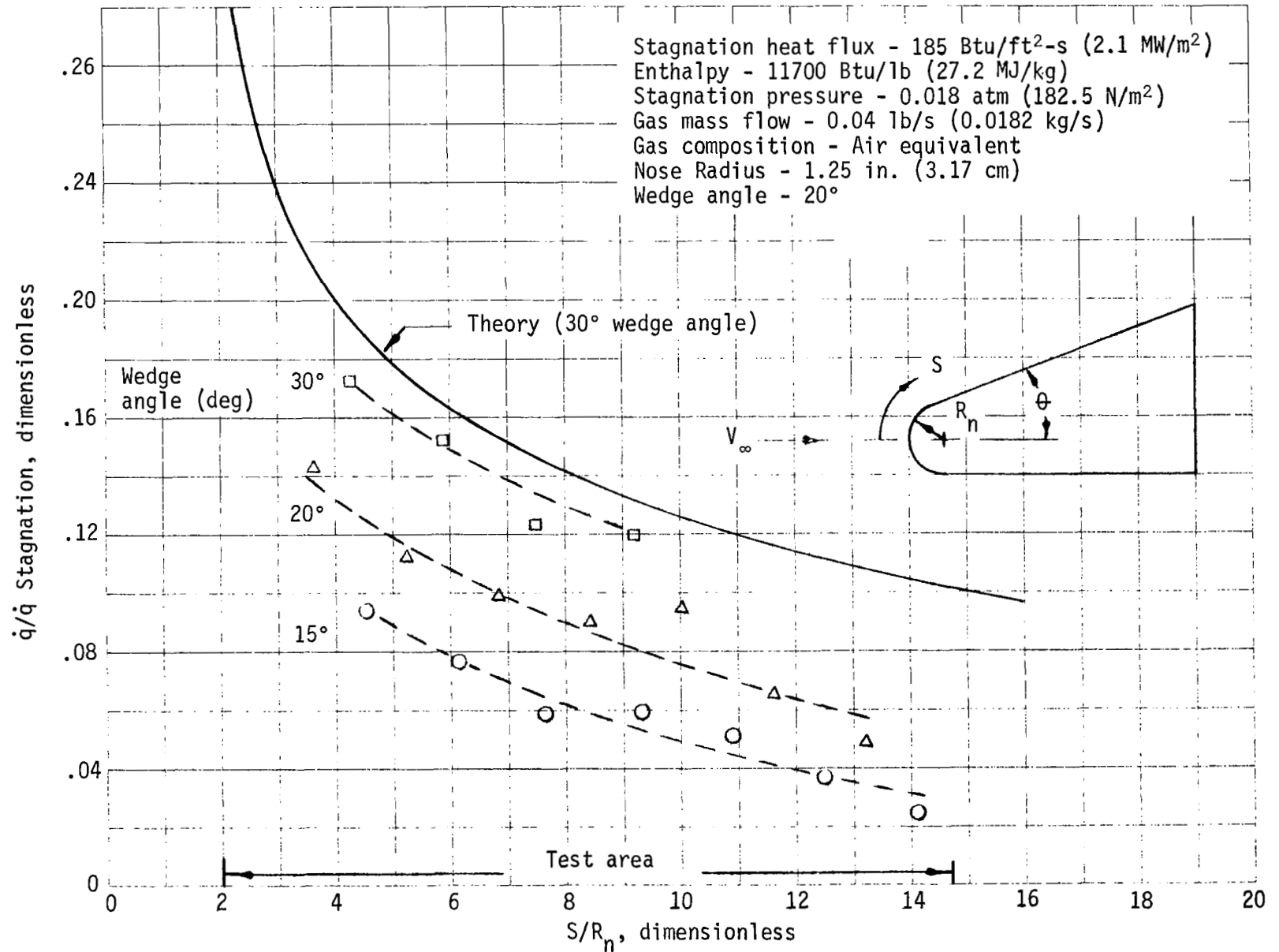


Figure 38.- Experimental Heating Distribution Over Cylinder-Wedge

## Thermal Performance Data (Splash Specimens)

Table VII summarizes the fabrication data, including "material defects," geometry, and density for the specimens used in this investigation as well as nominal test conditions. Actual test values of cold wall heating rates, enthalpy, and pressure are summarized in table VIII.

Table IX summarizes the pertinent test data including stagnation total heat, weight loss, length change, uncharred depth, and back surface temperatures.

Peak back surface temperature.— The results of all specimens containing the fabrication variances previously described are shown in figures 39 through 44. Since three replicas were tested at each test point, results have been averaged and data values have been connected by a straight line to aid in interpreting results. The effect on results of initial temperature and heating rate variations has been minimized by plotting temperature rise versus total heat input.

Bond coat effect: Figure 39 shows the results of core precoating. These results indicate a significant thermal difference between the silicone, the phenolic, and the uncoated core specimens. These differences, 20 to 60°F (11 to 33K), are not explained by data scatter nor are bulk density variations considered a factor since density was nearly constant for all three groups. One possible explanation is that the silicone concentration near the face sheet, identified in MCR-71-14,\* resulted in high conductivity near the face sheet. The differences between the phenolic and the uncoated core specimens, while small, could be the result of effectively increasing the higher conductivity core cross-sectional area by application of the phenolic bond coat. Most likely, however, the differences are explained by the scatter in data and a lower average surface temperature for the uncoated core specimens as indicated by figure 45.

Density effect: Bulk density effects are shown in figure 40 for a density range from 15.0 lb/ft<sup>3</sup> (240 kg/m<sup>3</sup>) to 17.3 lb/ft<sup>3</sup> (277 kg/m<sup>3</sup>). Note that temperature rise increases with a decrease in density (see also fig. 46). The data therefore indicate that the thermal diffusivity ( $K/\rho C_p$ ) parameter is controlling heat conduction for the density range investigated.

Density uniformity effects: The effect of a density variation from front surface to back surface is presented in figure 41. Since both models are approximately equal in bulk density, the differences in data averages could be interpreted as evidence that a "composite" ablative material with high density and storage near the surface and low density and conductivity near the back surface is thermally more efficient. Unfortunately, data scatter at both test conditions is greater than the differences and thus results are inconclusive.

---

\* *op cit*:

TABLE VIII.- PLASMA ARC TEST INPUTS

Model no.	Cold wall heating rates <sup>a</sup>								Enthalpy		Stagnation pressure		Test time, s
	Sensor 1		Sensor 2		Sensor 3		Sensor 4						
	Btu/ft <sup>2</sup> -s	MW/m <sup>2</sup>	Btu/ft <sup>2</sup> -s	MW/m <sup>2</sup>	Btu/ft <sup>2</sup> -s	MW/m <sup>2</sup>	Btu/ft <sup>2</sup> -s	MW/m <sup>2</sup>	Btu/lb	MJ/kg	atm	kN/m <sup>2</sup>	
19S-1	22.8	0.259	24.6	0.279	26.4	0.300	22.8	0.259	3803	8.84	0.0056	0.572	1200
19S-2	22.8	0.259	24.6	0.279	26.4	0.300	22.8	0.259	3803	8.84	0.0056	0.572	1200
19S-3	22.8	0.259	24.6	0.279	26.4	0.300	22.8	0.259	3803	8.84	0.0056	0.572	1200
19S-4	55.0	0.624	62.4	0.708	-	-	-	-	6404	14.90	0.0088	0.891	900
19S-5	53.6	0.608	55.6	0.631	-	-	-	-	6404	14.90	0.0089	0.902	900
19S-6	51.6	0.586	58.0	0.658	-	-	-	-	6386	14.85	0.0087	0.881	900
4B-1	22.0	0.256	24.1	0.273	24.8	0.281	22.1	0.251	3790	8.81	0.0052	0.533	1200
4B-2	22.6	0.256	24.1	0.273	24.8	0.281	22.1	0.251	3790	8.81	0.0052	0.533	1200
4B-3	22.6	0.256	24.1	0.273	24.8	0.281	22.1	0.251	3790	8.81	0.0052	0.533	1200
4B-4	55.5	0.630	60.0	0.681	-	-	-	-	6420	14.93	0.0084	0.851	800
4B-5	50.7	0.575	62.4	0.708	-	-	-	-	6320	14.70	0.0089	0.902	900
4B-6	45.5	0.516	46.7	0.530	42.3	0.480	42.3	0.480	5428	12.62	0.0065	0.658	800
5B-7	22.3	0.253	26.0	0.295	25.6	0.290	21.1	0.239	3825	8.89	0.0054	0.547	1200
5B-8	-	-	-	-	-	-	-	-	-	-	-	-	-
5B-9	22.3	0.253	26.0	0.295	25.6	0.290	21.1	0.239	3825	8.89	0.0054	0.547	1200
5B-10	50.7	0.575	62.4	0.708	-	-	-	-	6320	14.70	0.0089	0.902	900
5B-11	55.5	0.630	60.0	0.681	-	-	-	-	6420	14.93	0.0084	0.851	900
5B-12	54.5	0.618	56.2	0.638	-	-	-	-	6135	14.27	0.0084	0.851	1000
6B-13	23.1	0.262	24.2	0.275	25.5	0.289	22.4	0.254	3657	8.50	0.0052	0.533	1200
6B-14	23.1	0.262	24.2	0.275	25.5	0.289	22.4	0.254	3657	8.50	0.0052	0.533	1200
6B-15	23.1	0.262	24.2	0.275	25.5	0.289	22.4	0.254	3657	8.50	0.0052	0.533	1200
6B-16	54.5	0.618	56.2	0.638	-	-	-	-	6135	14.27	0.0084	0.851	900
6B-17	55.5	0.630	60.0	0.681	-	-	-	-	6420	14.93	0.0084	0.851	900
6B-18	50.7	0.575	62.4	0.708	-	-	-	-	6320	14.70	0.0087	0.881	900
10D-1	22.8	0.259	24.0	0.272	25.1	0.285	21.2	0.241	3582	8.33	0.0052	0.533	1200
10D-2	22.8	0.259	24.0	0.272	25.1	0.285	21.2	0.241	3582	8.33	0.0052	0.533	1200
10D-3	22.8	0.259	24.0	0.272	25.1	0.285	21.2	0.241	3582	8.33	0.0052	0.533	1200
10D-4	53.6	0.608	55.6	0.631	-	-	-	-	6406	14.90	0.0089	0.902	900
10D-5	55.0	0.624	62.4	0.708	-	-	-	-	6406	14.90	0.0088	0.891	900
10D-6	55.5	0.630	59.0	0.670	-	-	-	-	6390	14.86	0.0086	0.871	900
11D-7	23.6	0.268	25.0	0.284	25.6	0.290	22.4	0.254	3788	8.81	0.0052	0.533	1200
11D-8	23.6	0.268	25.0	0.284	25.6	0.290	22.4	0.254	3788	8.81	0.0052	0.533	1200
11D-9	23.6	0.268	25.0	0.284	25.6	0.290	22.4	0.254	3788	8.81	0.0051	0.533	1200
11D-10	55.5	0.630	59.0	0.670	-	-	-	-	6390	14.86	0.0086	0.871	900
11D-11	55.0	0.624	62.4	0.708	-	-	-	-	6406	14.90	0.0088	0.902	900
11D-12	53.6	0.608	55.6	0.631	-	-	-	-	6406	14.90	0.0089	0.902	900
12D-13	23.5	0.267	24.4	0.277	25.1	0.285	22.2	0.252	3823	8.89	0.0054	0.547	1202
12D-14	23.5	0.267	24.4	0.277	25.1	0.285	22.2	0.252	3823	8.89	0.0054	0.547	1200
12D-15	23.5	0.267	24.4	0.277	25.1	0.285	22.2	0.252	3823	8.89	0.0054	0.547	1200
12D-16	51.6	0.586	58.0	0.658	-	-	-	-	6386	14.85	0.0087	0.881	900
12D-17	51.6	0.586	58.0	0.658	-	-	-	-	6386	14.85	0.0087	0.881	900
12D-18	55.5	0.630	59.0	0.670	-	-	-	-	6390	14.86	0.0086	0.871	900
1V-1	23.7	0.269	26.8	0.304	27.1	0.308	23.0	0.261	3900	9.07	0.0054	0.547	1200
1V-2	23.7	0.269	26.8	0.304	27.1	0.308	23.0	0.261	3900	9.07	0.0054	0.547	1200
1V-3	23.7	0.269	26.8	0.304	27.1	0.308	23.0	0.261	3900	9.07	0.0054	0.547	1200
2V-10	50.7	0.575	57.0	0.647	-	-	-	-	6375	14.83	0.0086	0.871	900
2V-11	51.6	0.586	60.2	0.683	-	-	-	-	6448	15.00	0.0086	0.871	900
2V-12	52.4	0.595	63.0	0.715	-	-	-	-	6190	14.40	0.0087	0.881	900
1V-4	22.1	0.251	25.0	0.284	24.2	0.275	20.2	0.229	3828	8.90	0.0054	0.547	1200
1V-5	22.1	0.251	25.0	0.284	24.2	0.275	20.2	0.229	3828	8.90	0.0054	0.547	1200
1V-6	22.1	0.251	25.0	0.284	24.2	0.275	20.2	0.229	3828	8.90	0.0054	0.547	1200
2V-13	51.6	0.586	60.2	0.683	-	-	-	-	6448	15.00	0.0086	0.871	900
2V-14	50.7	0.575	57.0	0.647	-	-	-	-	6375	14.83	0.0086	0.871	900
2V-15	52.4	0.595	63.0	0.715	-	-	-	-	6190	14.40	0.0087	0.881	900
1V-7	22.1	0.251	25.5	0.289	24.6	0.279	20.0	0.227	3897	9.06	0.0054	0.547	1200
1V-8	22.1	0.251	25.5	0.289	24.6	0.279	20.0	0.227	3897	9.06	0.0054	0.547	1200
1V-9	22.1	0.251	25.5	0.289	24.6	0.279	20.0	0.227	3897	9.06	0.0054	0.547	1200
2V-16	52.4	0.595	63.0	0.715	-	-	-	-	6190	14.40	0.0084	0.851	900
2V-17	50.7	0.575	57.0	0.647	-	-	-	-	6375	14.83	0.0086	0.871	900
2V-18	51.6	0.586	60.2	0.683	-	-	-	-	6448	15.00	0.0086	0.871	900
15H-1	22.1	0.251	24.1	0.273	25.3	0.287	22.0	0.250	3735	8.68	0.0054	0.547	1200
15H-2	22.1	0.251	24.1	0.273	25.3	0.287	22.0	0.250	3735	8.68	0.0054	0.547	1200
15H-3	22.1	0.251	24.1	0.273	25.3	0.287	22.0	0.250	3735	8.68	0.0054	0.547	1200
15H-4	22.1	0.251	24.3	0.276	26.0	0.295	21.1	0.239	3892	9.05	0.0056	0.573	1200
15H-5	22.1	0.251	24.3	0.276	26.0	0.295	21.1	0.239	3892	9.05	0.0056	0.573	1200
15H-6	22.1	0.251	24.3	0.276	26.0	0.295	21.1	0.239	3892	9.05	0.0056	0.573	1200
16C-1	21.4	0.243	24.6	0.280	24.5	0.278	21.4	0.243	3675	8.54	0.0054	0.547	1200
16C-2	21.4	0.243	24.6	0.280	24.5	0.278	21.4	0.243	3675	8.54	0.0054	0.547	1200
16C-3	21.4	0.243	24.6	0.280	24.5	0.278	21.4	0.243	3675	8.54	0.0054	0.547	1200

<sup>a</sup> See figure 22 for sensor locations.

TABLE IX.- SUMMARY OF PLASMA ARC TEST DATA

Model	Stagnation total heat		Weight loss		Length change		Uncharred depth		Back surface temperature				Time of T <sub>max</sub> , s
	Btu/ft <sup>2</sup>	MJ/m <sup>2</sup>	oz	gm	in.	cm	in.	cm	T <sub>o</sub>		T <sub>max</sub>		
									°F	K	°F	K	
19S-1	27 300	209.8	1.03	29.3	0.069	0.175	-	-	84.1	28.9	302.4	150.2	2461.4
19S-2	27 300	209.8	1.05	29.9	0.079	0.201	-	-	78.1	25.6	273.6	134.2	2461.7
19S-3	27 300	309.8	1.01	28.6	0.075	0.190	0.93	2.36	80.8	27.1	271.8	133.2	2410.8
19S-4	49 500	561.9	16.3	46.2	0.149	0.378	-	-	81.8	27.7	428.3	220.2	1747.2
19S-5	48.240	547.5	1.63	46.1	0.161	0.409	0.50	1.27	76.4	24.7	409.7	209.8	1788.3
19S-6	46 440	527.0	1.70	48.2	0.136	0.345	-	-	70.7	21.5	386.5	196.9	1747.2
4B-1	27 100	307.6	1.15	32.7	0.075	0.190	-	-	86.6	30.3	281.9	138.8	2357.9
4B-2	27 100	307.6	1.17	33.1	0.068	0.173	1.00	2.54	86.9	30.5	270.5	132.5	2307.3
4B-3	27 100	307.6	1.18	33.5	0.066	0.168	-	-	79.1	26.1	270.5	132.5	2308.8
4B-4	44 400	503.9	1.56	44.3	0.130	0.330	-	-	86.6	30.3	353.6	178.7	1787.4
4B-5	45 700	518.6	1.80	51.0	0.134	0.340	0.54	1.37	78.2	25.7	391.0	199.4	1870.7
4B-6	36 400	413.1	1.16	32.8	0.095	0.241	-	-	76.1	24.5	247.1	119.5	1913.9
5B-7	26 700	303.0	1.13	32.0	0.069	0.175	-	-	81.6	27.6	293.4	145.2	2153.1
5B-8	-	-	-	-	-	-	-	-	-	-	-	-	-
5B-9	26 700	303.0	1.13	32.0	0.079	0.201	0.84	2.13	77.2	25.1	278.4	136.9	2308.2
5B-10	45 900	518.6	1.69	48.0	0.133	0.338	-	-	84.0	28.9	464.2	240.1	1725.4
5B-11	50 000	576.4	1.69	47.9	0.124	0.315	-	-	82.9	28.3	422.1	216.7	1746.1
5B-12	54 500	618.5	1.62	45.9	0.135	0.343	0.40	1.02	84.4	29.1	484.1	251.2	1636.0
6B-13	27 700	314.4	1.30	36.8	0.075	0.194	-	-	80.9	27.2	271.4	133.0	2435.7
6B-14	27 700	314.4	1.26	35.7	0.084	0.213	0.90	2.27	80.0	26.7	262.1	127.8	2358.5
6B-15	27 700	314.4	1.30	36.9	0.080	0.203	-	-	76.6	24.8	269.2	131.8	2437.1
6B-16	49 100	557.2	1.60	45.3	0.120	0.305	-	-	82.2	27.9	380.6	193.7	1973.3
6B-17	50 000	576.4	1.62	46.0	0.129	0.328	-	-	79.9	26.6	344.6	173.7	1912.0
6B-18	45 700	518.6	1.75	49.7	0.135	0.343	0.52	1.32	78.4	25.8	407.6	208.7	1869.2
10D-1	27 300	309.8	1.33	37.7	0.070	0.178	-	-	84.8	29.3	262.6	128.1	2539.0
10D-2	27 300	309.8	1.33	37.8	0.073	0.185	0.98	2.49	83.0	28.3	265.2	129.6	2615.1
10D-3	27 300	309.8	1.27	36.1	0.81	0.206	-	-	76.6	24.8	268.7	131.5	2514.0
10D-4	48 240	547.5	1.75	49.7	0.132	0.335	-	-	86.0	30.0	401.3	205.2	1848.8
10D-5	49 500	561.8	1.69	48.0	0.123	0.312	0.58	1.47	82.9	28.3	567.1	186.2	1891.0
10D-6	49 950	566.9	1.68	47.6	0.129	0.328	-	-	80.0	26.7	359.0	181.7	1784.0
11D-7	28 300	321.2	1.18	33.4	0.067	0.170	-	-	78.6	25.9	270.9	132.7	2461.1
11D-8	28 300	321.2	1.18	33.6	0.74	0.188	0.90	2.29	77.4	25.2	276.2	135.6	2436.0
11D-9	28 300	321.2	1.20	33.9	0.069	0.175	-	-	71.5	21.9	269.2	131.8	2488.7
11D-10	49 950	566.9	1.69	47.9	0.136	0.345	-	-	85.4	29.7	431.0	221.7	1725.1
11D-11	49 950	561.8	1.69	47.9	0.135	0.345	0.56	1.42	80.1	26.7	386.0	196.7	1848.1
11D-12	48 240	547.5	1.72	48.7	0.130	0.330	-	-	78.8	26.0	369.8	187.7	1930.6
12D-13	28 200	320.0	1.13	23.1	0.083	0.2108	-	-	80.0	26.7	281.5	138.6	2333.0
12D-14	28 200	320.0	1.17	33.3	0.079	0.201	0.85	2.16	79.1	26.2	278.0	136.7	2487.2
12D-15	28 200	320.8	1.12	31.7	0.062	0.157	-	-	75.1	23.9	265.6	129.8	2513.7
12D-16	46 440	527.0	1.65	46.7	0.154	0.391	-	-	80.5	26.9	419.5	215.3	1890.1
12D-17	46 400	527.0	1.65	46.9	0.147	0.373	0.45	1.14	77.0	25.0	401.5	205.3	1746.2
12D-18	49 950	566.9	1.62	45.9	0.151	0.384	-	-	79.6	26.4	395.5	201.9	1747.2
1V-1	28 400	322.3	1.23	34.8	0.091	0.231	-	-	77.7	25.4	380.0	193.3	1819.2
1V-2	28 400	322.3	1.20	34.0	0.090	0.228	-	-	76.2	24.6	347.5	175.3	1750.0
1V-3	28 400	322.3	1.17	33.1	0.81	0.206	0.58	1.47	77.0	25.0	365.5	185.3	1820.0
2V-10	46 440	527.0	1.56	44.1	0.131	0.333	-	-	85.5	29.7	467.5	241.9	1550.0
2V-11	47 160	535.2	1.59	45.1	0.110	0.279	0.40	1.02	80.5	26.9	477.4	247.4	1499.5
2V-12	46 800	531.1	1.62	45.8	0.135	0.343	-	-	78.8	26.0	474.3	245.7	1455.3
1V-4	26 500	300.7	1.13	32.0	0.096	0.244	-	-	78.2	25.7	250.0	176.7	2000.0
1V-5	26 500	300.7	1.10	31.2	0.077	0.196	1.04	2.64	78.2	25.7	356.3	180.2	2025.3
1V-6	26 500	300.7	1.15	32.5	0.075	0.190	-	-	75.6	24.2	330.6	165.9	2077.8
2V-13	46 440	527.0	1.59	45.2	0.118	0.300	-	-	81.5	27.5	523.6	273.1	1414.0
2V-14	45 360	517.8	1.51	42.8	0.107	0.272	0.40	1.02	80.9	27.2	482.1	250.4	1417.2
2V-15	47 100	534.5	1.50	42.6	0.121	0.307	-	-	80.6	27.0	531.4	277.4	1458.3
1V-7	26 500	300.7	1.32	37.5	0.075	0.190	-	-	79.6	26.4	388.1	198.2	1900.0
1V-8	26 500	300.7	1.15	32.6	0.075	0.190	0.94	2.39	83.4	28.6	264.4	184.7	1922.5
1V-9	26 500	300.7	1.17	33.3	0.074	0.188	-	-	78.1	25.6	350.9	177.2	1923.8
2V-16	47 100	534.5	1.56	44.3	0.115	0.292	-	-	86.5	30.3	541.9	283.3	1334.0
2V-17	45 360	511.8	1.52	43.1	0.109	0.277	-	-	78.3	25.7	501.8	261.0	1376.9
2V-18	46 440	527.0	1.48	41.9	0.100	0.254	0.62	1.58	79.4	26.3	525.8	274.3	1397.9
15H-1	26 500	300.7	1.18	33.6	0.099	0.251	-	-	79.8	26.2	255.5	124.2	2410.5
15H-2	26 500	300.7	1.19	33.7	0.101	0.256	-	-	80.9	27.2	-	-	-
15H-3	26 500	300.7	1.15	32.6	0.088	0.224	1.03	2.62	77.5	25.3	245.4	118.6	2616.5
15H-4	26 500	300.7	1.14	32.3	0.074	0.188	-	-	85.2	29.6	281.1	138.4	2384.4
15H-5	26 500	300.7	1.15	32.5	0.810	0.206	0.98	2.49	83.2	28.4	267.0	130.6	2512.9
15H-6	26 500	300.7	1.18	33.4	0.081	0.206	-	-	81.0	27.2	259.0	126.1	2462.5
16C-1	25 700	291.7	1.14	32.3	0.062	0.156	-	-	82.4	28.0	257.3	125.2	2179.1
16C-2	25 700	291.7	1.10	31.1	0.061	0.155	0.97	2.46	79.6	26.4	258.6	125.9	2435.1
16C-3	25 700	291.7	1.13	32.1	0.066	0.168	-	-	73.0	22.7	241.9	116.6	2308.6

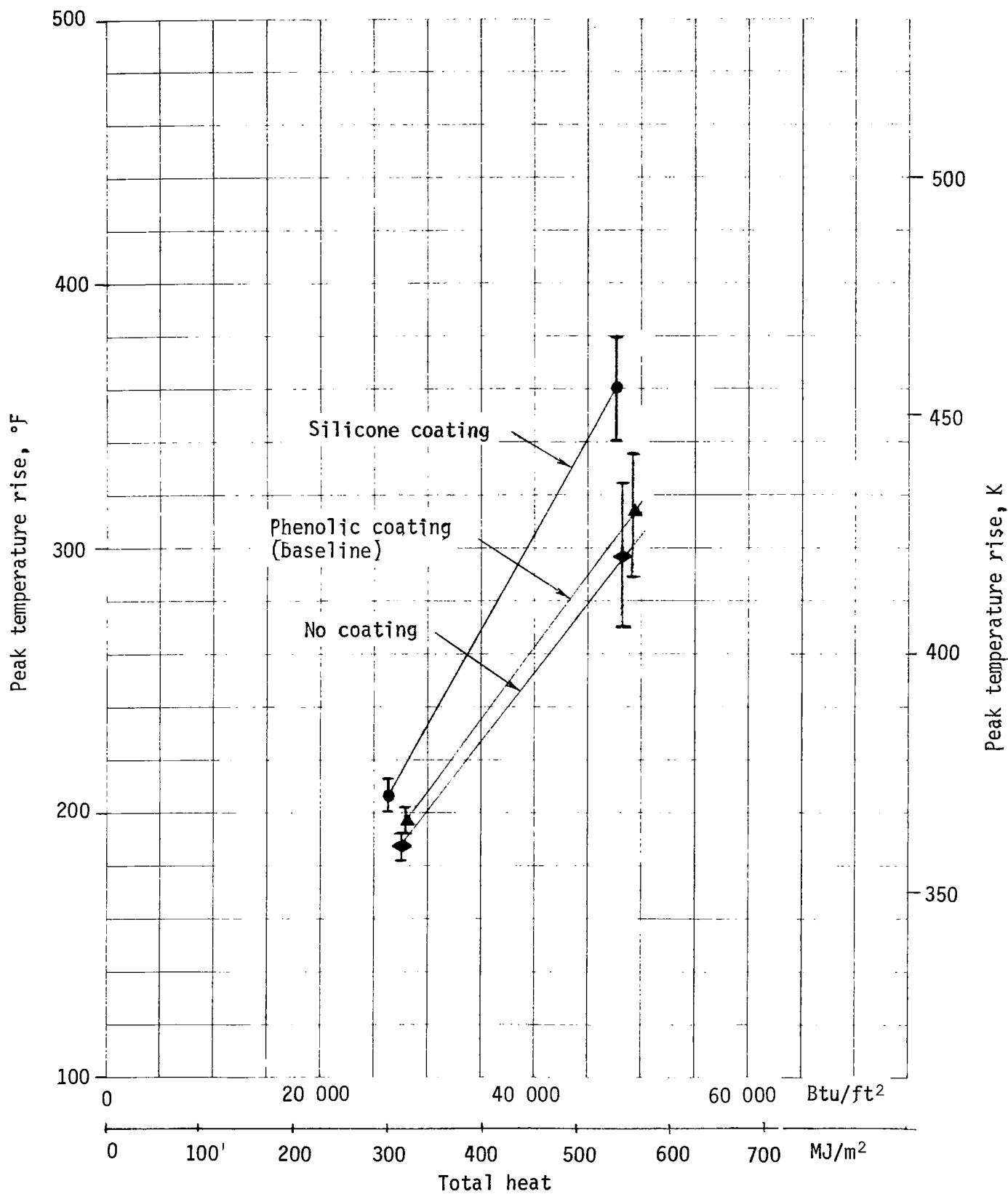


Figure 39.- Effect of Bond Coat on Peak Back Surface Temperature Rise



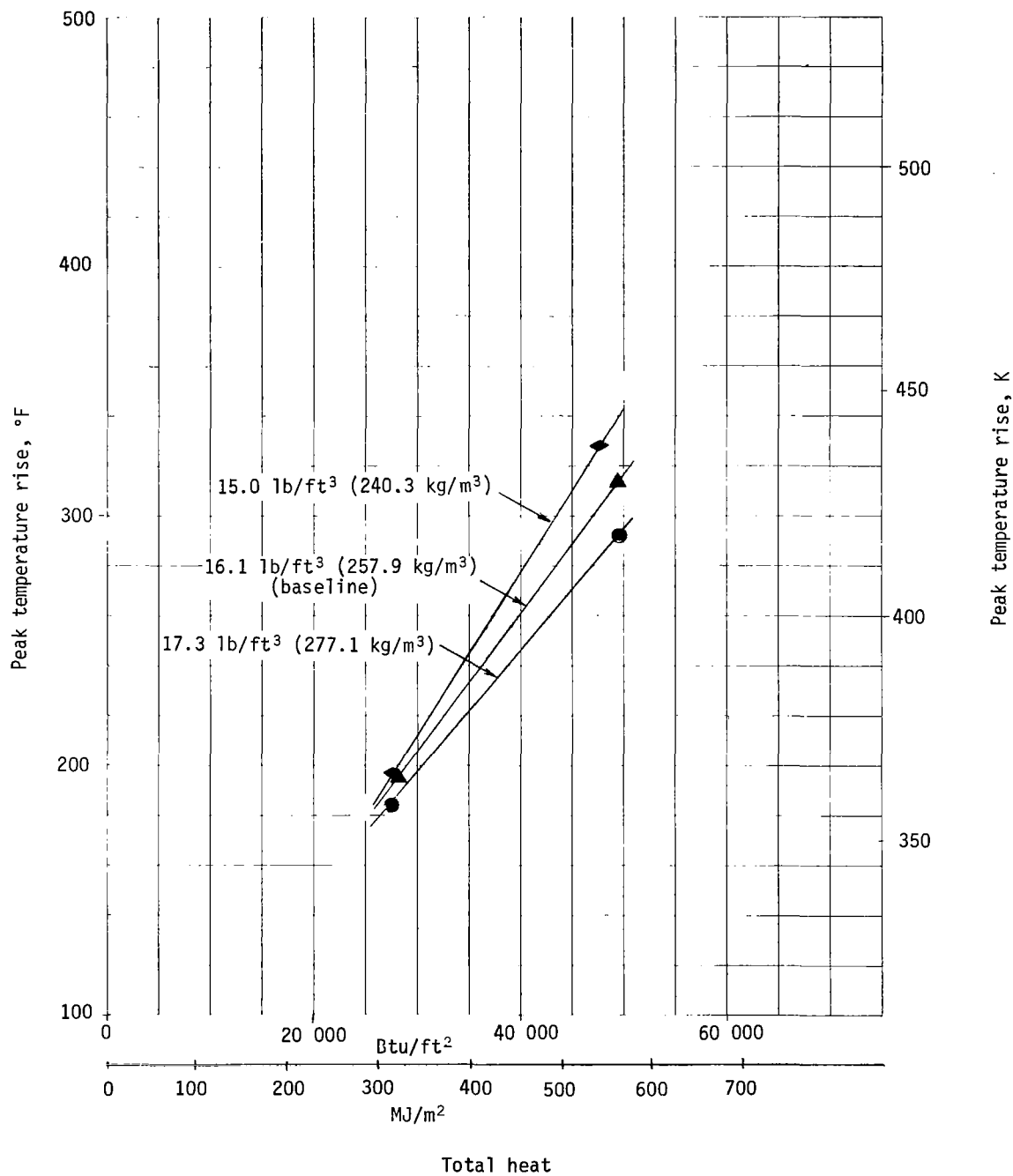


Figure 40.- Effect of Bulk Density Variations on Peak Back Surface Temperature Rise

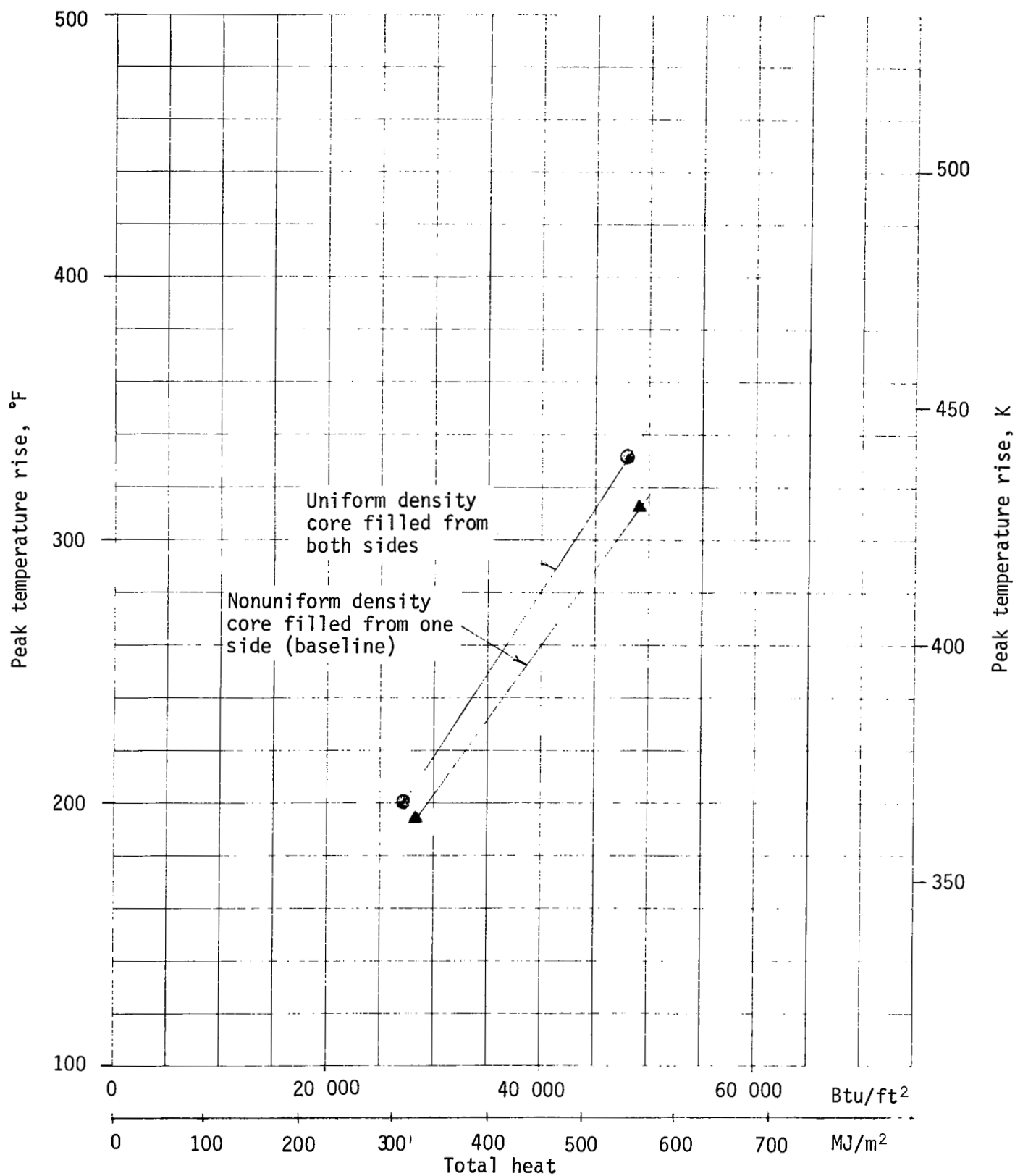


Figure 41.- Effect of Density Distribution on Peak Back Surface Temperature Rise

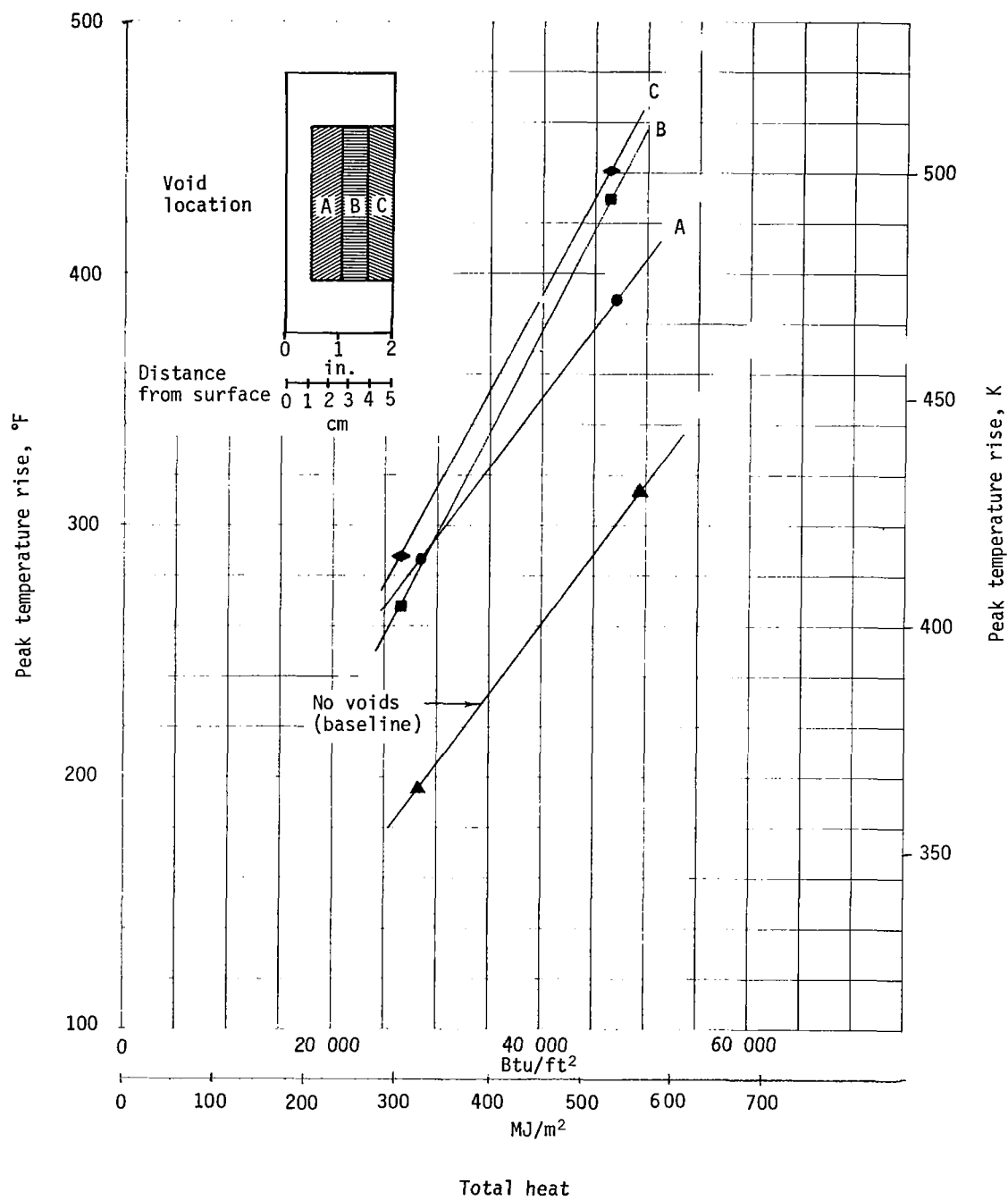


Figure 42.- Effect of Voids on Peak Back Surface Temperature Rise

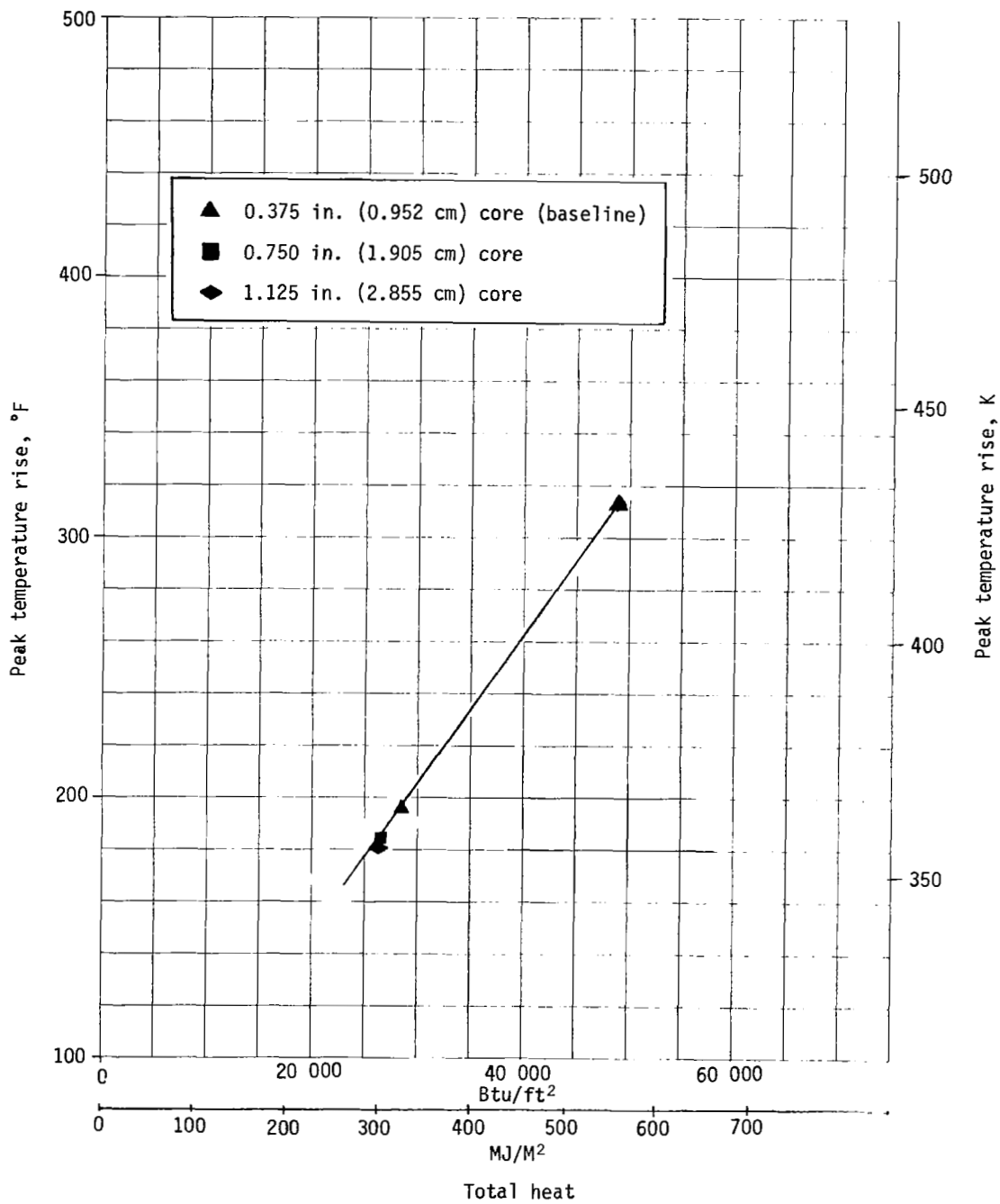


Figure 43.- Effect of Core Size on Peak Back Surface Temperature Rise

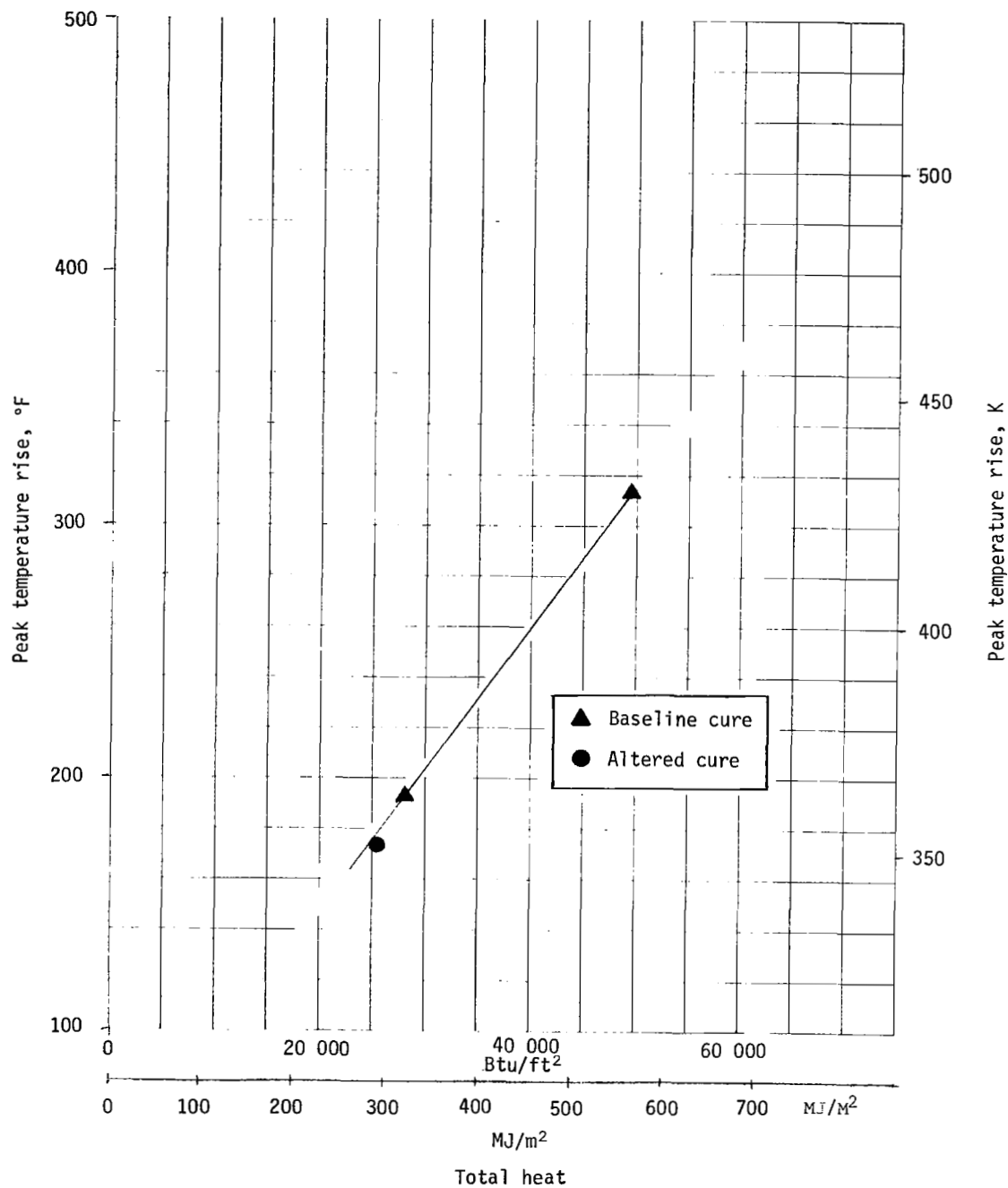


Figure 44.- Effect of Cure Cycle on Peak Back Surface Temperature Rise

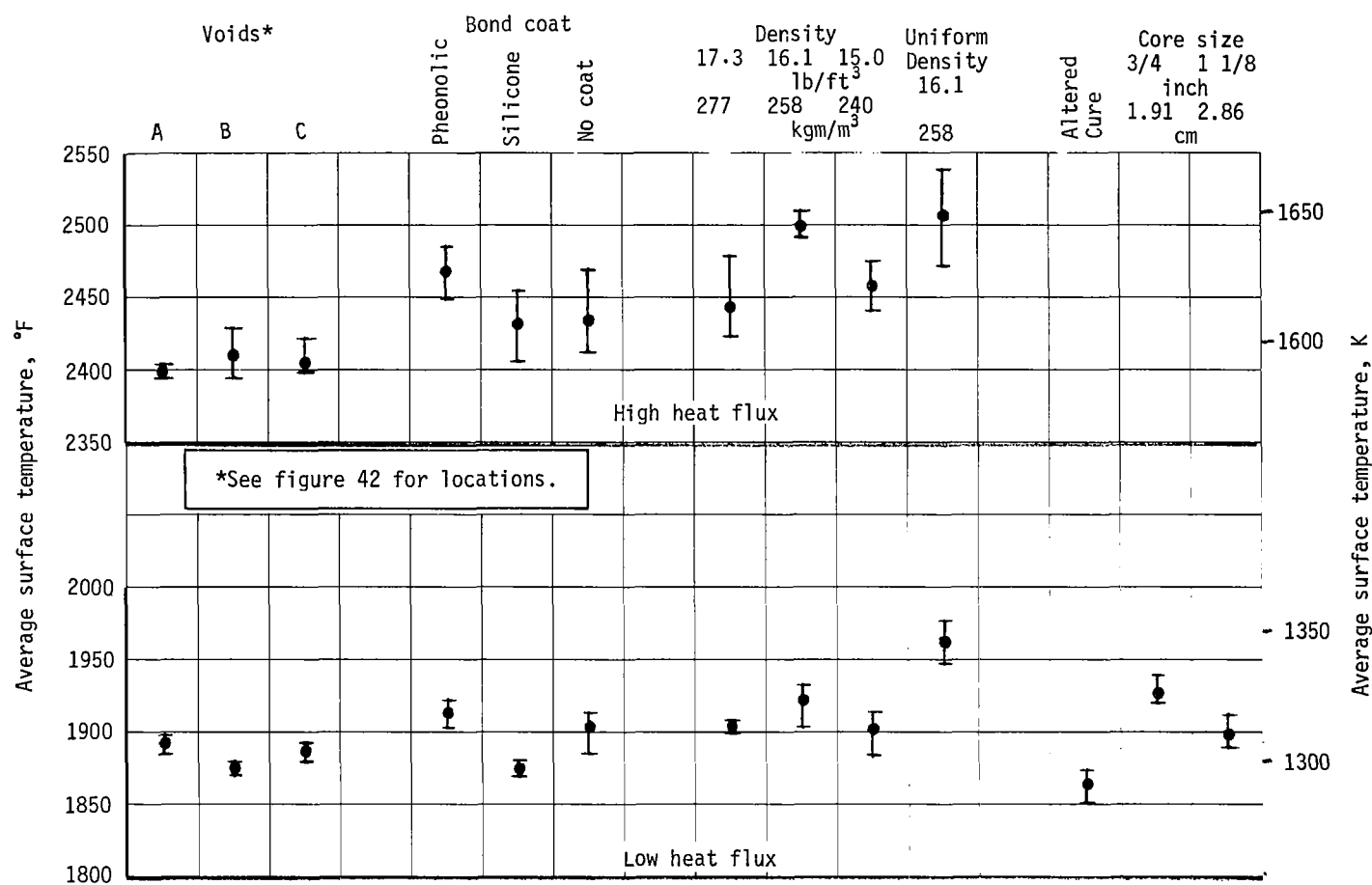


Figure 45.- Average Surface Temperature for Defects Studied

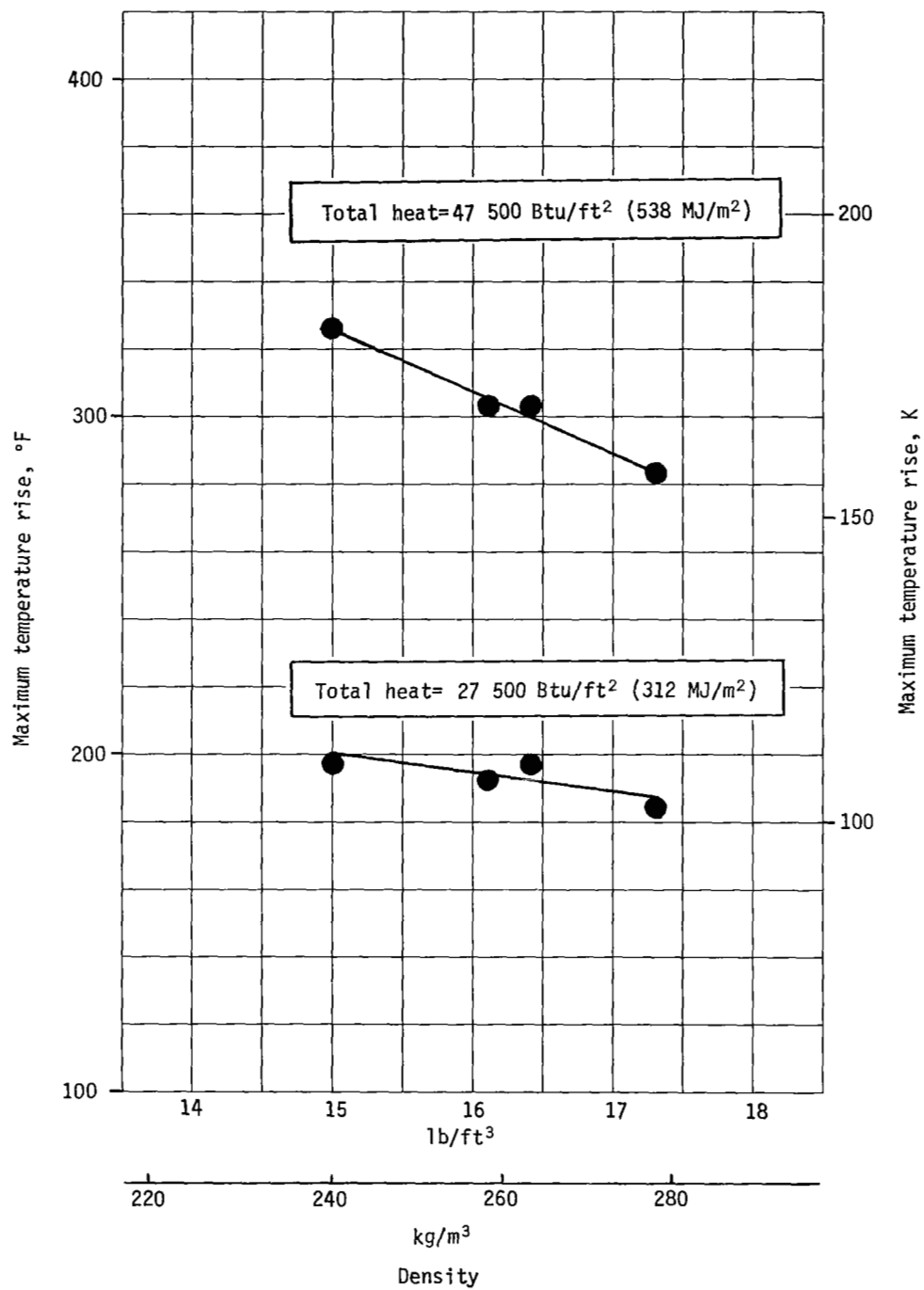


Figure 46.- Effect of Density on Backface Temperature Rise

**Voids:** Figure 42 presents the results of voids and void location. These results indicate a significant back surface temperature increase with voids in all cells. This increase is partially explained by the reduction in specimen thermal mass (approximately 20%) indicated in figure 47, which shows maximum temperature rise versus composite unit weight. The following expression was used to determine the composite unit weight: Composite unit weight = ( $\rho_t$ ) ablative + ( $\rho_t$ ) honeycomb in void area. The data also indicate that void location affects back surface temperature, with voids near the back surface producing the largest temperature rise. Maximum back surface temperature rise is plotted against void distance from the back surface in figure 48 for both test points. A data correction was made for total heat effects. At the low heat flux, a below nominal surface temperature was noted for voids centered 0.75 inch (1.91 cm) from the back surface. This possibly explains the difference in curve shape.

**Core size effect:** The effect of core size on back surface temperature is presented in figure 43 and is minimal. The minor differences noted at the low heating point are predictable in that reducing the amount of high conductivity core reduces the back surface temperature.

**Cure effect:** The altered cure cycle results are plotted in figure 44. A 20°F (11.1K) lower temperature is noted for the altered cure specimens and can be explained by a slightly higher bulk density and lower total heat input.

**Thermal distributions.-** Temperature distributions were determined at the end of heating for specimens containing honeycomb bond coating variations, density uniformity variations, and void location variations. The results are shown in figures 49 and 51. Each curve presented was obtained by plotting the individual specimen temperatures at their respective locations below the surface. These locations were determined from pretest specimen X-rays and are reported in MCR-71-201.\* Then a smooth curve was fitted to the data to obtain an average value for the three specimens tested as illustrated in figures 52 and 53. A comparison of the thermal distribution between test conditions was obtained by plotting the results from specimens are shown in 4B-1, 4B-2, and 4B-3 in figure 54. It was noted that projection of thermocouple temperatures to the surface were in excellent agreement with measured pyrometer surface temperatures for both test conditions.

**Bond coat effect.-** The temperature distributions for the specimens containing bond coats of silicone and phenolic resin, along with the specimens that received no bond coat, are plotted together in figure 49. The data seem to indicate a higher conductivity for the specimens fabricated with a silicone core bond coating. The temperatures in the char zone are lower than the other two cases and the temperatures in the virgin material are higher for the silicone case. We can probably rule out the heating rate factor, which is within  $\pm 1\%$  for these specimens. Thus the most plausible reasoning would point to a higher conductivity for the silicone-coated specimen.

---

\*Thompson, R. L.; and Driver, W. W.: Study of Critical Defects in Ablative Heat Shield Systems (Task III Summary). MCR-71-201, July 1971.



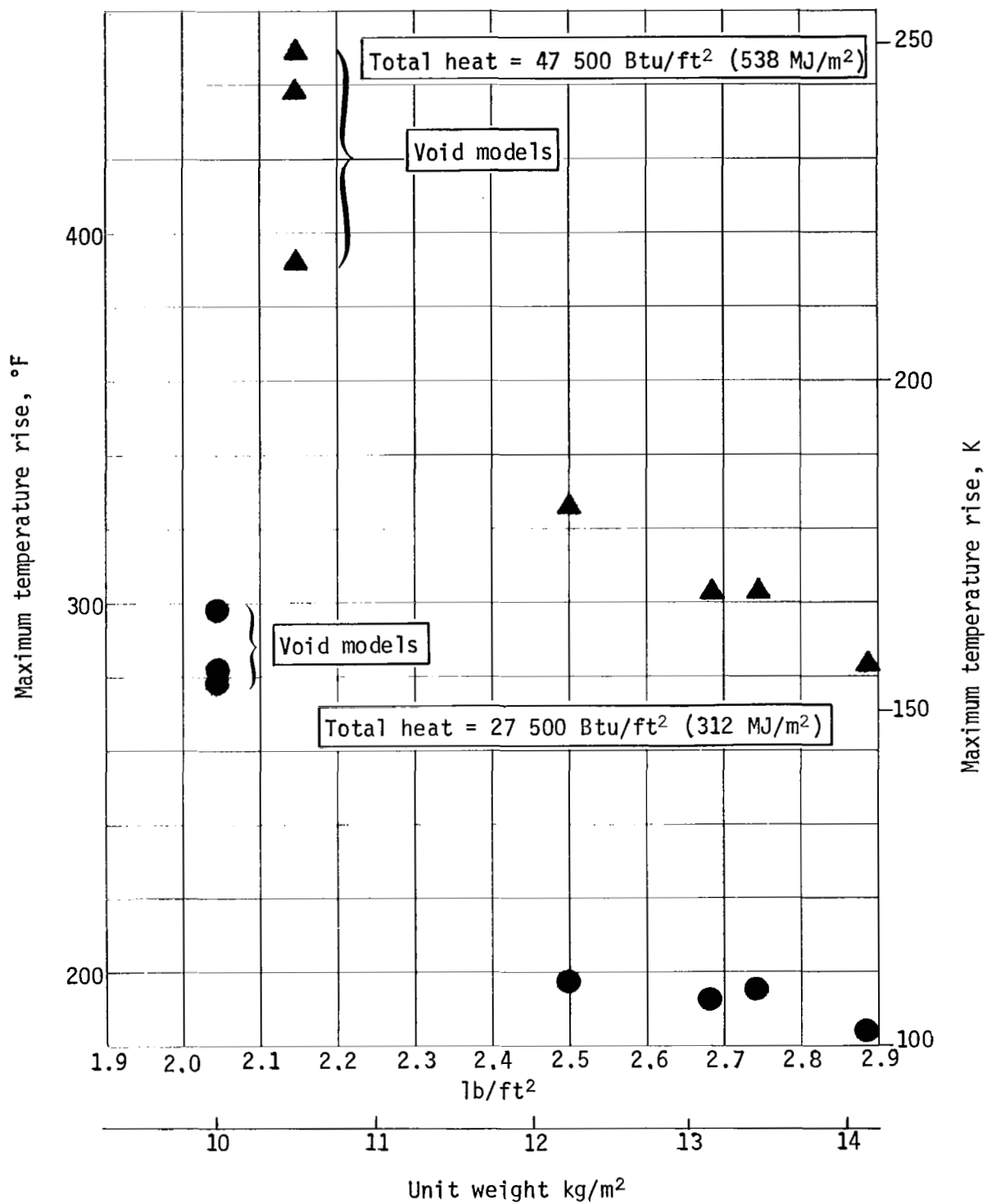


Figure 47. - Effect of Unit Weight on Backface Temperature Rise

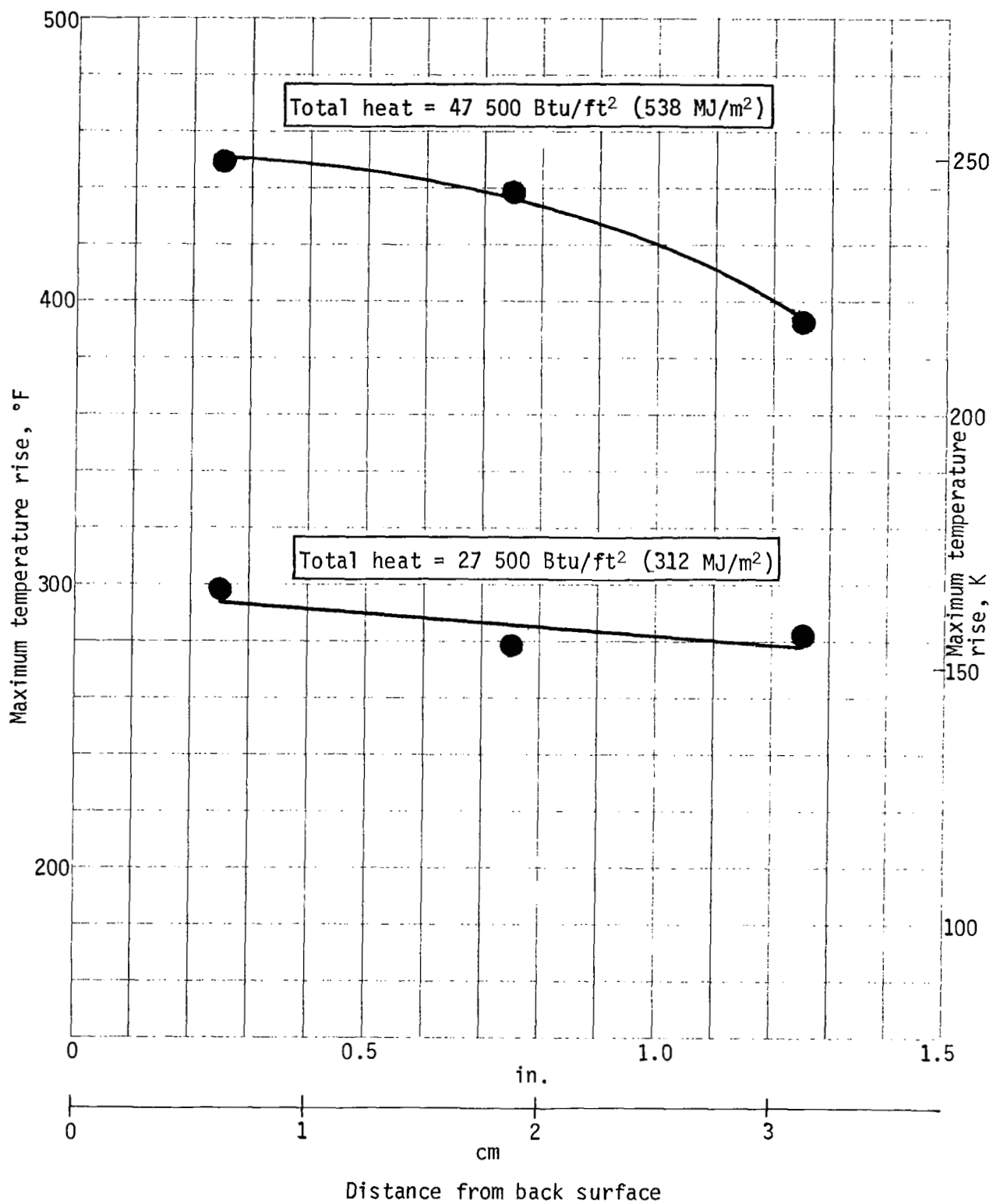


Figure 48. - Effect of Void Location on Backface Temperature Rise

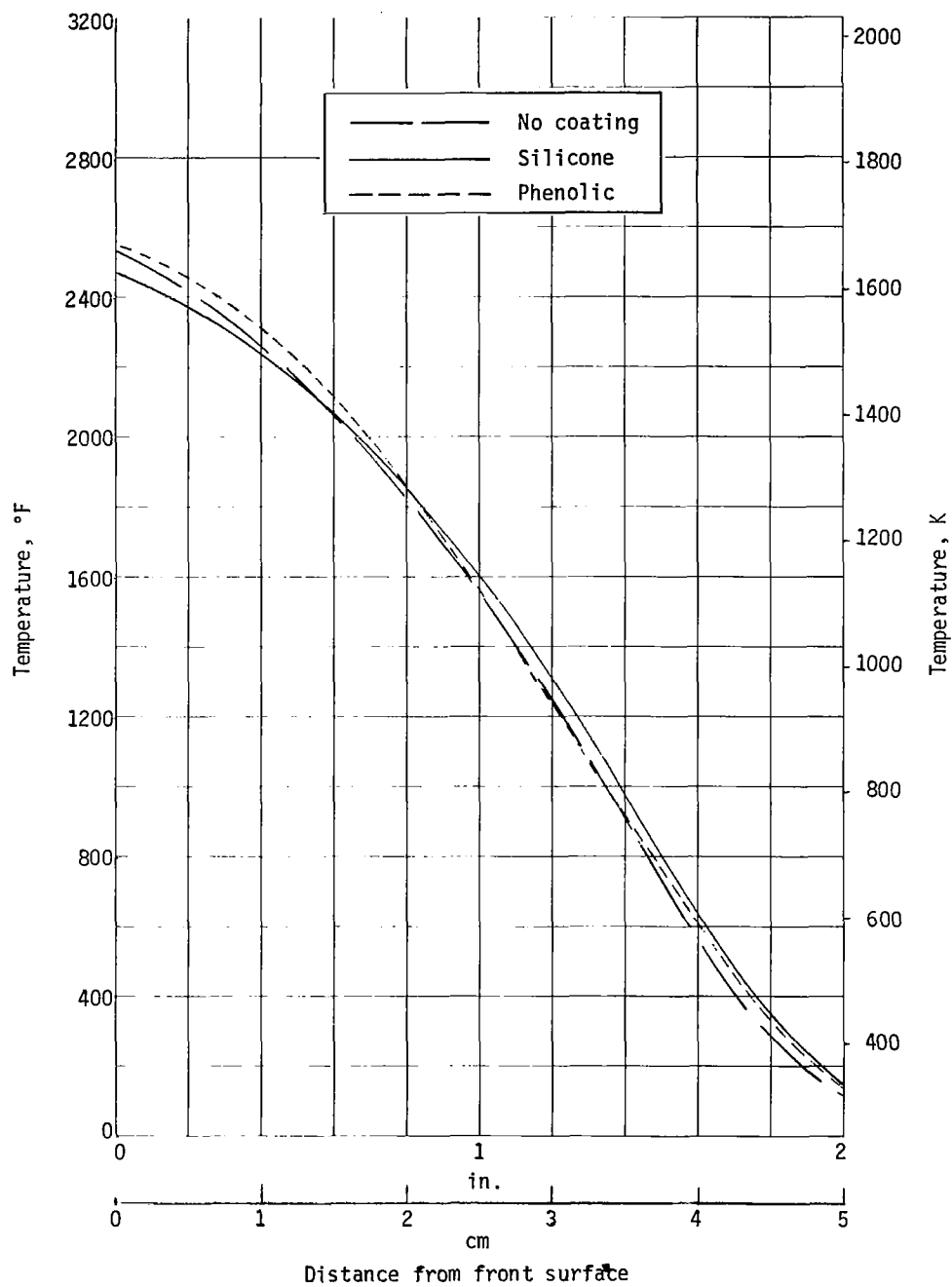


Figure 49. - Bond Coat Effects on Temperature Profile, High-Flux End of Heating

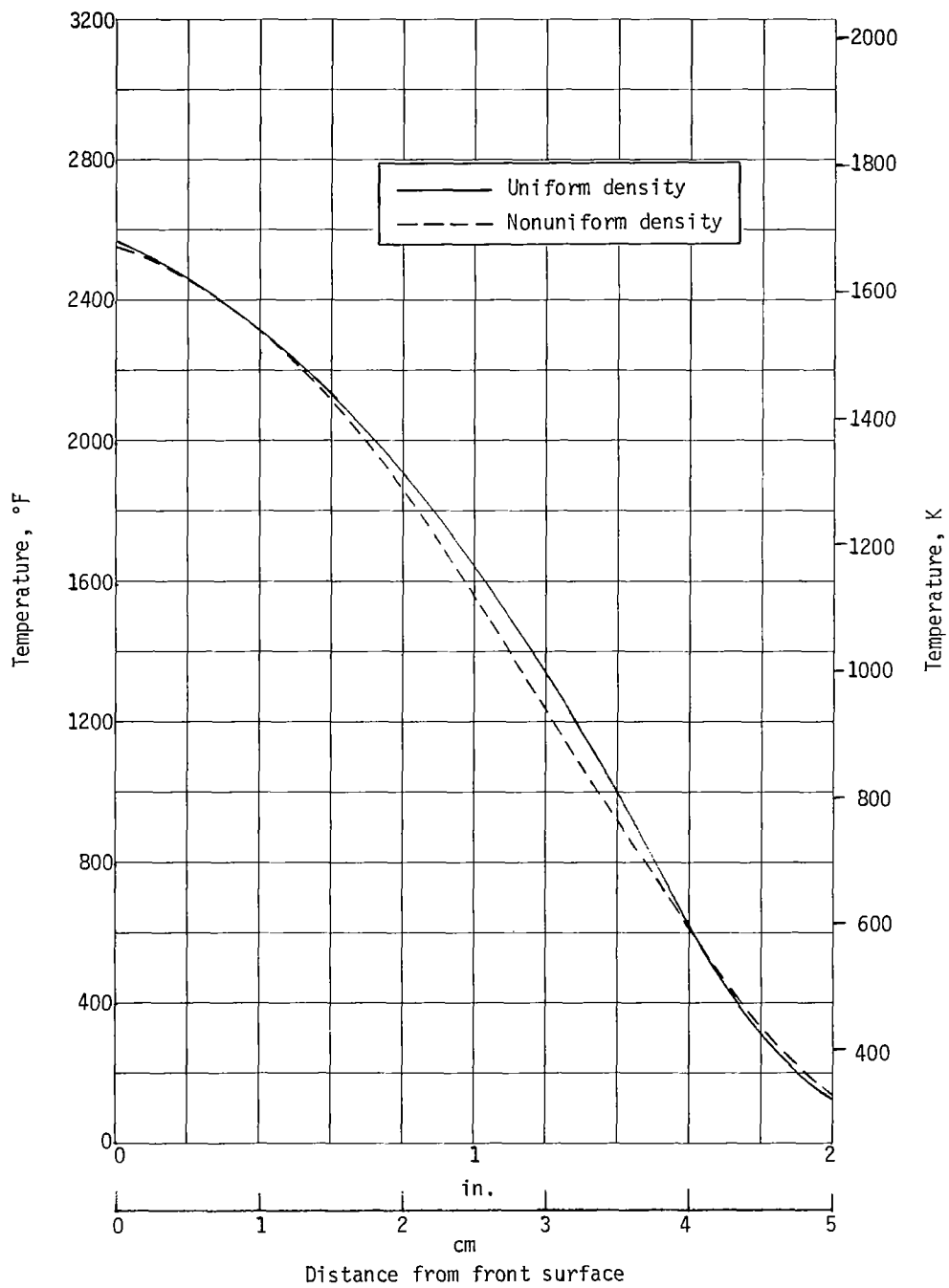


Figure 50. - Density Uniformity Effects on Temperature Profile, High-Flux End of Heating

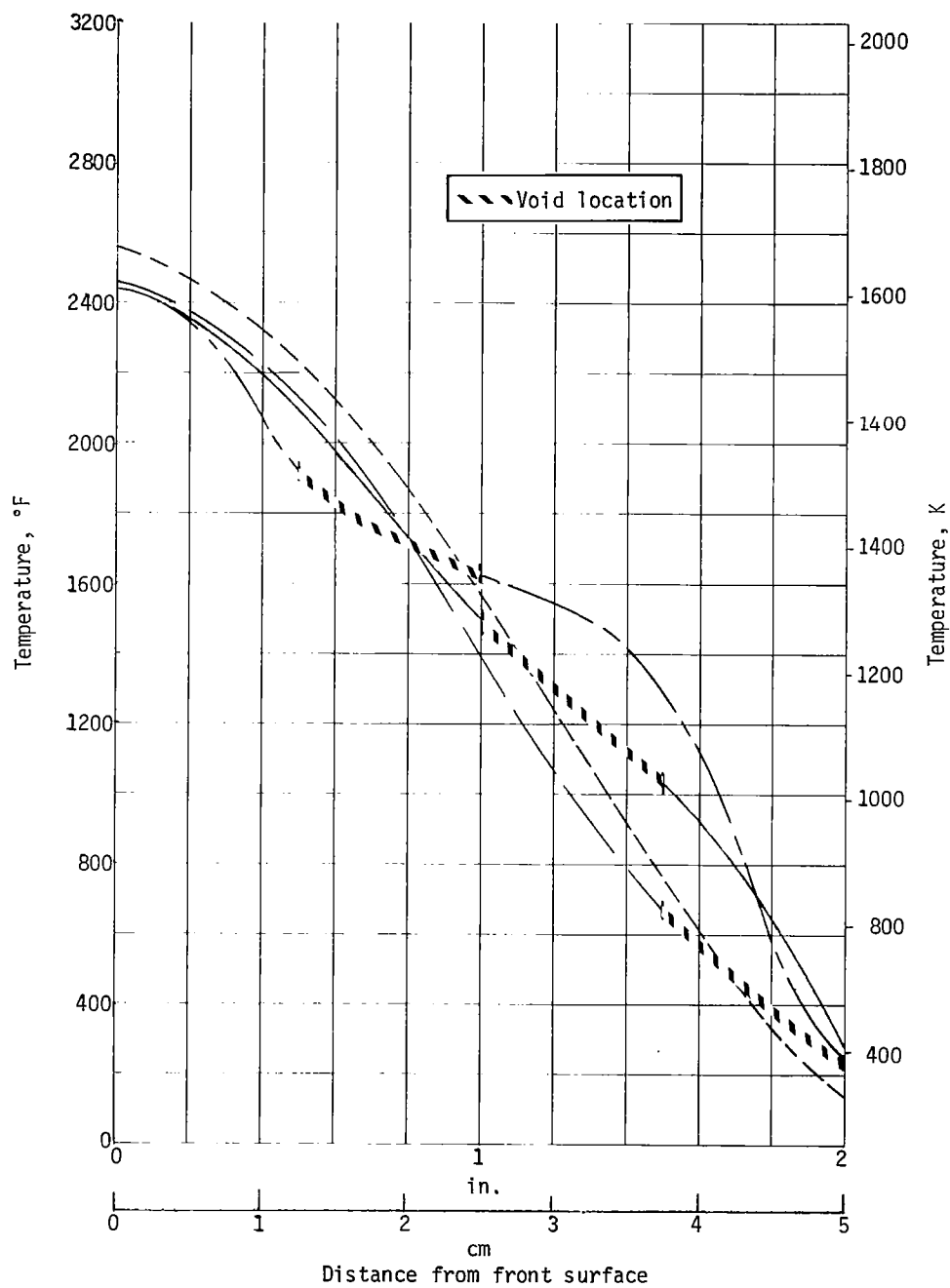


Figure 51. - Void Effects on Temperature Profile, High-Flux  
End of Heating

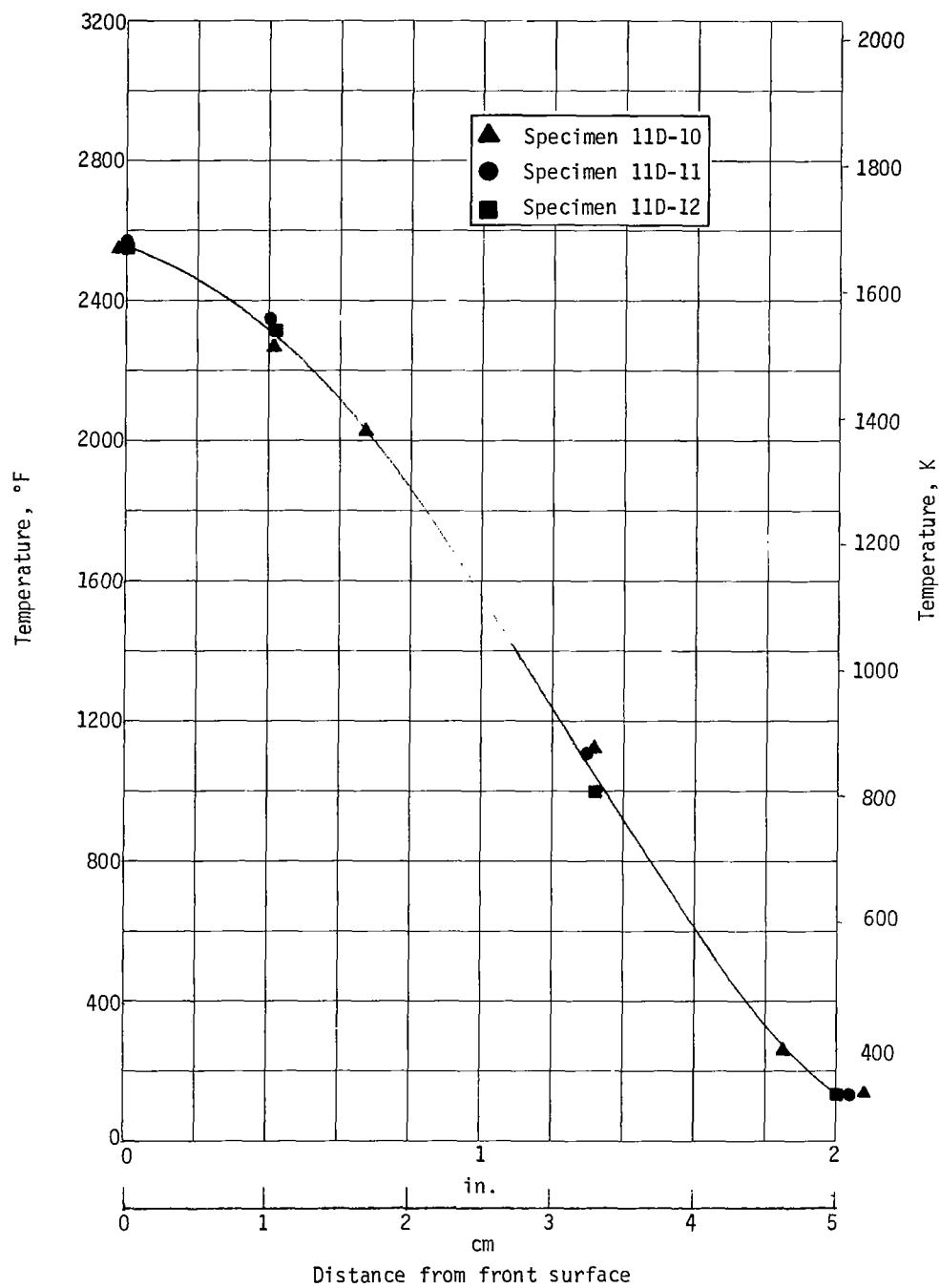


Figure 52. - Baseline Temperature Profile, High-Flux  
End of Heating

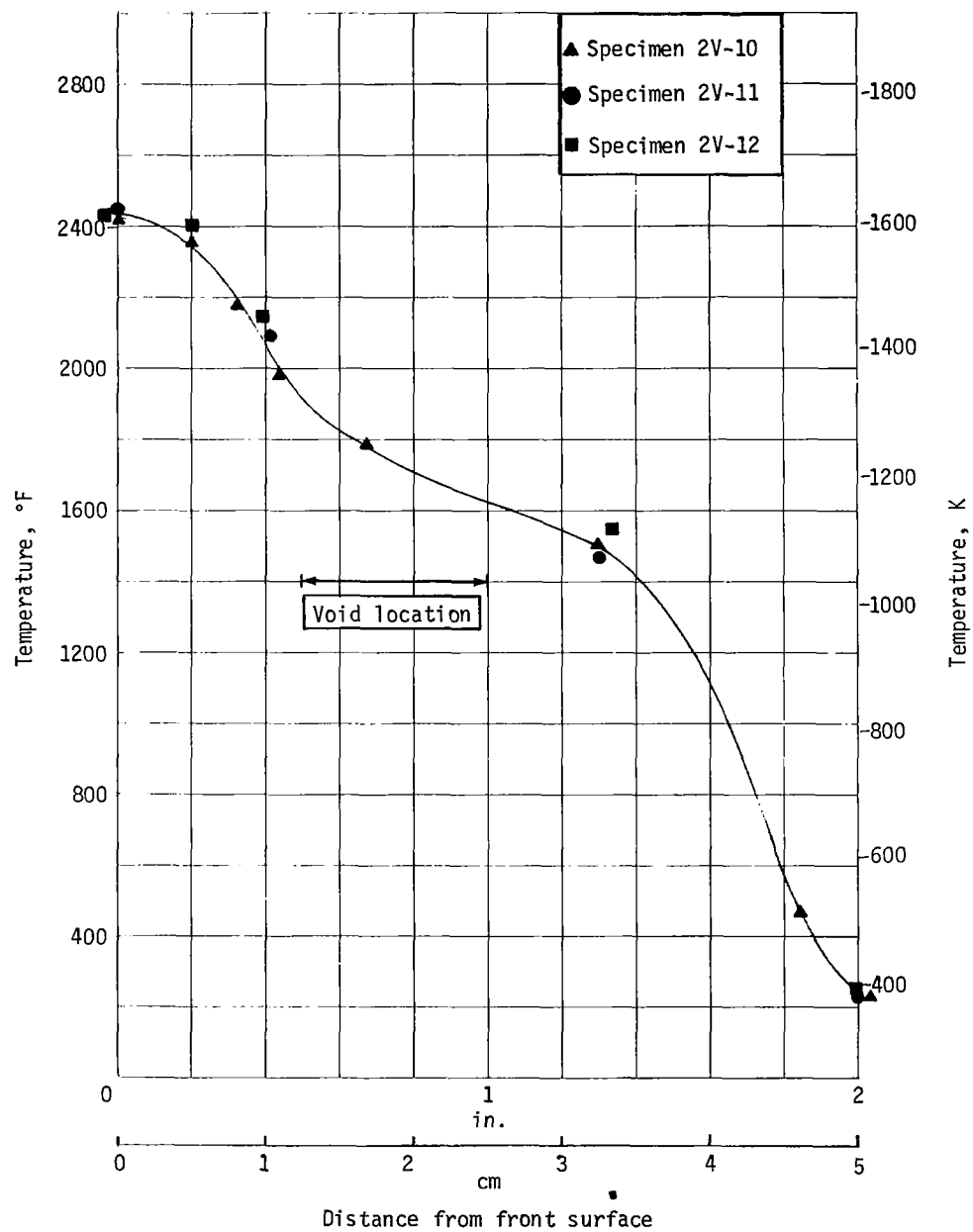


Figure 53. - High Void Temperature Profile, High-flux  
End of Heating

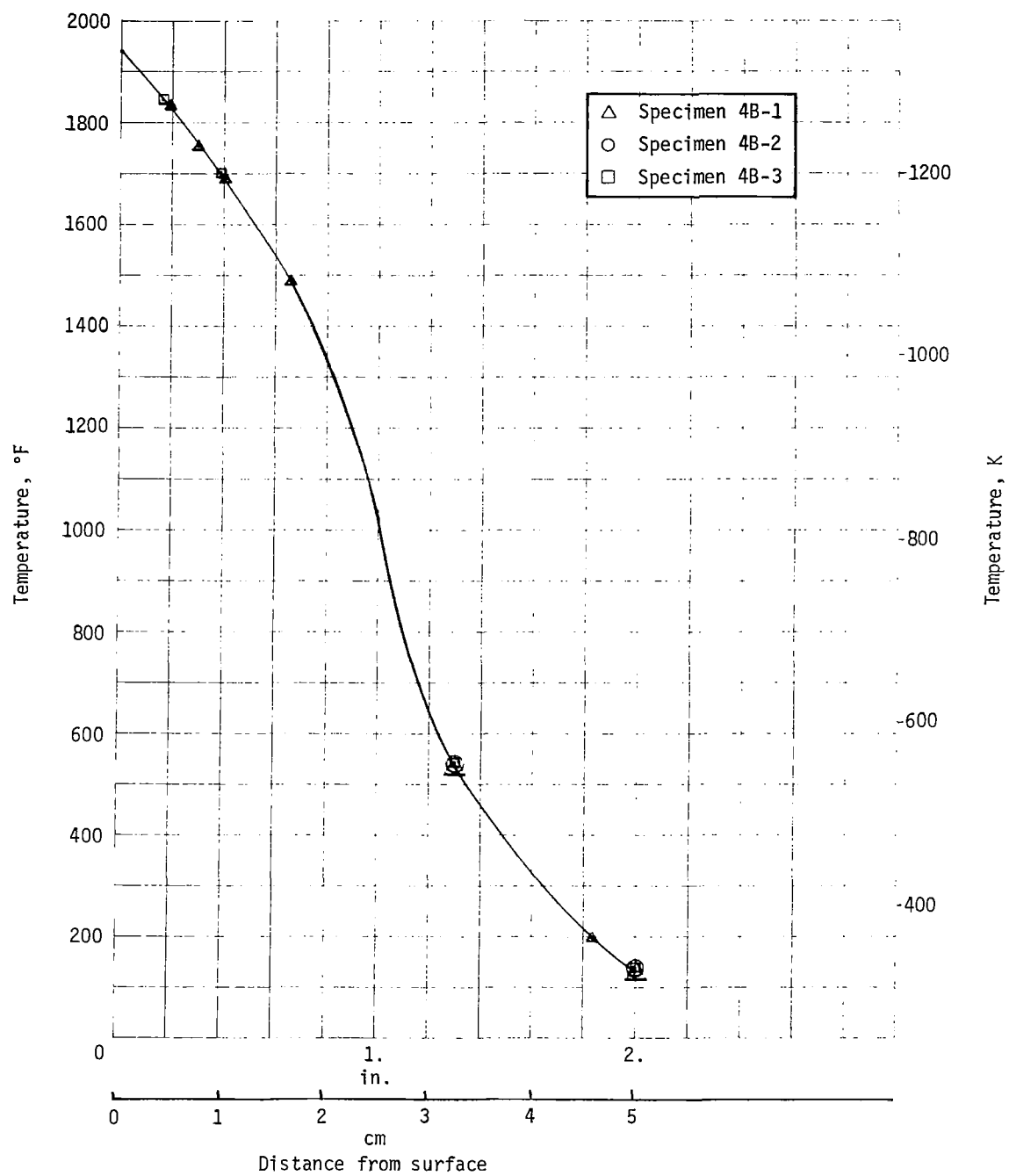


Figure 54. - Baseline Temperature Profile, Low-Flux  
End of Heating



Density uniformity.- In figure 50, the effect of density uniformity from front to back surface on temperature distributions is shown for the 11D and 19S series specimens. The density distribution was verified by electronically determining the relative radiographic densities by a video analyzer system. A video presentation of a radiograph of specimen 11D-11 illustrating a relative density increase from the face sheet to the panel surface was shown in figure 6. Relative radiographic density measurements were obtained along the ordinate line through the center of the image. A video presentation of the relative radiographic density of specimen 19S-1 also shown illustrates the uniformity produced by the "two-side" packing method. Noise in the trace on this specimen is due to the glass cloth wrapped around the specimen after installation of the thermocouples.

Both sets of specimens had essentially the same surface temperature, although the 11D series exhibits higher temperatures in the char layer and pyrolysis zone with a subsequent crossover to lower temperatures within the virgin material. The diffusivity argument used previously does not seem to explain this difference. Since total mass is a constant for these specimens, perhaps we are seeing only the conductivity effects. Thus, near the surface the conductivity is higher in billet 11D due to both higher density and the local breakage of microspheres during core loading. Nearer the face sheet, the density drops below billet 19S and conductivity drops accordingly.

Voids location effect: The effect of void location on temperature distribution is presented in figure 51. The results of the 11D control specimen tests are shown for reference. It can be seen that the surface temperature is roughly 150°F (83K) cooler for all the void specimens despite the fact that measured heating rates are within the specified  $\pm 5\%$  tolerance. This can be explained by the temperature distributions within the void specimens. The temperatures immediately behind the voids are about 500°F (533K) higher than those at corresponding locations in the control specimens, indicating that heat transferred by radiation at the char temperature is greater than that conducted by the ablative filler. This same effect was true for all three void placements.

Weight loss.- Weight loss was not significantly affected by any of the defects investigated, with the exception of density uniformity specimens (fig. 55). Uniform density specimens showed lower weight loss at both high and low heat flux levels, because of the difference in mass distribution within these specimens.

Surface temperature.- Surface temperatures (average values) and scatter bands for the two test conditions are compared in figure 45.

Data scatter and trends.- Data scatter present in the back surface temperature measurements is presented in figures 56 and 57. Minimal scatter  $\pm 3$  to 15°F (1.7 to 8.3K), between "identical" specimens is noted in figure 56 as expected since all three specimens were tested together at the low heat flux condition. At the high heating condition, typical scatter was  $\pm 8$  to 30°F (4.5 to 16.5K) and can be attributed in part to test condition variations from one facility operation to the next.

Maximum temperature rise trends are shown in figures 46 through 48 for density, ablative composite unit weight, and void location.

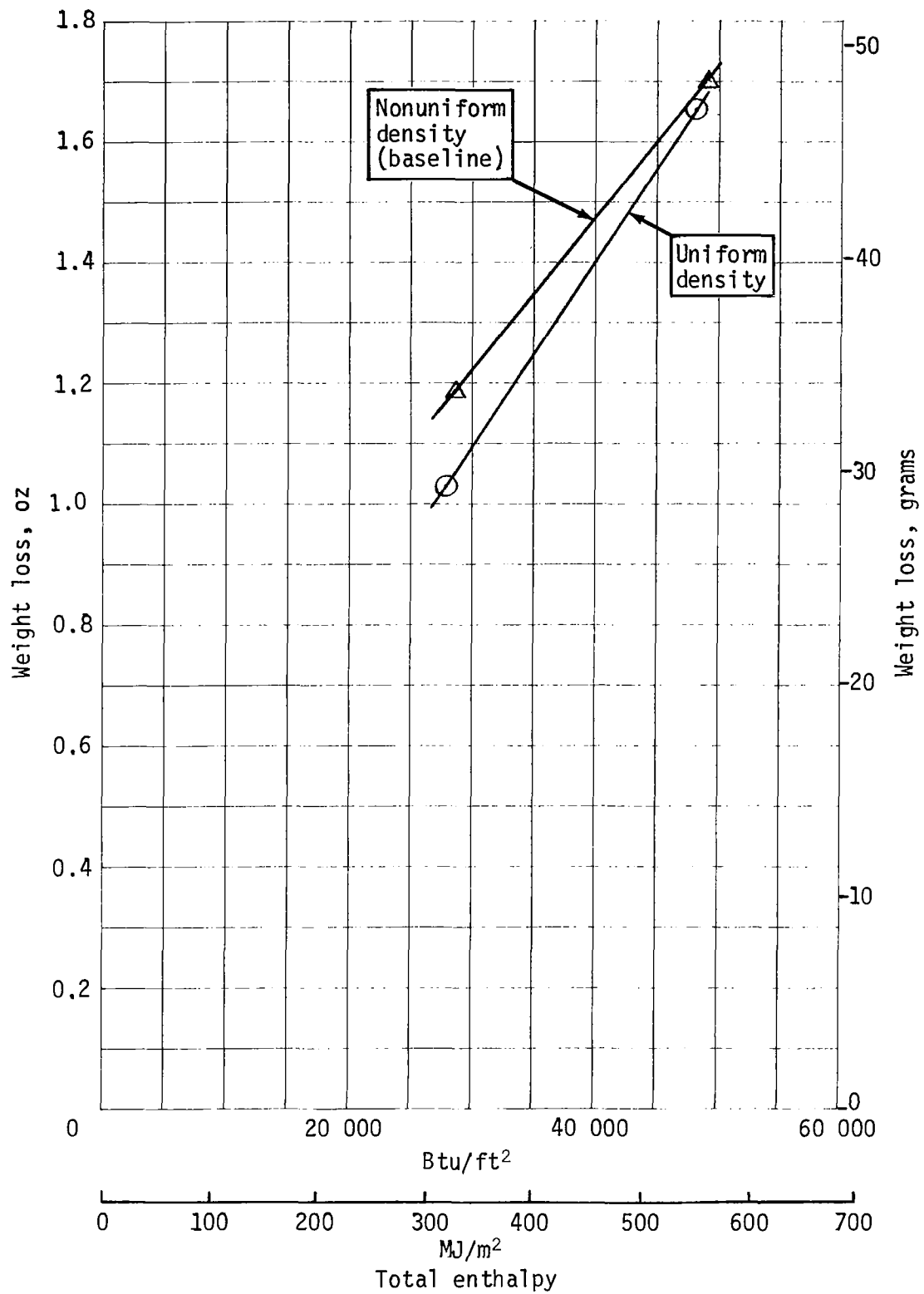


Figure 55. - Effect of Density Distribution on Weight Loss

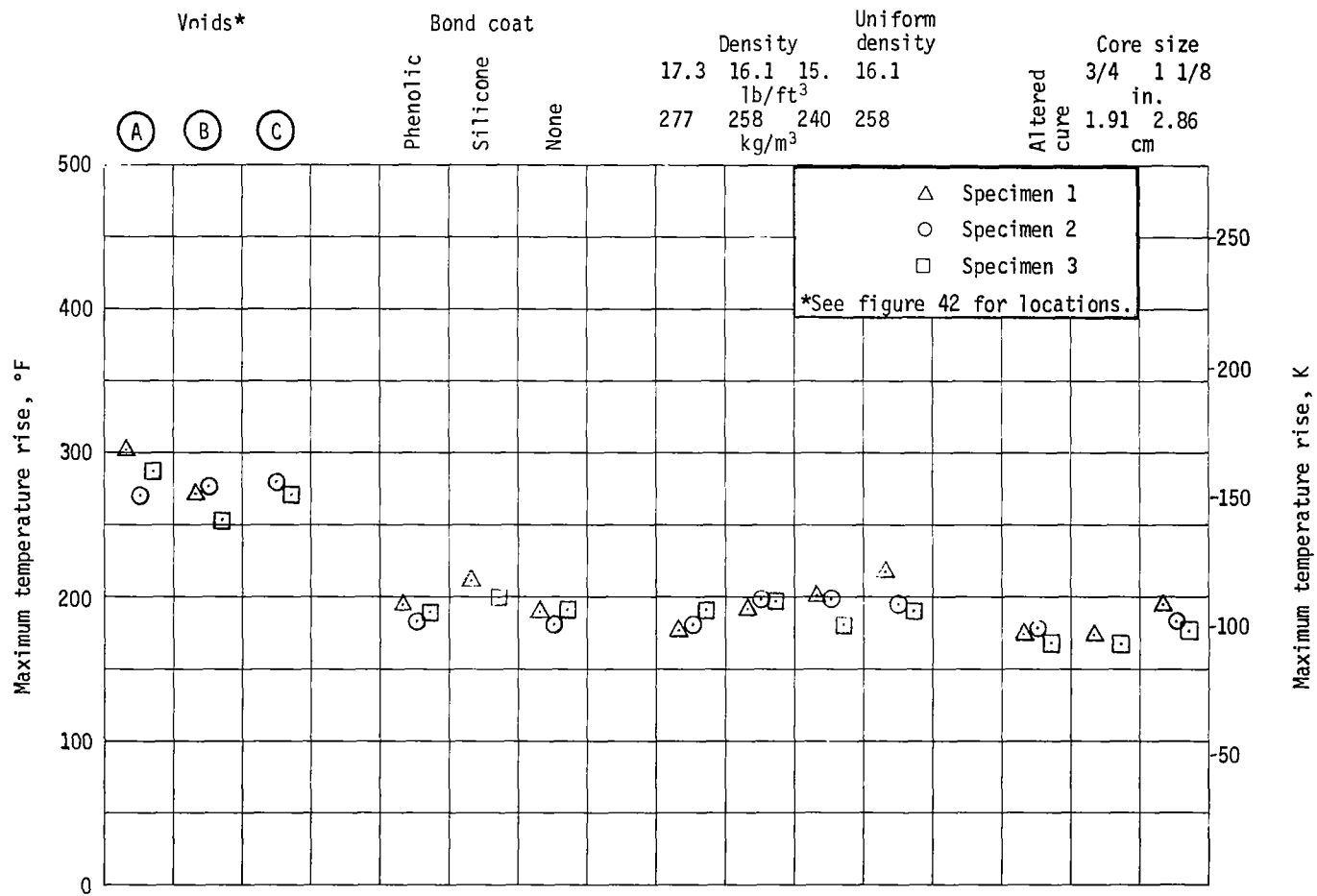


Figure 56. - Data Scatter, Low Flux

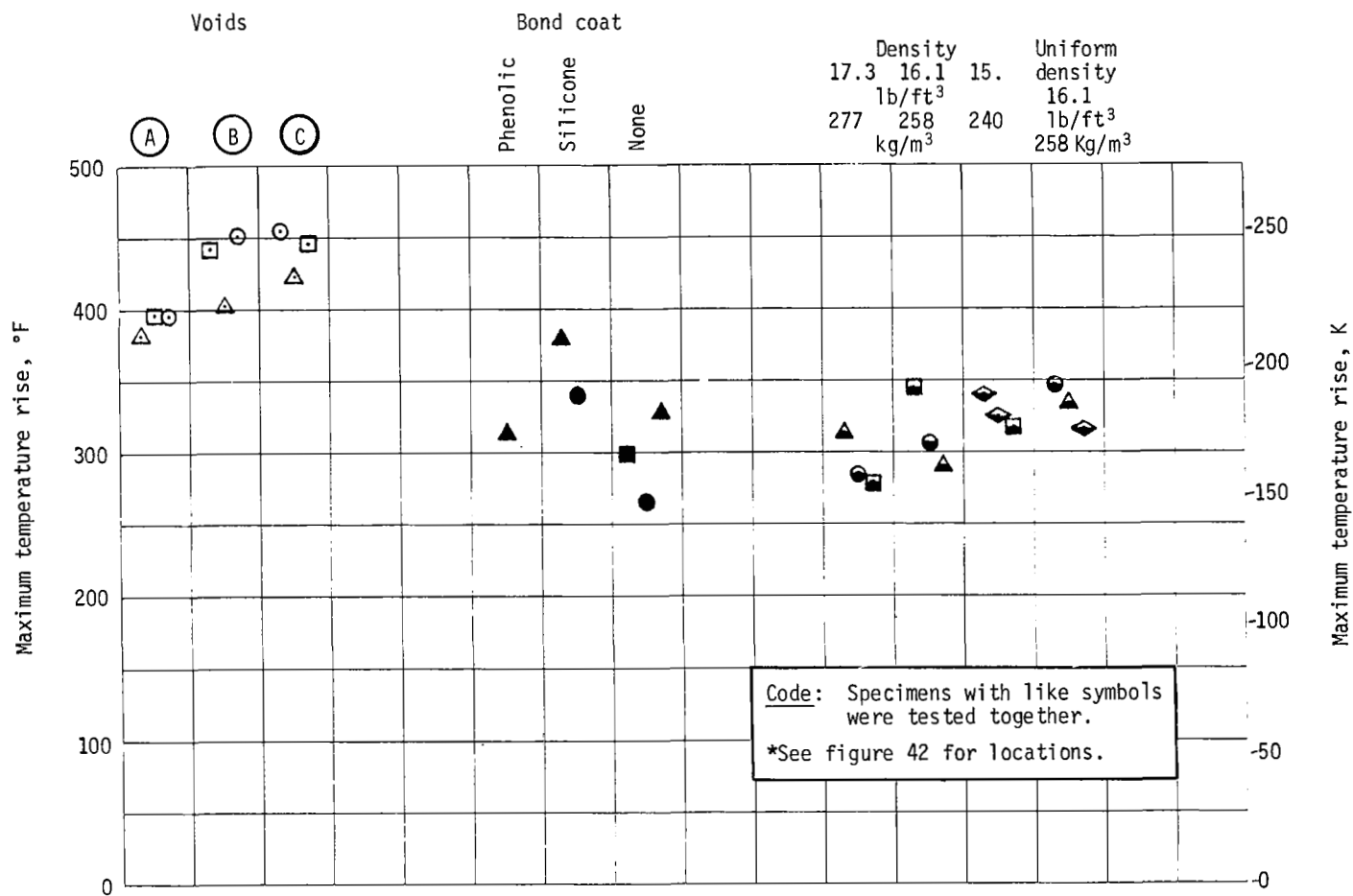


Figure 57. - Data Scatter, High Flux

Visual observations.— Typical ablation characteristics are shown in figures 58 through 71. These characteristics are discussed in the following paragraphs.

**Low heat flux, general:** The low heat flux specimens generally had a reddish brown solid surface without cracks or loss of char. Below the surface the char was very weak with cracks predominantly parallel to the surface. A 0.06- to 0.1-inch (0.152- to 0.254-cm) high void or large crack was noted just below the surface (fig. 60). The honeycomb in these specimens was intact with the surface, and ablation depths reached 0.95 to 1.15 inch (2.41 to 2.94 cm) below the surface.

**High heat flux, general:** High heat flux specimens had a black surface coating on very weak silica ash. This silica layer was typically 0.07-inch (0.178-cm) thick and the honeycomb was gone to the same depth. The char below the surface was very weak and showed multiple cracks parallel to the surface (fig. 61). The char was not attached to the honeycomb and was free to shift in most models while the ablation depth ranged from 1.28 to 1.60 inches (3.5 to 4.07 cm).

**Bond coating specimens:** All low heat flux specimens had the typical void just below the surface. Below this void, the noncoated models had integral char that was not bonded to the core and therefore shrank without cracking. The bond-coated models had one or more cracks in the char in addition to the void next to the surface.

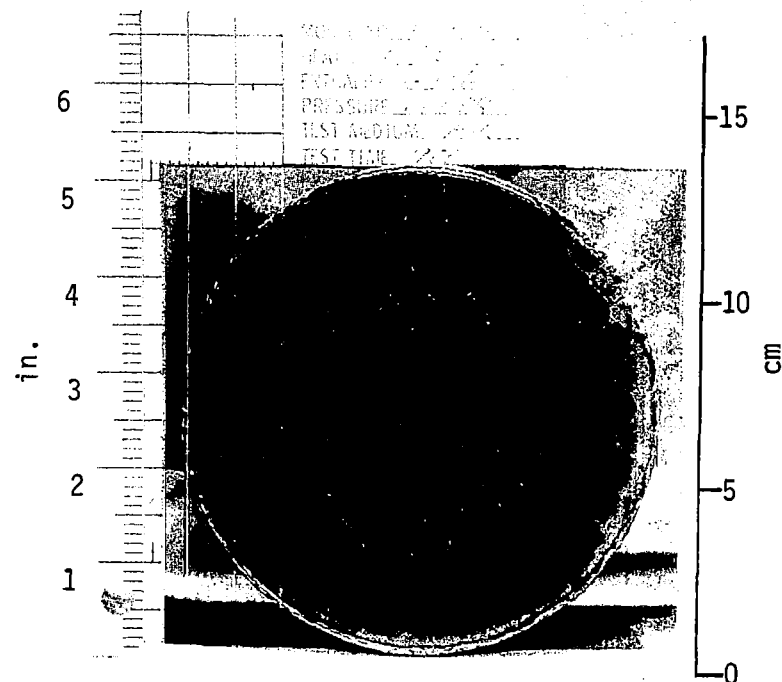
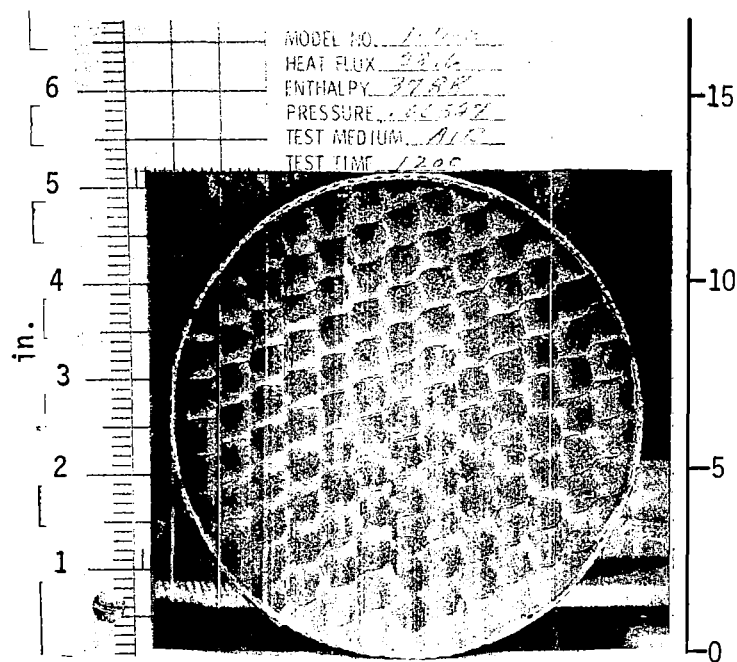
The high heat flux models had multiple cracks in the char regardless of the type of bond coating. The silicone bond-coated models experienced deeper ablation penetration than the phenolic and uncoated models, 1.60 versus 1.46 inches (4.07 versus 3.71 cm) respectively, thus substantiating temperature measurements.

**Density:** The low heat flux models all had an integral char surface, while the char appearance for the low-density models had more cracks than the models with normal and high density. At the high heating rate, char strength was directly proportional to density, and ablation depth was inversely proportional to density at both high and low heat fluxes (fig. 62).

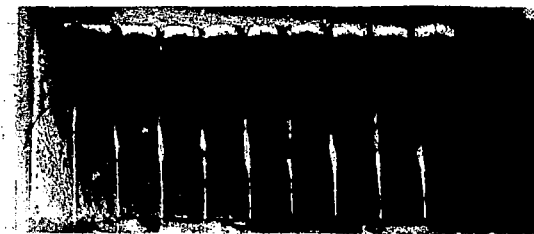
**Voids:** The ablation depth on these models was significantly higher than for models without voids (fig. 59) and, for the high heat flux, the char extended to both sides of the voids located at positions A and B.

**Large honeycomb:** Honeycomb with 3/4-inch (1.905-cm) and 1-1/8-inch (2.86-cm) cell sizes were tested at low heating conditions only. The 3/4-inch (1.905-cm) honeycomb did not significantly affect the surface or char characteristics (fig. 60). Tests with the 1 1/8-inch (2.86-cm) honeycomb resulted in a strong surface but some cracks. The char had the typical void below the surface except that it was larger. Cracks in the char were perpendicular to the surface (fig. 60) and the ablation depth was less than normal at 0.97 inch (2.46 cm).

**Density uniformity:** The uniform-density models tested at the low heat flux did not have the typical void below the surface; however, a series of parallel cracks was evident and similar to the typical high-flux models. Other char characteristics at high and low flux were typical.

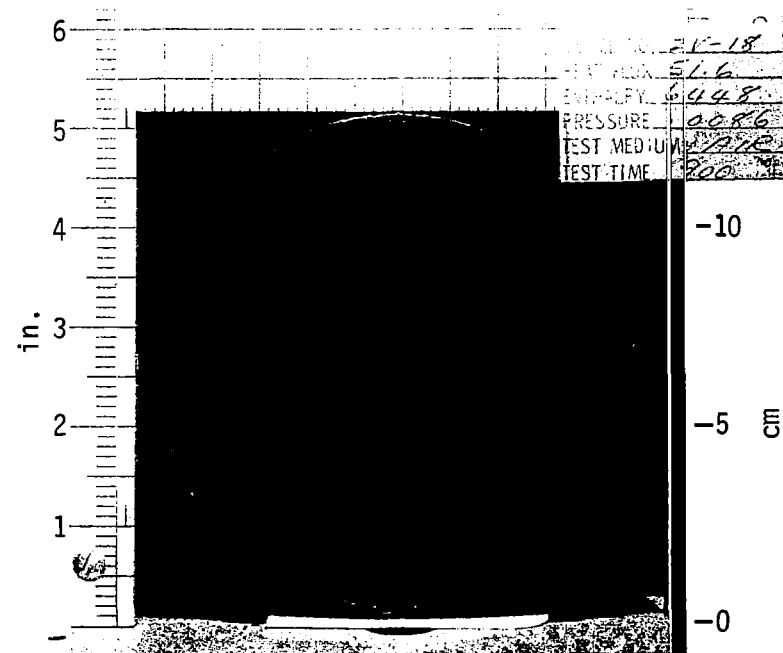
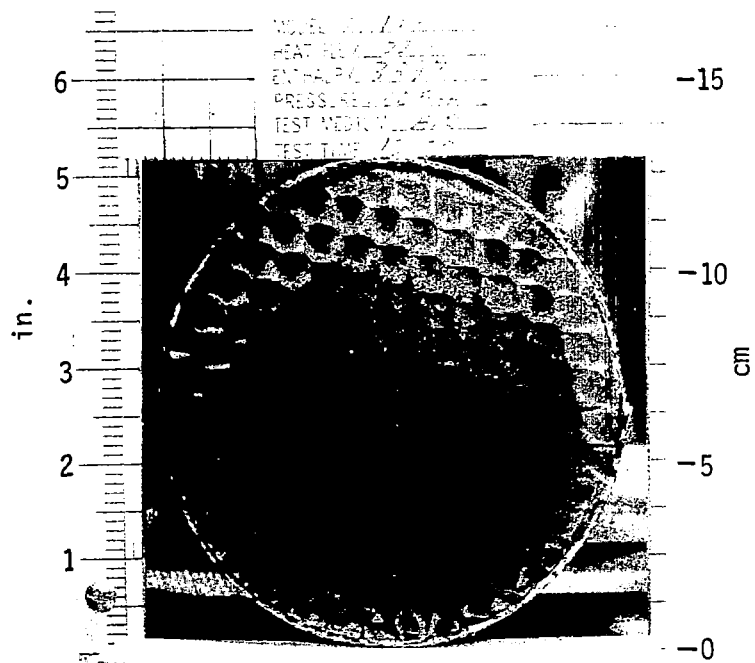


11D-8 Low flux

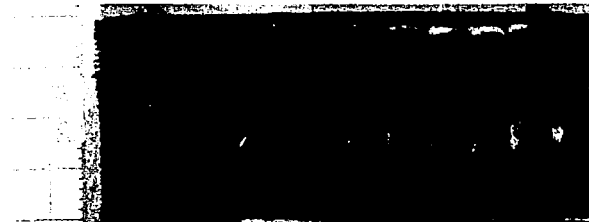


11D-11 High flux

Figure 58. - Charred Plasma Arc Specimens, Nominal Density

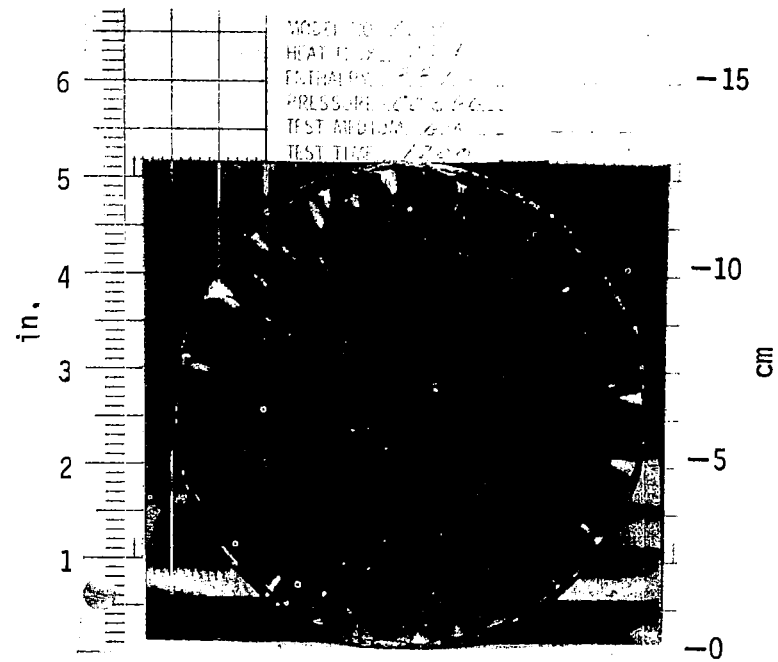
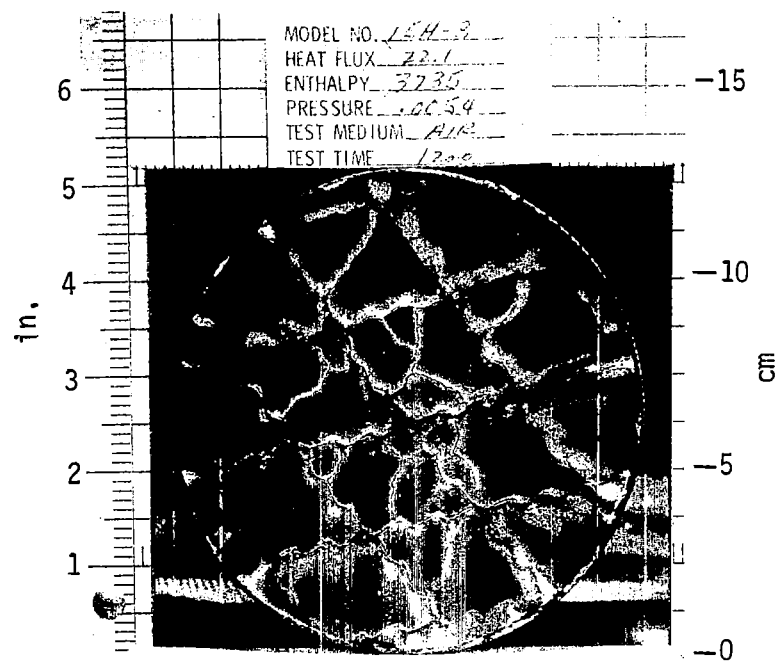


1V-8 Low flux



2V-18 High flux

Figure 59. - Charred Plasma Arc Specimens, Backface Void



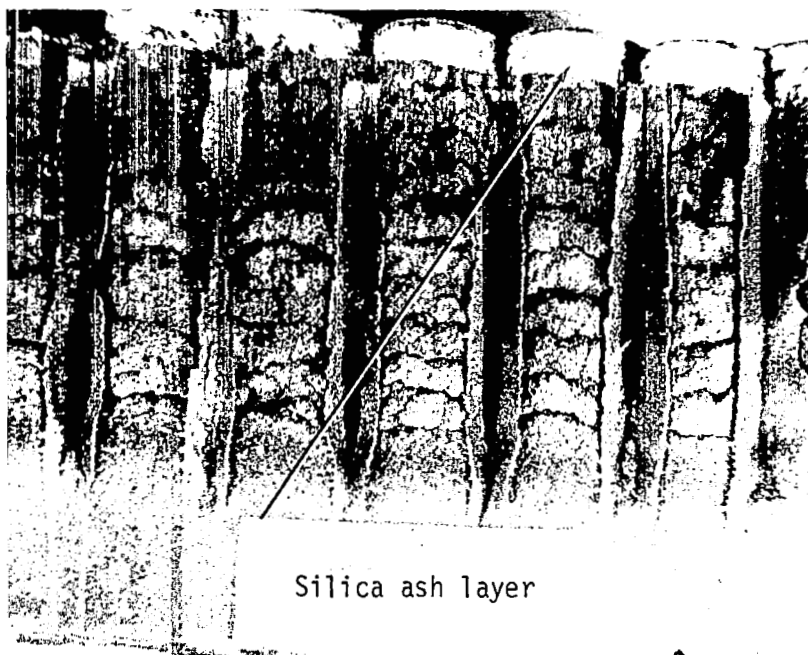
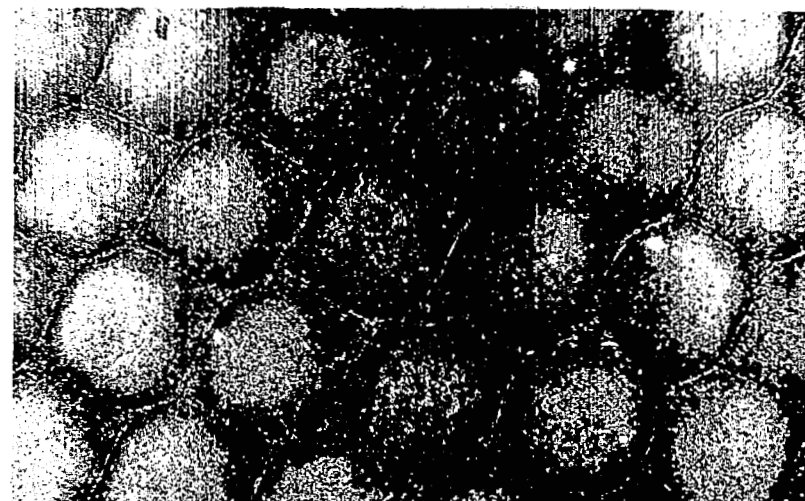
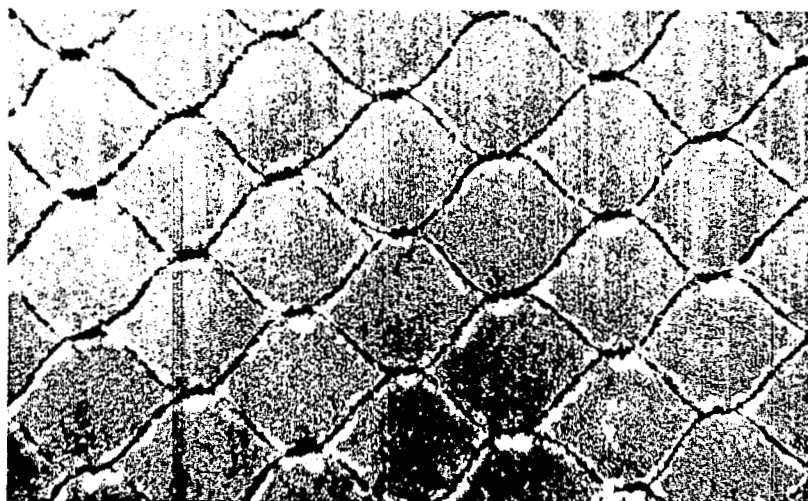
15H-3 1 1/8-in. (2.855-cm) Honeycomb, low flux



15H-5 3/4-in. (1.905-cm) Honeycomb, low flux

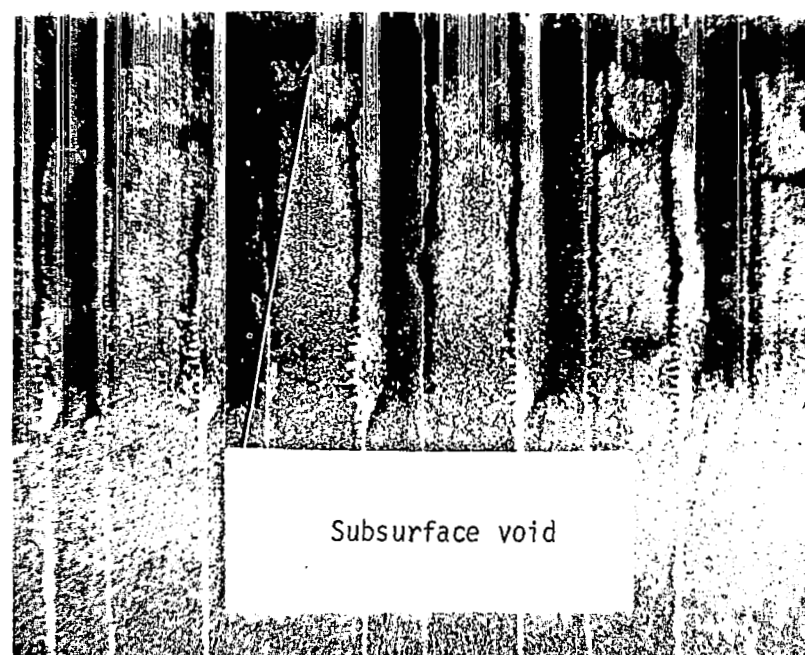
Figure 60. - Charred Plasma Arc Specimens, Large honeycomb





Silica ash layer

High flux



Subsurface void

Low flux

Figure 61. - Typical Char Surface and Cross Section, 2X Magnification

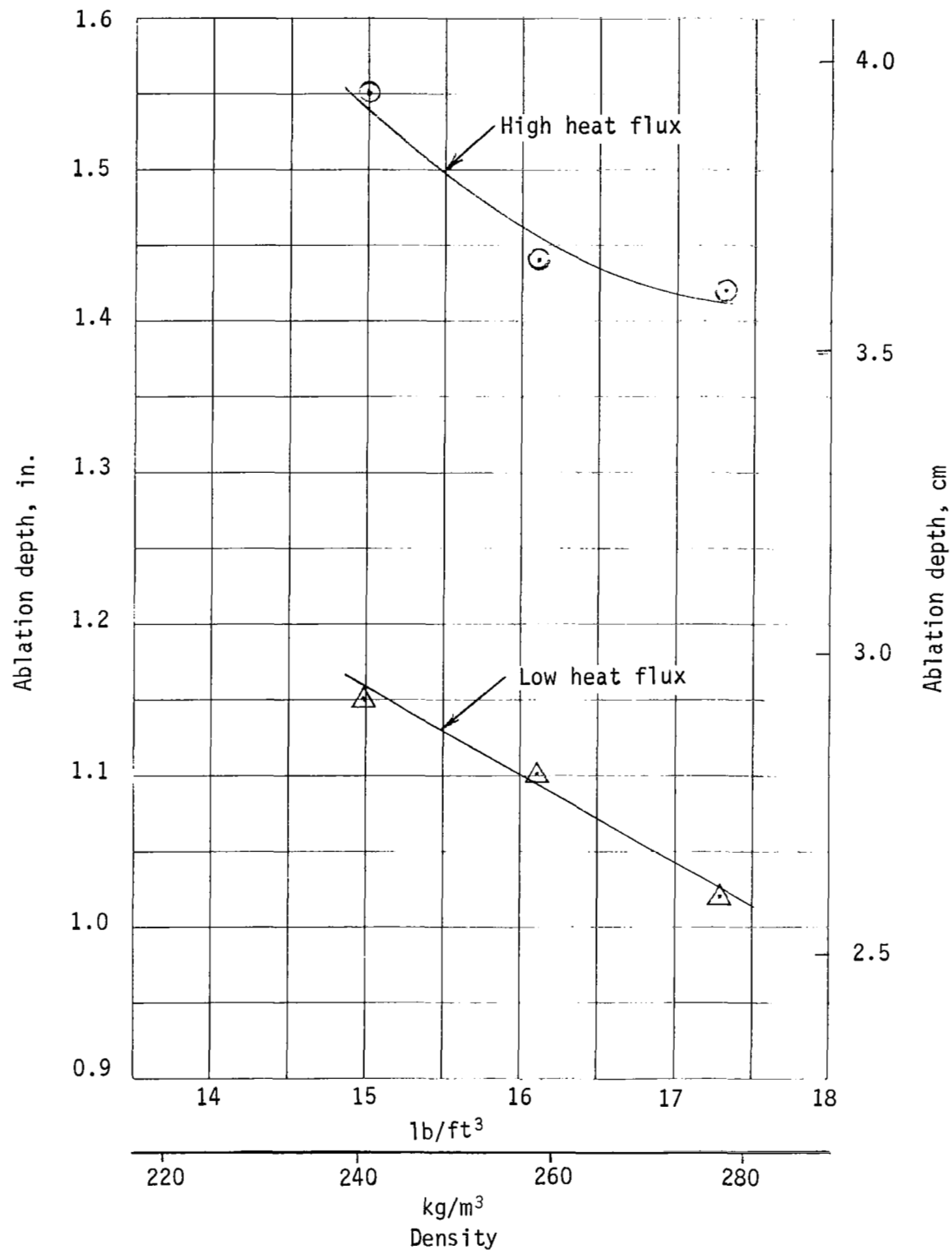


Figure 62.- Ablation Depth vs Density

## Physical Property Data

Tensile tests were run with the honeycomb ribbon direction transverse to the direction of loading and five specimens were tested at each condition. This type of material is subject to more variations than a homogeneous material. Thus, the strength of each specimen is subject not only to normal variations such as machining, minute voids, etc, but also to honeycomb node bond, honeycomb filler bond, and filler strength. This results in more panel-to-panel and specimen-to-specimen scatter than with a homogeneous material. Figures 63 through 65 demonstrate this type of variation.

Tensile specimens were tested to evaluate the following parameters:

- 1) Honeycomb bond coating;
- 2) Density variations of ablative filler;
- 3) Cure cycle variations;
- 4) Omission of fibers;
- 5) No honeycomb core.

Honeycomb bond coating.— The tensile strength of filled honeycomb ablators strongly depends on the bond between the honeycomb and filler. Low strength and/or low ultimate elongation can result in bond failures during thermal cycling.

Task I of this program pointed out problems using silicone as a bond coating.\* A review of other contracts suggested the use of SC1008 phenolic varnish as a bond coating. A series of tests was completed to evaluate the use of silicone and phenolic bond coating compared with no coating. Tensile properties are shown in figures 66 through 68. Typical failures are shown in figure 69.

No coating: A bond coating appears to be necessary to achieve tensile strength in the ablative composite. Without any coating, tensile failure occurs at the honeycomb/ablator interface. Strength and ultimate elongation were less than half those of the bond-coated panels (fig. 66 and 67).

Silicone bond coat: Dow Corning 182 resin was selected for the silicone bond coat so it would cure in with the resin in the ablative mix. Although adhesion with this system was very good, tensile strength of the panels was somewhat less than that of the phenolic bond coat (fig. 66). These specimens failed across the ablative material without any sign of unbonding.

---

\**op cit.*

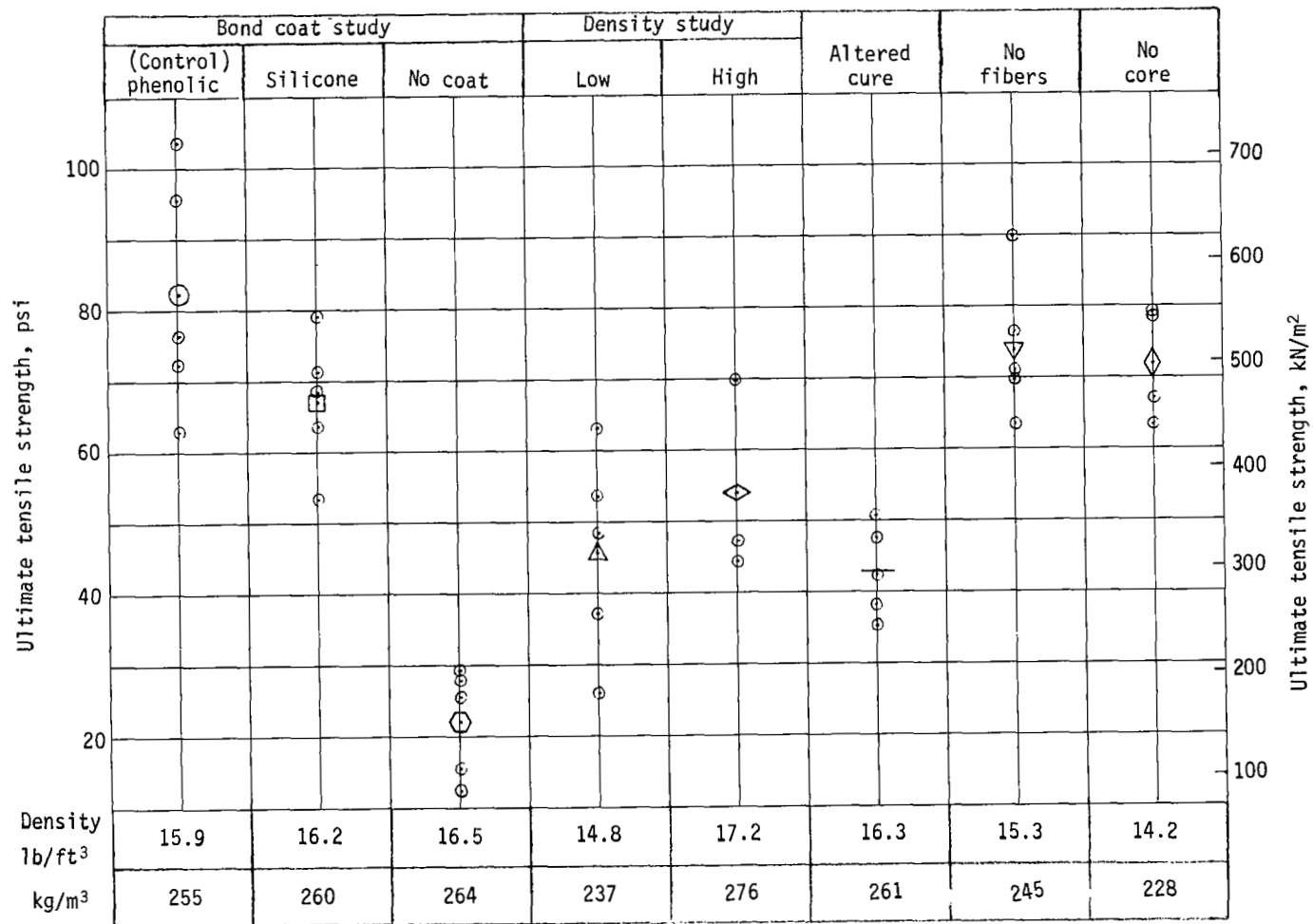


Figure 63.- Tensile Strength at Ambient Temperature



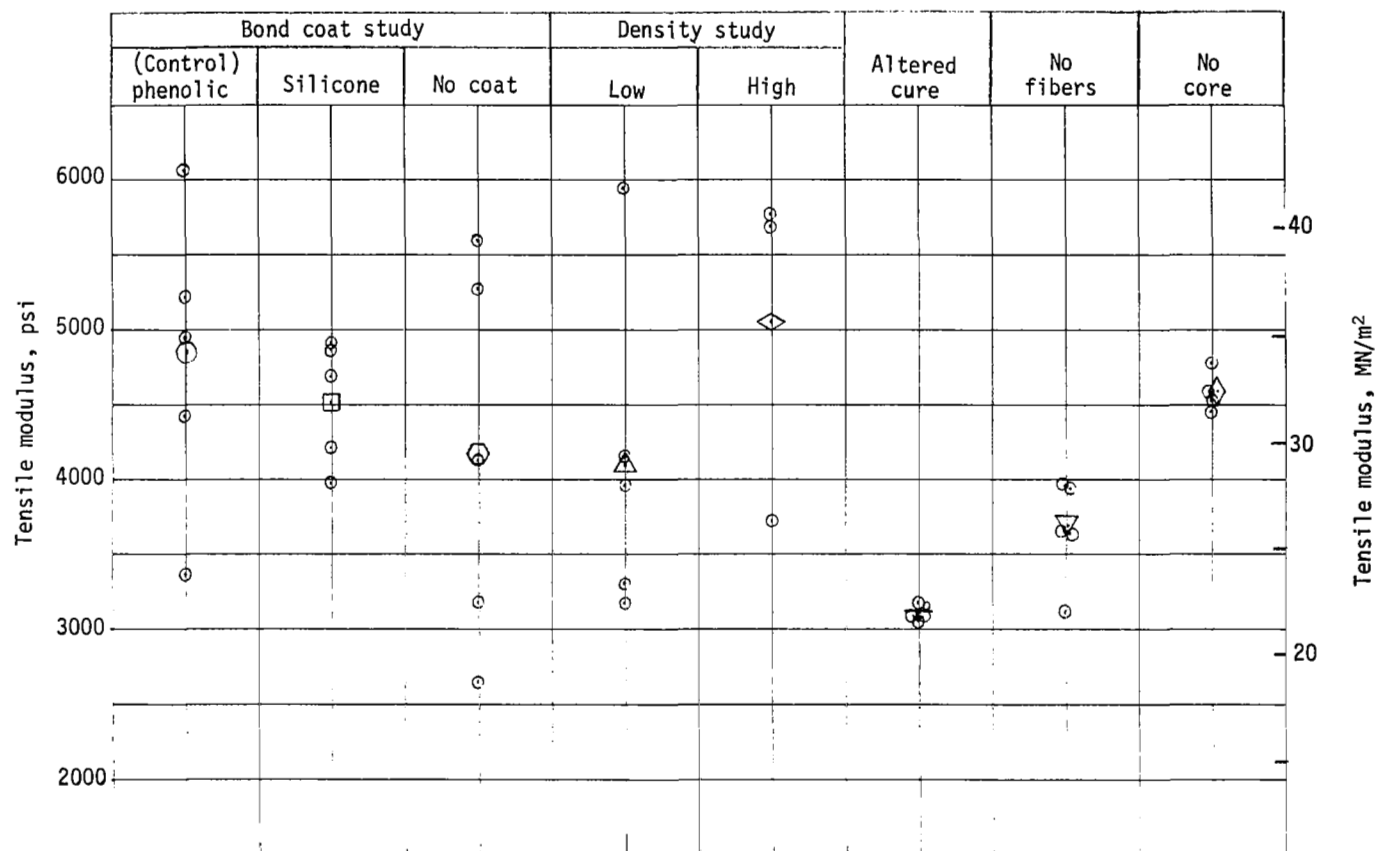


Figure 65.- Tensile Modulus at Ambient Temperature

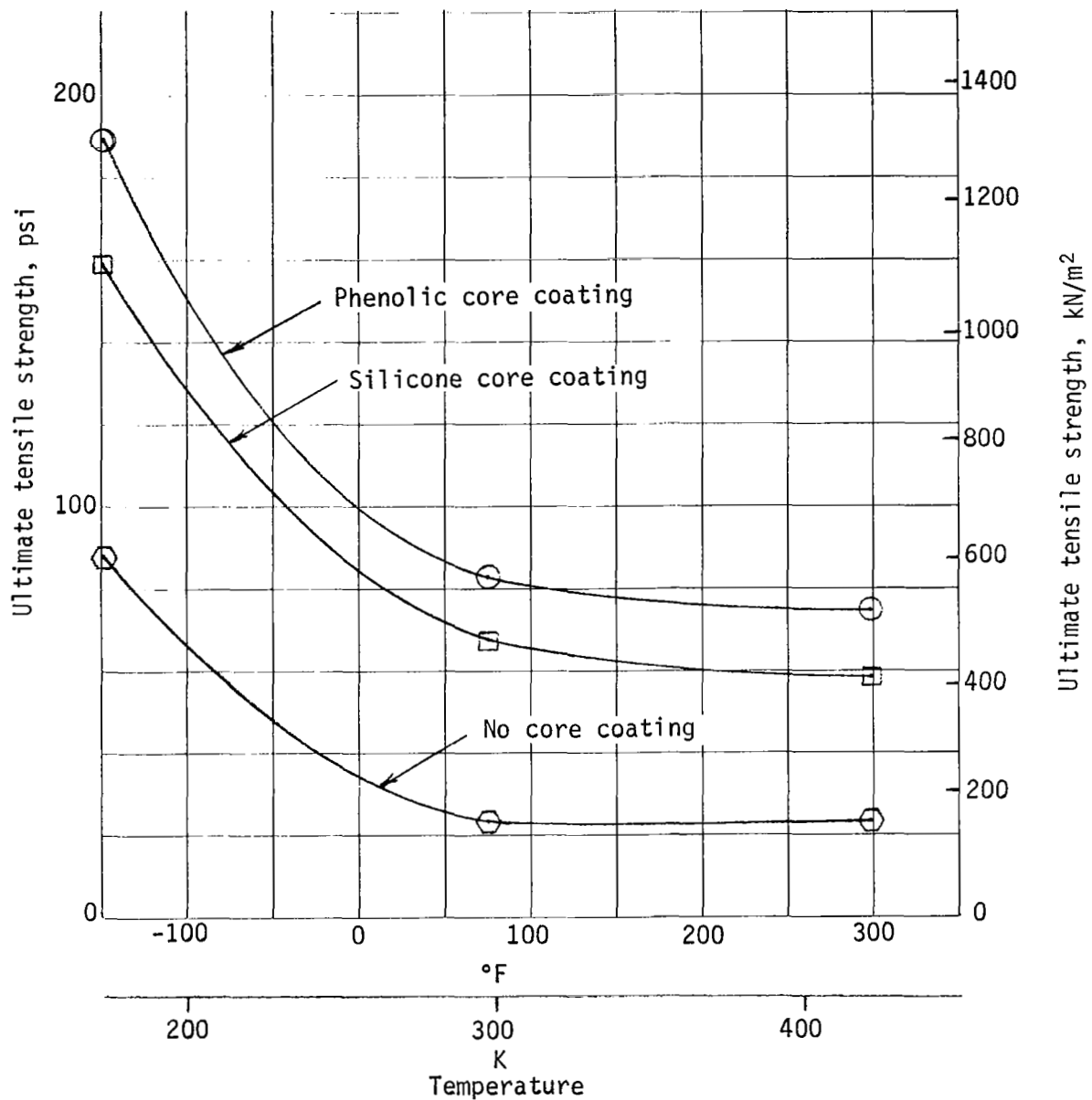


Figure 66.- Effect of Core Coating on Tensile Strength

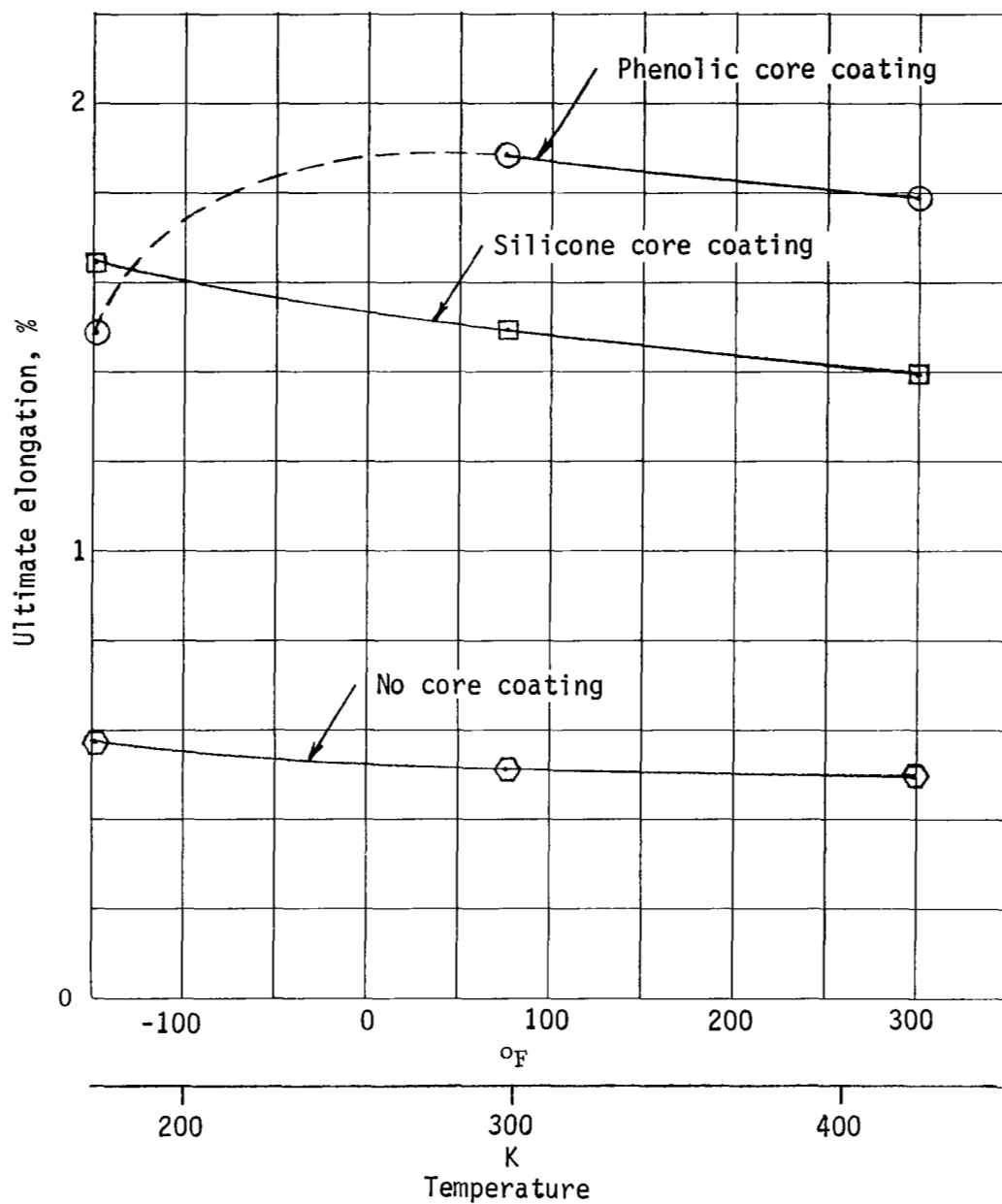


Figure 67.- Effect of Core Coating on Elongation



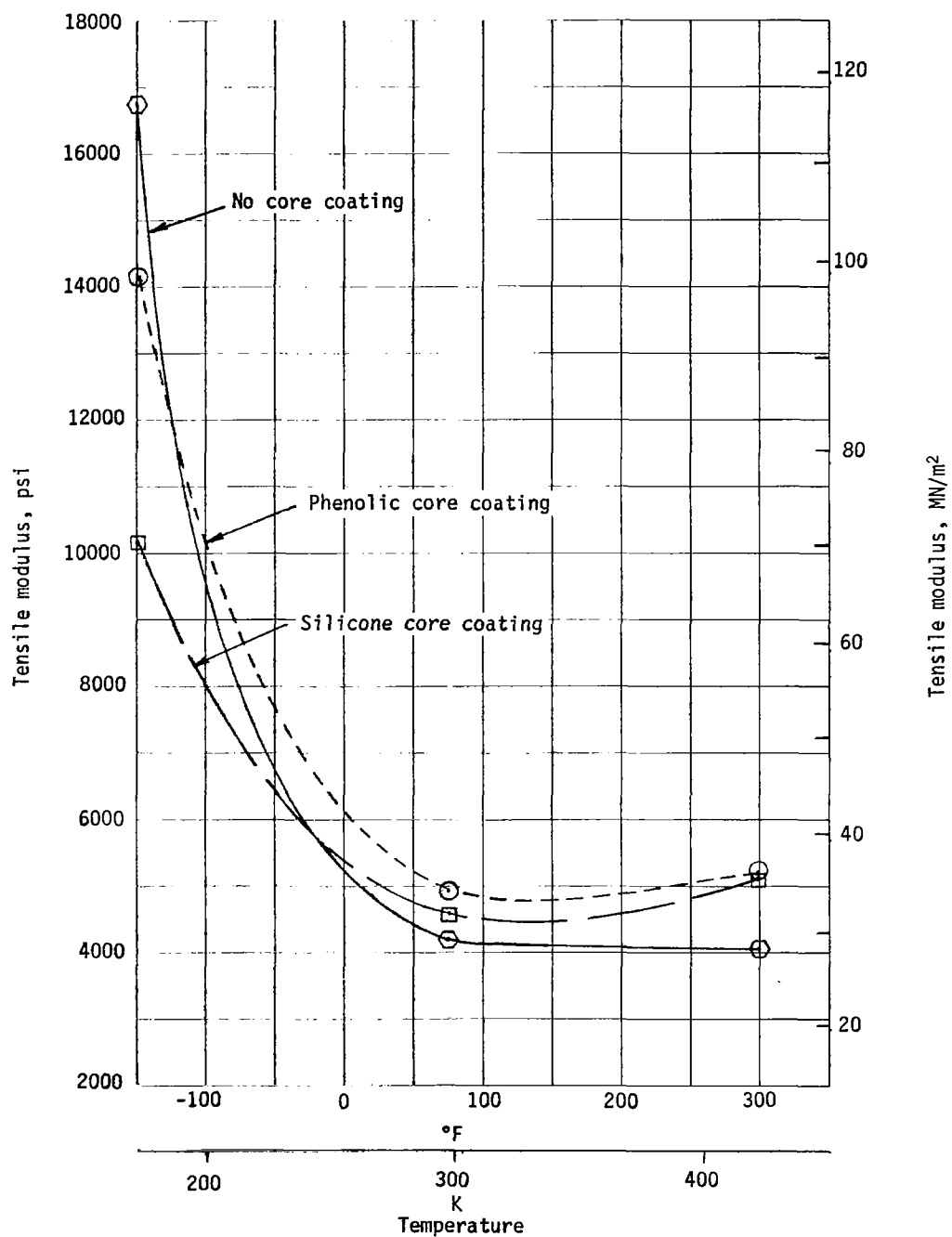


Figure 68.- Effect of Core Coating on Tensile Modulus

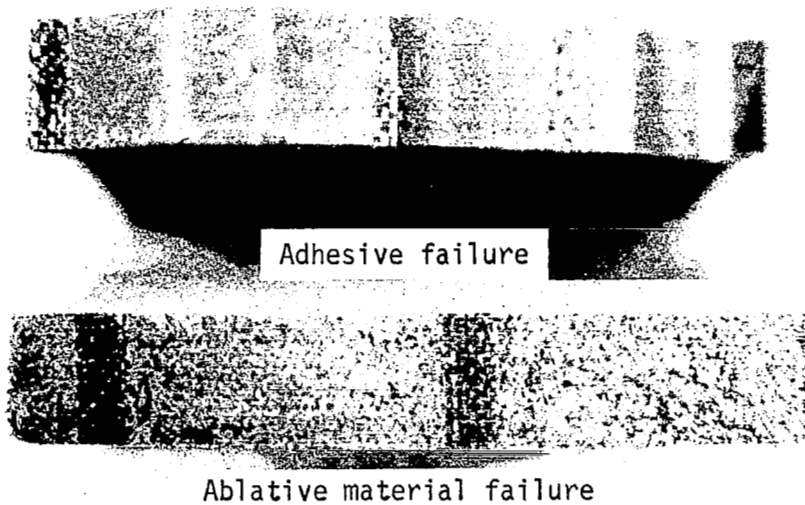
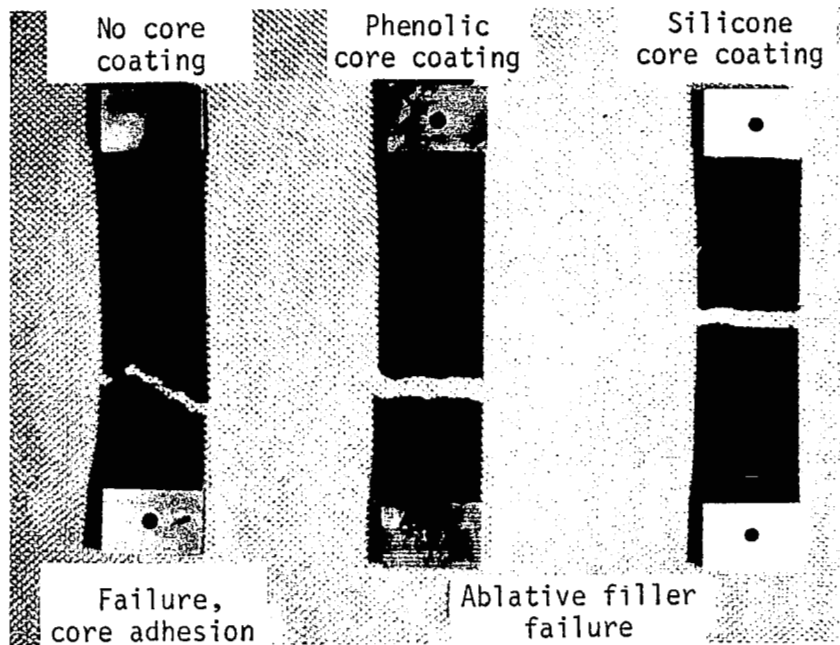


Figure 69.- Tensile Specimens, Bond Coat Study

Phenolic bond coat: Phenolic varnish (Monsanto SC1008) produces very good bonds between honeycomb and the ablative filler. The bond coat was B-staged on the core and actually improved packing because of its low coefficient of friction. During cure of the silicone ablative material, a strong bond was formed. Tensile tests of the composite resulted in failures through the ablative material as shown in figure 69.

The ultimate elongation is also higher than with the silicone bond coat except at -150°F (172K). At this temperature, the two coatings have essentially the same elongation. It is postulated that the phenolic bond coat has gone through a transition, whereas the silicone bond coat still has flexibility.

Density of ablative filler.- Three panels were tested at room temperature with phenolic bond coat and different packing densities. The results are shown in figure 70. It appears that there is an optimum density of around 16 lb/ft<sup>3</sup> (255.0 kg/m<sup>3</sup>). This does not agree with normal experience that shows that increased density of materials increases strength. It is possible, however, that overpacking may degrade the honeycomb and filler strengths.

Altered cure cycle.- One panel was fabricated for tensile tests using the cure cycle discussed under the section called Material Billets. These specimens were tested at room temperature and the results are given in figures 63, 64, and 65. Data scatter was minimal, particularly for modulus. The average strength and modulus were significantly lower than other phenolic bond-coated samples.

No fibers.- The omission of fibers had little effect on tensile strength. The modulus was reduced, however, because of an increase in the ultimate elongation (figs. 63, 64, and 65).

No honeycomb core.- Ambient tensile properties without core are very close to values obtained with the core. This does not necessarily indicate that the strength is equivalent with and without core. All tensile tests with core on this program were tested perpendicular to the ribbon. Testing along the ribbon would undoubtedly give different results (figs. 71, 72, and 73).

## Large Panels

Both the defect panel and the control panel survived the pre-reentry environmental tests without problems. Visual and X-ray examination failed to show any degradation of the panels or the attachments, or any change to the included anomalies. Surface hardness increased as anticipated during the temperature conditioning.

Acoustic.- Both panels were subjected to an overall sound pressure level of 156 decibels for 15 seconds. This was followed by 159 decibels for 50 seconds. Posttest visual examination showed no degradation of face sheet bond, attachments, or panel integrity.

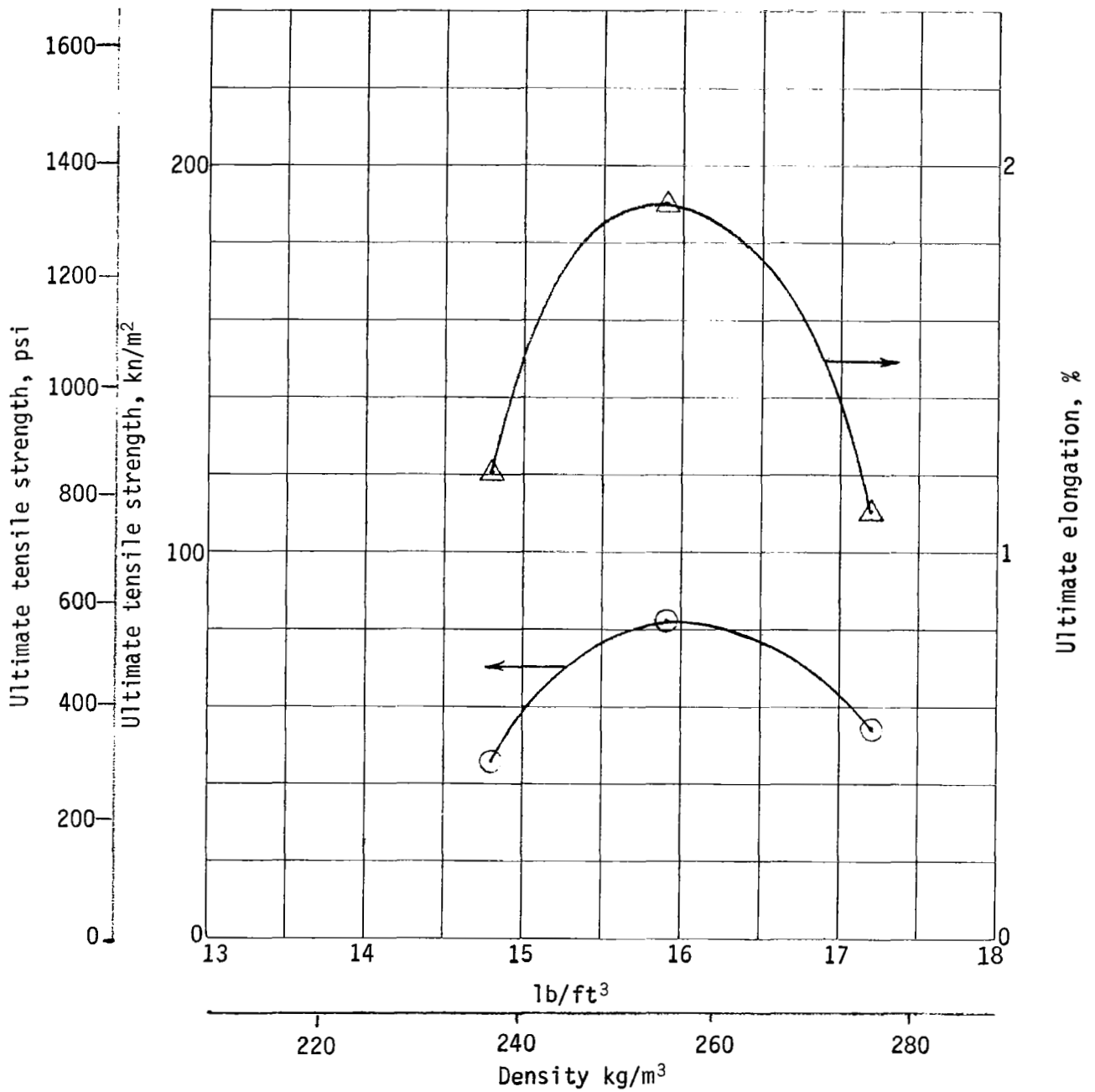


Figure 70.- Effect of Density on Tensile Properties

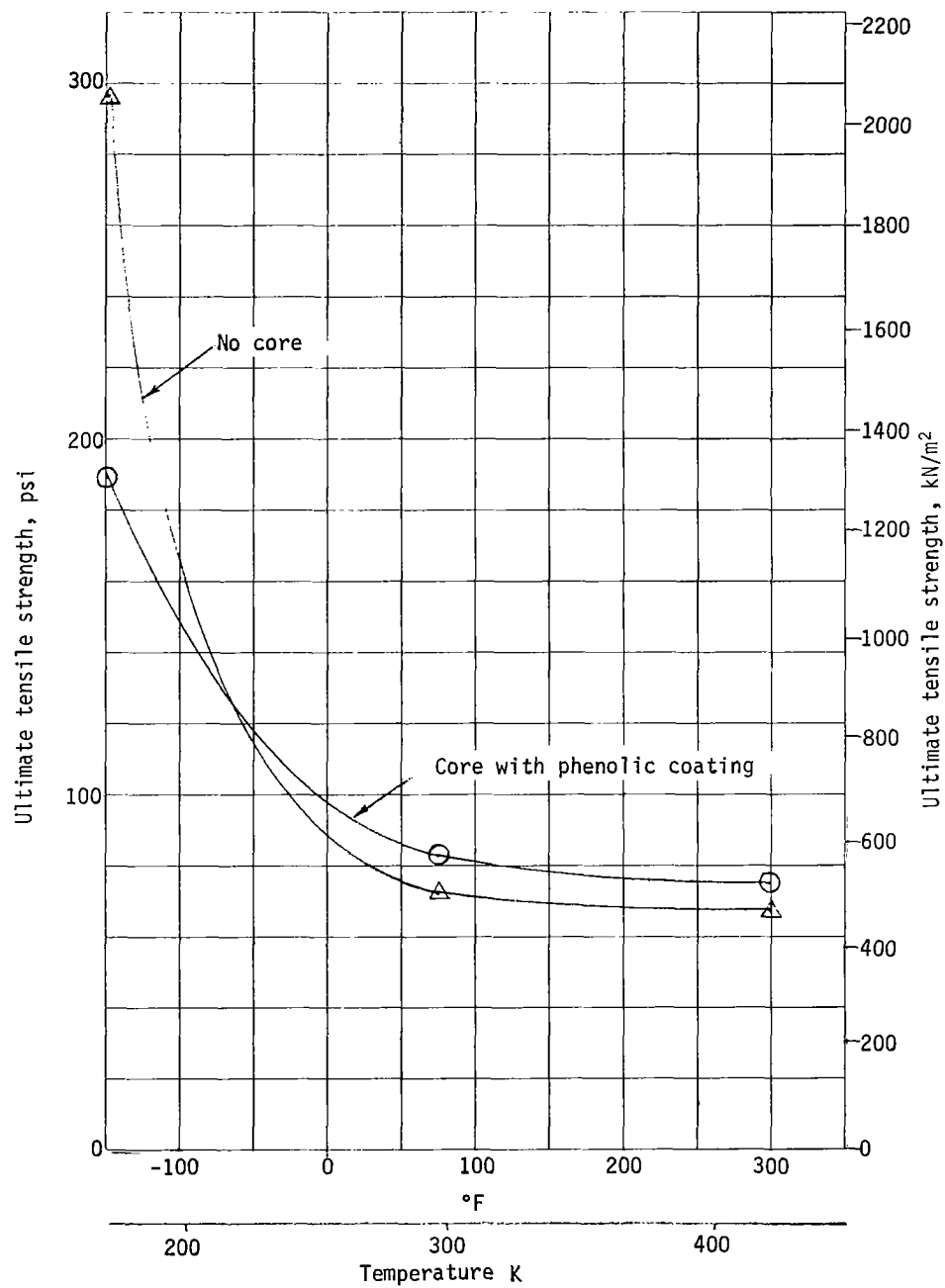


Figure 71.- Effect of Honeycomb on Tensile Strength

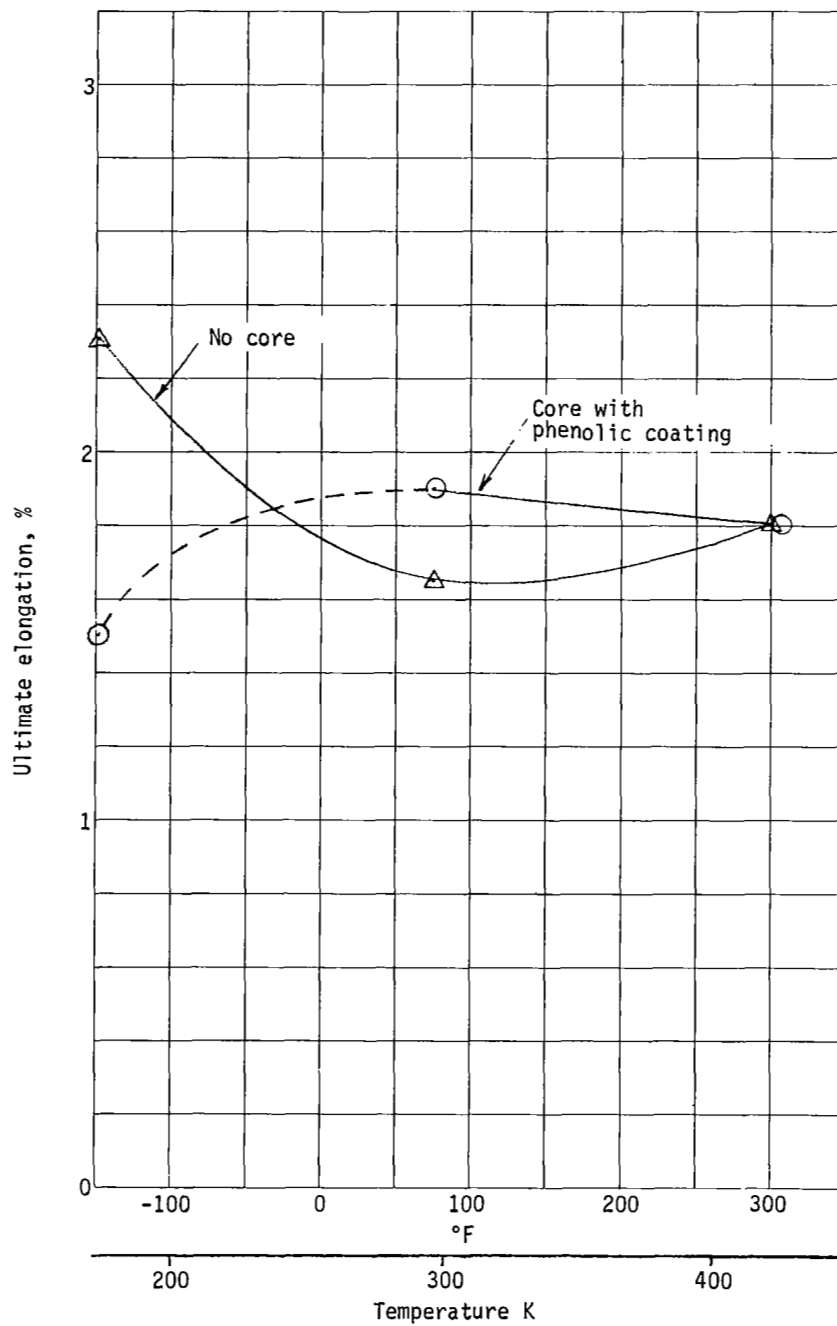


Figure 72.- Effect of Honeycomb on Elongation

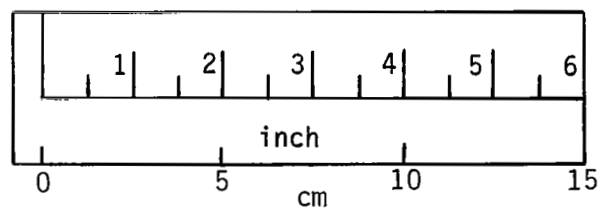
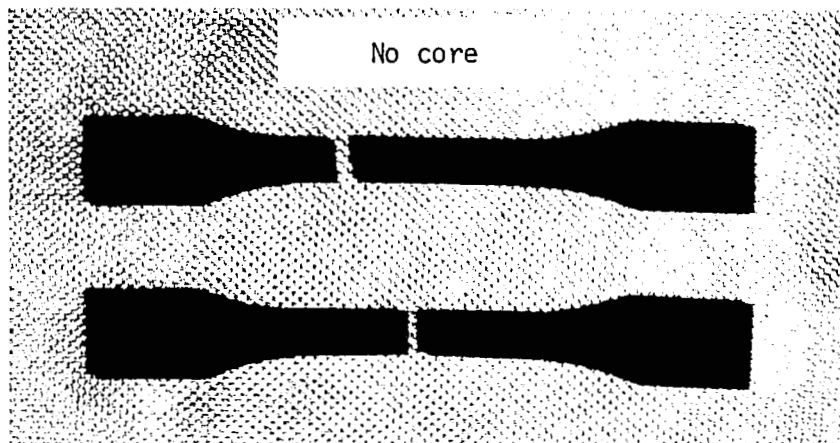


Figure 73.- Tensile Specimens, No Core

Hot vacuum test. - The test and control panels were subjected to vacuum and heat simultaneously. The test conditions were:

- 1) Heating - Quartz lamps, one side only;
- 2) Front face temperature - 290 to 305°F (416 to 425 K);
- 3) Backface temperature - 70 to 110°F (294 to 316K);
- 4) Vacuum -  $7 \times 10^{-5}$  torr ( $9.3 \times 10^{-3}$  N/m<sup>2</sup>) start to  $6 \times 10^{-6}$  torr ( $8 \times 10^{-4}$  N/m<sup>2</sup>) finish;
- 5) Duration - 72 hr.

Some outgassing was evident during initial heating as the vacuum increased from  $5 \times 10^{-6}$  torr ( $6.6 \times 10^{-4}$  N/m<sup>2</sup>) to  $7 \times 10^{-5}$  torr ( $9.3 \times 10^{-3}$  N/m<sup>2</sup>) while heating the ablative surface. The vacuum stabilized at  $6$  to  $7 \times 10^{-6}$  torr ( $8$  to  $9.3 \times 10^{-4}$  N/m<sup>2</sup>) after two days at temperature.

Visual observation through the chamber window did not show any problems during the test. The chamber temperature was then decreased for the cold test without breaking the vacuum. The increase in hardness during the hot vacuum exposure was from 5 to 10 points on the Shore A scale.

Cold vacuum test. - Cold soak followed immediately after the hot test. Liquid nitrogen was used in the shroud to reach the low temperature. Quartz lamps were used to control the panel temperature at -150°F (172K). The test conditions were:

- 1) Cold wall shroud temperature - -315 to -320°F (80 to 77K);
- 2) Heating - Quartz lamps both sides;
- 3) Front face temperature - -140 to -150°F (177 to 166K);
- 4) Backface temperature - -150 to -160°F (172 to 166K);
- 5) Vacuum -  $5 \times 10^{-6}$  torr ( $6.7 \times 10^{-4}$  N/m<sup>2</sup>) start, to  $4 \times 10^{-6}$  torr ( $5.3 \times 10^{-4}$  N/m<sup>2</sup>) finish;
- 6) Duration - 24 hr.

At the cold conditions, the ablative filler was dished in the honeycomb core due to differential thermal contraction. The filler-to-honeycomb bond, however, did not show any sign of failure. Posttest visual examination, figures 74 and 75, failed to show any degradation of bonds, face sheet, attachments, or change in face sheet defects.



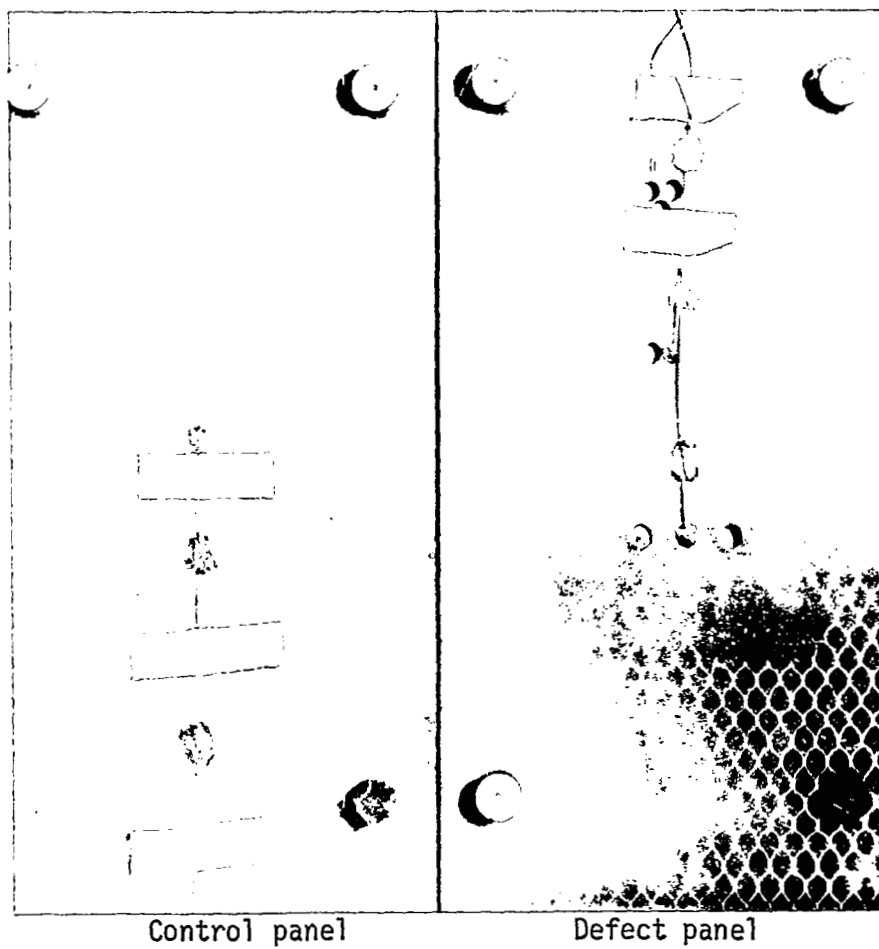


Figure 74.- Panels after Removal from Cold Soak

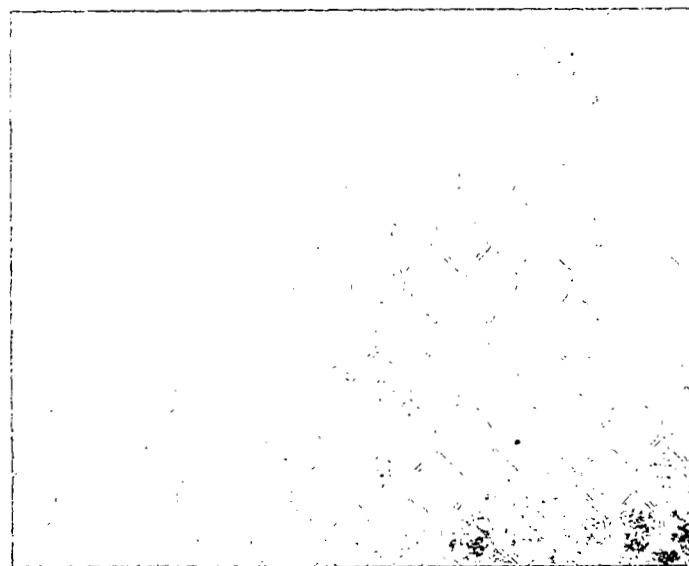


Figure 75.- Ablative Surface after Cold Soak;  
Core Frosted

Ablation tests.— The cold wall heat flux to the specimen surface varied from 30 Btu/ft<sup>2</sup>-s (0.341 MW/m<sup>2</sup>) at the leading edge to 10 Btu/ft<sup>2</sup>-s (0.113 MW/m<sup>2</sup>) at the trailing edge. The measured spanwise distribution was very nearly uniform as indicated by the test surface of the specimen shown in figure 76. The aerodynamic shear varied from 1.0 to 0.5 psf (47.9 to 23.9 N/m<sup>2</sup>) along the surface of the panels. Both panels were exposed to the environment for 1000 seconds.

The defective specimen performed extremely well with a strong smooth char surface formed over 85% of the specimen. Surface-connected anomalies had no apparent effect on the critical strength properties of the char or on the ablators-to-face sheet attachment. Surface temperatures, shown in figure 77, were very nearly uniform across the width of the panel,  $\pm 20^{\circ}\text{F}$  ( $\pm 11\text{K}$ ), and varied along the length from  $2100^{\circ}\text{F}$  (1420K) to  $1900^{\circ}\text{F}$  (1310K). Variations in internal and back-face temperatures, summarized in figure 77, are attributed to the variation in heating rate and were not noticeably altered by the presence of small surface voids (1 to 3 cells), varying in depth from 0.125 to 0.375 inch (0.318 to 0.952 cm), or by small holes up to 0.189 inch (0.48 cm) in diameter through the ablators. The 8 square inches (51.5 cm<sup>2</sup>) of unsupported char cracked into a random pattern with little difference noted between the area of crushed core and undercut core. Char retention was not noticeably affected by these localized core defects or by the surface discontinuities created by ablative material removal. The two upstream ablative plugs formed integral char with the adjacent material and were securely fastened. The two downstream ablative plugs did not form an integral char and were loose in their holes, probably the result of cooldown shrinkage. The areas containing face sheet delamination and core unbonding from the face sheet were not affected by this test.

The comparative data desired from the control specimen were invalidated because of the loss of a copper water plug on the specimen holder. This failure occurred at the beginning of the test and resulted in water being leaked into the test chamber. This resulted in an increase in chamber pressure and produced an unbalanced test stream with a corresponding strong shock cone emanating from the nozzle exit. A shock impingement with the specimen surface resulted from the interaction between this shock and the bow shock and created a "hot" spot on the forward 8 inches (20.3 cm) of the specimen (fig 78). The increased heating and turbulent flow that resulted produced significant char removal and a grooving of the receded surface as noted in figure 78. A contributing factor in producing these grooves may have been the fact that the core ribbon direction was parallel to the flow. The groove width was approximately one-half the cell width since the honeycomb nodes were left standing to a height of approximately 0.125 inch (0.318 cm) above the surface. The char "skin," which seems to be formed at heating rates of 10 to 30 Btu/ft<sup>2</sup>-s (0.113 to 0.341 MW/m<sup>2</sup>), exhibited good attachment strength during this test. Pressure gradients and shear forces did not remove this char from the many open cells around the perimeter of the surface burnthrough region. Surface temperatures of  $2500^{\circ}\text{F}$  (1600K) were measured in the receded area with a rapid falloff to  $2000^{\circ}\text{F}$  (1370K) near the trailing edge.


Stream flow 



Figure 76.- Defective Panel after Plasma Arc Test

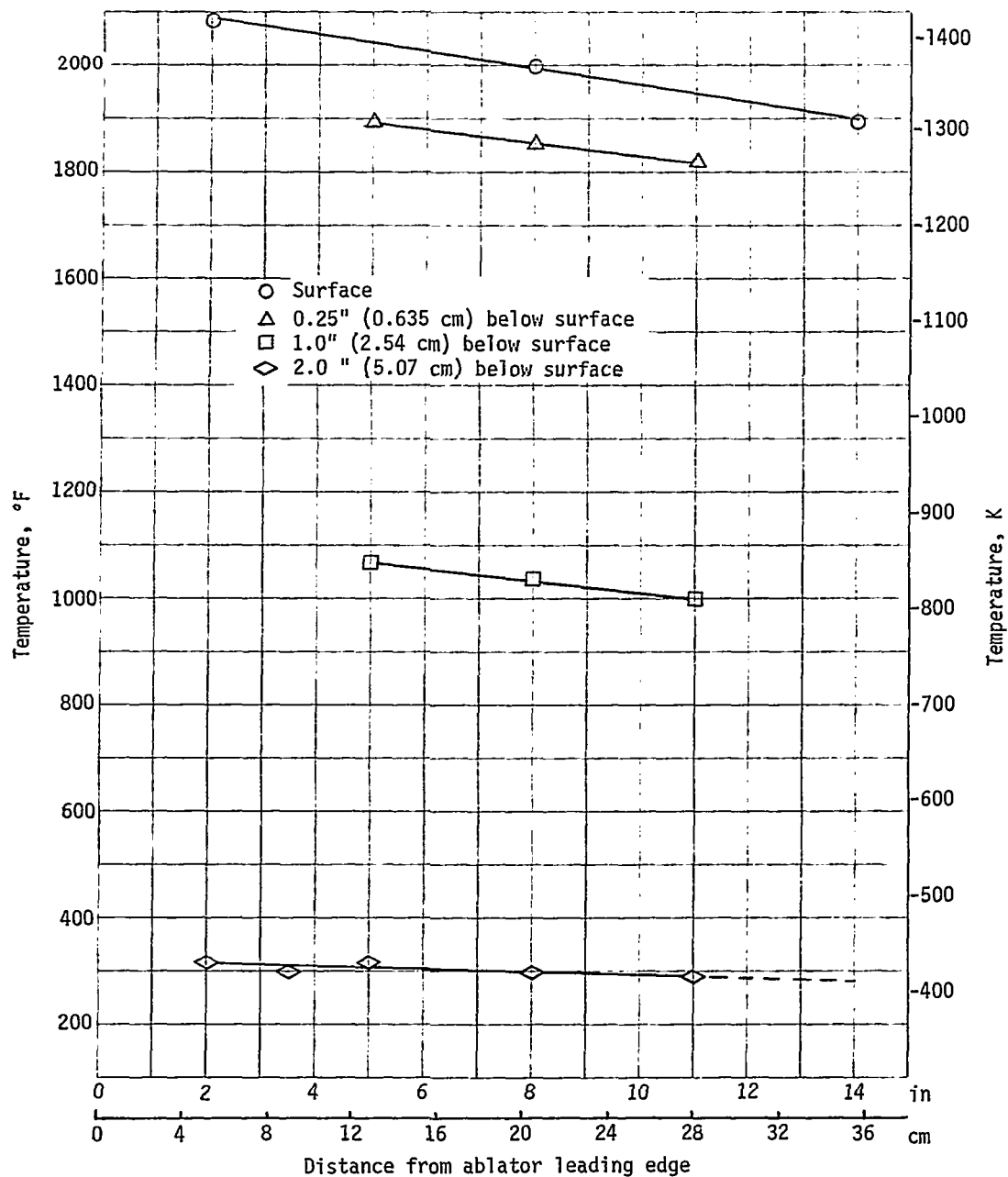


Figure 77.- Summary of Peak Temperature Measurements

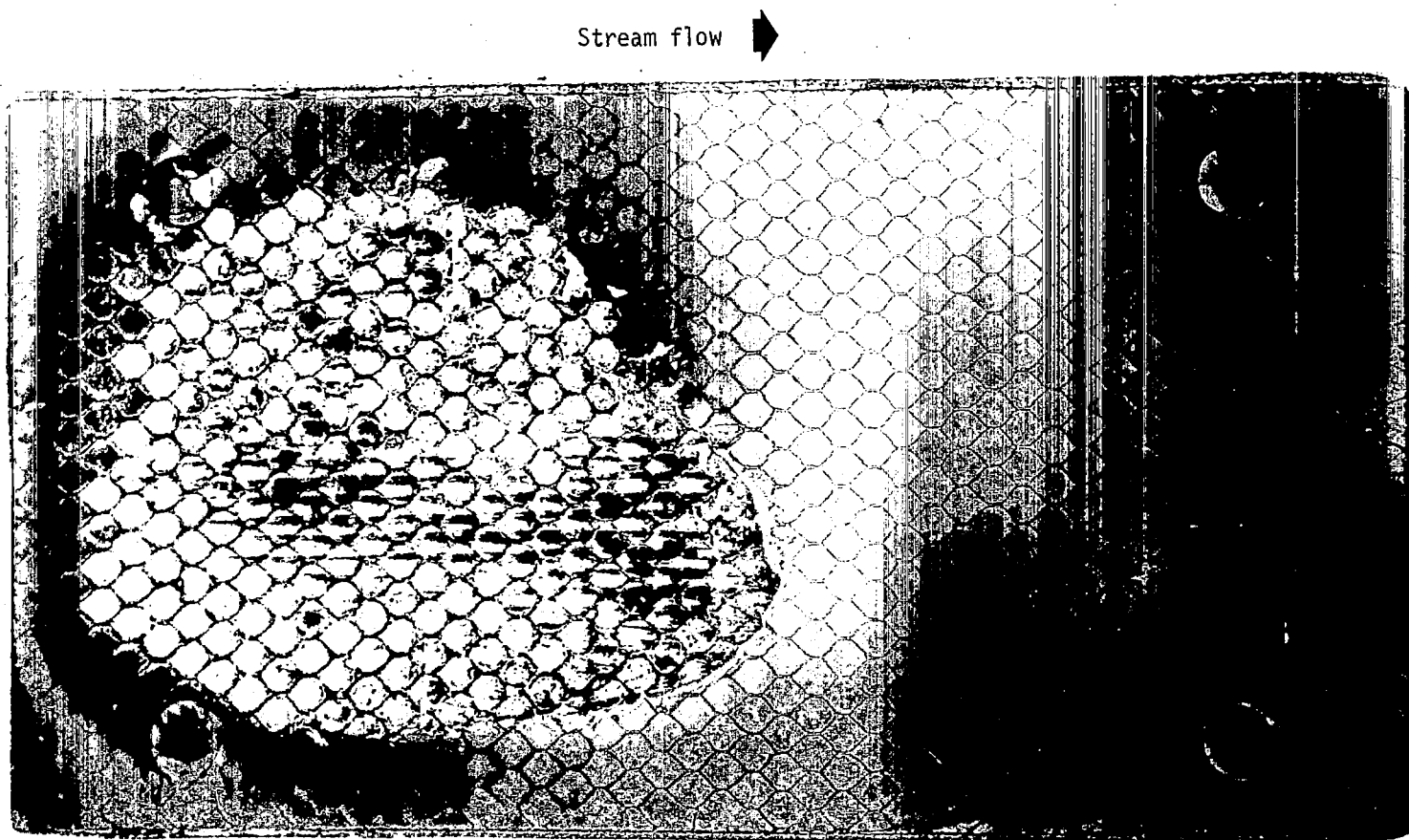


Figure 78.- Control Panel Showing Area of Shock Interaction

## CONCLUSIONS

The conclusions from this program are based on the performance requirements delineated in the section entitled Thermal Protection System Performance Requirements.

Density effects.- The density anomalies investigated during this study did not violate any of the specified performance requirements. The density gradients from the ablator surface to the back surface that resulted from the low-cost honeycomb core filling methods were found to be noncritical during the reentry heating environment. The nonuniform density distribution resulted in greater ablation weight loss but better insulative characteristics than the uniform distribution. This effect, however, was minor and not considered significant in terms of a material improvement.

Bulk density variations within the specified tolerance  $\begin{smallmatrix} +0 \\ -2 \end{smallmatrix} \text{ lb/ft}^3$  ( $\begin{smallmatrix} +0 \\ -32 \end{smallmatrix} \text{ kg/m}^3$ ), did not significantly affect thermal efficiency or weight loss. The lower density models did, however, experience a 40°F (22K) greater temperature rise at the back surface and greater ablation penetration. The temperature increase was well within the criteria of 75°F (42K) and is therefore considered noncritical. It is felt that an acceptance criteria based on a radiographic density standard is a feasible method for density certification.

Honeycomb core bond coating.- No structural criteria were violated by the honeycomb core bond coating variations investigated. The use of a bond coating, however, significantly improved the mechanical properties, and the phenolic resin resulted in superior processing, material homogeneity, and mechanical and ablative properties compared to the silicone-coated samples. The subsurface char attachment to the honeycomb seemed insensitive to the application of a bond coat since the char on all samples was generally found unattached. This may have occurred during specimen cooldown and, in any event, is not considered a fabrication defect. Formulation modifications, however, that increase char residue would certainly improve the overall strength and integrity of this subsurface char layer.

The use of a silicone bond coating was found to significantly degrade insulation performance. The variation from the control case was in excess of the temperature tolerance and thus, for a process using this coating, the amount of silicone coating applied could produce a critical defect.

Voids.- Large voids were evaluated at three locations within the ablator and no catastrophic effects were noted on char retention. Thermally, the large voids investigated degraded insulation efficiency and the degradation depended on void location. The magnitude of the temperature overshoot was 100 to 140°F (56 to 78K), and exceeded the tolerance mainly because of the large reduction (20%) in material density. It is thought that voids that do not reduce local ablator density below 15 lb/ft<sup>3</sup> (240 kg/m<sup>3</sup>) are noncritical. The area over which a void can be averaged is expected to be highly dependent on the lateral thermal conductance of the ablator substructure. Thus the maximum acceptable void size or collection of voids can be estimated for a given substructure and allowable temperature rise.

Core effect.— The tests conducted indicated local core crushing (25 to 30 cells) and core cell size up to 1.125 inch (2.85 cm) to be noncritical defects. The larger honeycomb core was found to give slightly lower backface temperatures without degradation in char layer integrity. Thus, lower core packing costs might be realized by using larger cell honeycomb core.

Cure variations.— Large variations in cure temperature, pressure, and time did not affect thermal efficiency. The lower temperature cure produced very consistent tensile property data, although strength and elongation were lower than for the baseline cure. This resulted in a lower modulus; however, unless thermal stresses are a problem, it is not recommended because of the 50% increased cure time.

Fiber bundles.— Fiber bundles were not found to be critical; indeed, no evidence was found that warranted the inclusion of fibers in the formulation. Fabrication costs could be reduced by their omission.

Surface voids and ablator holes.— Backface temperatures were not significantly affected by the presence of small drilled holes up to 0.189 inch (0.48 cm) in diameter through the ablator, or surface voids in 3-cell clusters and 0.25 inch (0.635 cm) in depth.

Metal inclusions.— The addition of small metal inclusions 0.0312 inch (0.0792 cm) in diameter and 2.5% by weight did not significantly affect backface temperature.

Attachment defects.— The two attachment point defects investigated -- face sheet delamination and core disbonding from the face sheet -- survived all the environmental exposures without consequence. In conclusion, delaminations and unbonds likely caused by process or machining operations and of less than 1.77 square inches (11.35 cm<sup>2</sup>) are probably tolerable and are classified noncritical based on study results.

Ablative plugs.— Although the ablative plugs performed quite well during the wedge tests, we recommend that these plugs be bonded in place by using a silicone bond coat. This would reduce the probability of plug loss in the absence of an integral char surface formation or due to material shrinkage during cooldown.

General.— In summary, the following conclusions were reached:

- 1) Tensile tests showed that the ablative composite had maximum strength and modulus at low temperature. Mechanical properties were essentially the same at 76 and 300°F (297.5 and 422K). Fibers and honeycomb core had only a minor effect on mechanical properties, while a density of 16 lb/ft<sup>3</sup> (256 kg/m<sup>3</sup>) produced the maximum tensile strength;
- 2) Maximum ablator ultimate elongation was approximately 2%. This seems adequate for present Shuttle requirements;

- 3) Ablative tests at low heat flux resulted in an integral charred surface with a void area below this surface crust. At high heat flux, the specimens had a very weak char consisting of a layer of silica ash on weak carbonaceous char. The char had many cracks parallel to the surface. In addition, at the high heating condition, the honeycomb was eroded to a depth of 0.07 to 0.1 inch (0.178 to 0.254 cm) and the char was self-supporting. None of the defects investigated caused char loss, spallation, or collapse of the char layer;
- 4) Surface roughing was not significant at either test condition since the char surface seemed to be protected from recession by an oxidation-resistant coating. At a temperature of 2450 to 2500°F (1618 to 1645K), the glass honeycomb was vaporized or melted away, thus producing some roughness. Under higher shear and pressure forces, the char may be lost resulting in a very rough surface. The use of an improved grade of glass honeycomb and/or ablator formulation changes would alleviate this problem at these temperatures;
- 5) Several processing improvements incorporated during Task III resulted in higher quality panels than any of the panels inspected during Task I or Task II. Material homogeneity was greatly improved by the elimination of the heptane extender and the use of phenolic resin to provide a honeycomb core bond coat. Bulk density and panel uniformity were controlled very closely with the fixed volume packing procedure employed.

## RECOMMENDATIONS

The following recommendations are based on the experience gained in performance of this contract:

- 1) Since tensile strength reached a maximum at about 16 lb/ft<sup>3</sup> (256 kg/m<sup>3</sup>), it is possible that the percent of silicone in the formulation could be increased and packing pressure decreased to maintain this density. The increased resin content should provide more char residue for a stronger char formation. The increased core filling difficulties might be offset by using larger core. Another approach would be to use a more highly phenylated resin system that would yield a more carbonaceous char;
- 2) The heating rate change during the reentry trajectory after initial char formation should be investigated to determine its effect on char integrity and the thin oxidation coating formed on the surface;
- 3) Bond coating can impose significant thermal penalties. Although phenolic resin produced the best results in this program, strength dropped off significantly at low temperature. Other bond coating resins such as "staged" silicones could be investigated for this application. This should combine the advantages of phenolic resin with the temperature capability of silicones;



- 4) To more fully explore the effect of bond coat on thermal insulation, we recommend that thermal conductivity tests be conducted. This should be followed by additional plasma arc tests;
- 5) An additional improvement in thermal conductivity might be achieved by using honeycomb core with a lower resin content;
- 6) Large honeycomb core looked practical at low heat flux. This should be investigated further as a way to reduce fabrication cost and improve processibility.

# APPENDIX A

## CONVERSION OF U.S. CUSTOMARY UNITS TO SI UNITS

The International System of Units, abbreviated SI (System International), was adopted in 1960 by the Eleventh General Conference on Weights and Measures held in Paris, France. The conversion factors required for units used herein are given in the following tabulation.

Physical Quantity	U.S. Customary Unit	Conversion Factor*	SI Unit
Aerodynamic shear stress	lb/ft <sup>2</sup>	47.88	N/m <sup>2</sup>
Coefficient of heat transfer	Btu/ft <sup>2</sup> -sec-°R	2.04 x 10 <sup>4</sup>	W/m <sup>2</sup> -K
Density	lb/ft <sup>3</sup>	16.02	kg/m <sup>3</sup>
Dynamic pressure	lbf/ft <sup>2</sup>	47.88	N/m <sup>2</sup>
	lbf/in. <sup>2</sup>	6894.76	N/m <sup>2</sup>
Atmospheric pressure	atm	101 325.0	N/m <sup>2</sup>
Barometric pressure	in. of Hg (60°F)	3376.85	N/m <sup>2</sup>
Enthalpy	Btu/lb	2.32 x 10 <sup>3</sup>	J/kg
Heat transfer rate	Btu/ft <sup>2</sup> -sec	1.135 x 10 <sup>4</sup>	W/m <sup>2</sup>
Length	ft	0.3048	m
	in.	2.54	cm
Mass distribution	lb/ft <sup>2</sup>	4.88	kg/m <sup>2</sup>
Mass flow per unit area	lb/ft <sup>2</sup> -sec	4.85	kg/m <sup>2</sup> -s
Specific heat	Btu/lb-°R	4.18 x 10 <sup>3</sup>	J/kg-K
Temperature	°F	$\frac{5}{9}(\text{°F} + 460)$	K
Temperature rise	°F	0.556	K
Velocity	fps,	0.305	m/s
Distance	nautical mile	1852.0	m
Volume	ft <sup>3</sup>	0.028	m <sup>3</sup>
*Multiply value given in U.S. customary unit by conversion factor to obtain equivalent value in SI unit.			

The prefixes to indicate multiples of units are tabulated.

Prefix	Multiple
mega (M)	$10^6$
centi (c)	$10^{-2}$
milli (m)	$10^{-3}$

## APPENDIX B

### FABRICATION OF LOW-DENSITY ELASTOMERIC HEAT SHIELD PANELS

This process establishes the materials, equipment, and methods used in the fabrication of low-density elastomeric heat shield panels for NASA-Langley Contract NAS1-10289. This process does not establish test methods other than in-process and final inspection techniques of a quality control nature.

Application - This process presents the step-by-step methods from raw material handling through the final composite panel dimensioning for test panel configurations. In this sense, it is developmental and is not intended for fabrication of flight-configuration hardware.

The composite panel when finished is essentially a single-faced honeycomb panel with the cell structure filled with an elastomeric ablator bonded to the face and cell-wall surfaces.

Materials - The materials used are:

- 1) Epoxy-Glass Prepreg, Hexcel Corporation, Trevarno F-161-181, F-50 finish;
- 2) Honeycomb, Hexcel Corporation, HRP 3/8 GF-11-2.2;
- 3) Refrasil fibers, H.I. Thompson Co., F-100A-25;
- 4) Phenolic Microballoons, Union Carbide, BJO-0930;
- 5) Silicone elastomer, Dow Corning, Sylgard 182 Resin and curing agent;
- 6) Phenolic resin, Monsanto, SC-1008.

Equipment - The equipment included:

- 1) Vacuum pump;
- 2) Air circulating oven;
- 3) Vapor degreaser, trichloroethylene condensing vapor;
- 4) Binks, Spray gun and nozzles;
- 5) Laboratory balance;
- 6) No. 30 sieve;

- 7) Planetary mixer, Hobart N-50;
- 8) Planetary mixer, Hobart A-200;
- 9) Bandsaw;
- 10) Small drill motor.

Procedure - The procedure is detailed.

1. Fabrication of Honeycomb Core to Glass-reinforced Epoxy Face
  - 1.1 Honeycomb Core Preparation
    - 1.1.1 Cut core to proper dimension for tooling fitup.
    - 1.1.2 Check tooling fitup by assembling the core in tooling.
    - 1.1.3 Remove the core from tooling and visually inspect the core for defects such as broken cell walls and ends or delaminated node bonds. Cell wall and node defects shall be cause for rejection of core details.
    - 1.1.4 Clean core by using dry, filtered compressed nitrogen. Core shall then be degreased in condensing vapors of the trichloroethylene vapor degreaser.
    - 1.1.5 Visually inspect the core for residual contamination and if necessary repeat step 1.1.4 and record this fact in QC log.
    - 1.1.6 Immediately wrap cleaned core in clean kraft paper for storage until ready for use.
  - 1.2 Glass-Epoxy Face Laminate Preparation
    - 1.2.1 Remove preimpregnated glass fabric from cold storage and allow the material to warm up to room temperature.
    - 1.2.2 Cut two plies of the prepreg to the proper dimensions to make a 90° crossply laminate.
  - 1.3 Laminate/Core Layup
    - 1.3.1 Solvent-clean (MEK) and apply mold release to the tooling surfaces.
    - 1.3.2 Place a mold-release-coated Mylar film on the mold surface.

- 1.3.3 Place the first laminate ply on the Mylar and roll out flat and smooth; then remove the separator film.
- 1.3.4 Place the second ply on top of the first ply with a 90° weave orientation to the first ply. Smooth out and remove separator film.
- 1.3.5 Center the core support tool on the face laminate layup.
- 1.3.6 Insert the core in the core-support tool down against the face laminate.
- 1.3.7 Inspect the tooling and layup at this point to ensure that proper fitup is obtained, especially at the core/laminate junction.
- 1.3.8 Place glass fabric wicking over the layup assembly so it intersects with a vacuum outlet.
- 1.3.9 Construct a vacuum bag over this assembly and seal to the mold base.
- 1.3.10 Draw a vacuum on the part and check bag assembly for leaks.
- 1.4 Laminate/Core Laminating Cure
  - 1.4.1 Place the assembled part and tooling in a room-temperature air recirculating oven. Bring part temperature up to  $325 \pm 10^{\circ}\text{F}$  ( $437 \pm 5.6 \text{ K}$ ).
  - 1.4.2 Maintain part temperature for 1 hour at 23 inches of Hg ( $77.7 \text{ kN/m}^2$ ) minimum pressure.
  - 1.4.3 Cool part to  $100^{\circ}\text{F}$  ( $311 \text{ K}$ ) under vacuum pressure before disassembly.
  - 1.4.4 Inspect the laminated part for conformance to dimensional tolerances, warpage, broken cell walls, and filleting action at the laminate-to-core bond.
- 2. Preparation of Core/Laminate Panels for Ablation Material
  - 2.1 Drill relief holes 0.063 in. (0.16 cm) in diameter through the laminate face into each honeycomb cell. Use an abrasion-resistant drill such as carbide without lubrication. Drill must be cut and resharpened so only 1/4 of a twist exists.
  - 2.2 Apply a wet coat of phenolic varnish and alcohol mixture to the core and laminate by dip coating.

- 2.3 The wet-coat phenolic composition shall be as follows:  
     SC-1008 varnish - 50 parts by weight;  
     Alcohol (ethyl) - 50 parts by weight.
  - 2.4 Then place the panel with the open side of cells down and allow it to drain on absorbant paper or cloth for  $\frac{1}{2}$  hour.
  - 2.5 Place the panel in an air-circulating oven and dry the resin coating at 120°F (322 K) for 2 hours. A "tack-free" uncured resinous surface should result.
3. Ablative Material Formulation

Ingredient	Parts by Weight
Sylgard 182 resin	22.8
Sylgard 182 curing agent	2.2
Refrasil fibers	4.0
Phenolic microspheres	71.0

- 3.1 Raw Material Preparation
  - 3.1.1 Discard retained material and dry the fines under 23 inches Hg (77.7 kN/m<sup>2</sup>) minimum at 150 ± 10°F (339 ± 5.6 K) for 24 hours.
  - 3.1.2 Size the phenolic microspheres through a 30-mesh sieve.
  - 3.1.3 Store the dried microspheres in airtight polyethylene bags until ready for formulation.
- 3.2 Mixing
  - 3.2.1 Fiber/resin dispersion
    - 3.2.1.1 Weigh the necessary amount of the resin to accomplish the proportionality required on the batch being formulated and place in the N-50 planetary mixer.
    - 3.2.1.2 Weigh the required amount of catalyst and add to the resin.
    - 3.2.1.3 Mix for 2 minutes at speed setting No. 1 followed by 3 minutes at speed setting No. 2 (5 minutes total mix).
    - 3.2.1.4 Weigh the proper amount of fibers and add to the resin mixture and mix for 10 minutes at speed setting No. 1.

- 3.2.1.5 Slowly and evenly, over a period of approximately 5 minutes, add 20% of the phenolic microspheres to the running mixer to obtain complete wetting of the microspheres.
  - 3.2.1.6 Transfer the contents of the small planetary mixer to the large A-200 planetary mixer and add the remaining microspheres. Mix for 45 minutes.
  - 3.2.1.7 Examine the ablative mixture to assure homogeneity.
4. Preparation and Packing of the Panel
- 4.1 Tooling Preparation
    - 4.1.1 Solvent-clean all tooling and fixtures.
    - 4.1.2 Apply release-type agent to tooling and fixtures.
    - 4.1.3 Position 1 ply of coarse fiberglass bleeder cloth on tool base. Overlay 1 ply of fine-weave bleeder fiberglass fabric. Both plies shall be sufficiently large to extend beyond the edge of the subsequently superimposed "picture frame" fixture.
    - 4.1.4 Center the previously wet-coated honeycomb panel on the bleeder and release plies with the open-ended cells up.
    - 4.1.5 Install a "picture frame" fixture around the honeycomb panel. The fixture shall be the same height as the honeycomb panel and shall fit the panel periphery snugly but without distorting the honeycomb cells.
    - 4.1.6 Inspect the alignment of all tooling and part. Correct as necessary.
    - 4.1.7 Position a clean piece of Mylar film across the top of the honeycomb panel and extending beyond the picture frame edges.
    - 4.1.8 Superimpose another picture frame fixture, of the same dimensions, over the lower one with Mylar film sandwiched between.
    - 4.1.9 Inspect the alignment of all tooling and part. Correct as necessary.



## 4.2 Panel Packing

- 4.2.1 Calculate the total weight of material required to fill the panel and leave a  $\frac{1}{2}$ -inch (1.27-cm) head. Place 40% of the mixed ablative material evenly in the top picture frame.
- 4.2.2 Pull the Mylar film from between the two picture frames.
- 4.2.3 Gently press the ablative material into the cell cavities using a  $2\frac{1}{2}$ -inch (6.35-cm) diameter hand tamper. Material shall penetrate between partial cells and picture frame inner surfaces.
- 4.2.4 Repeat steps 4.2.1 through 4.2.3 twice. The second material loading weight is to be 20% of the total weight.
- 4.2.5 Carefully remove top picture frame disturbing the ablative material head as little as possible.
- 4.2.6 Cover the partially compacted assembly with a release-treated fiberglass bleeder ply. The bleeder shall be sufficiently large to extend down to the tool base and overlap the bottom bleeder plies.
- 4.2.7 Assemble a vacuum bag (nylon) over the assembly and seal to the tool base.
- 4.2.8 Evacuate and maintain a minimum of 23 inches Hg (77.7 kN/m<sup>2</sup>) vacuum on the panel.
- 4.2.9 Vibrate the assembly using a pneumatic rivet gun with a 2-inch (5.08-cm) diameter head and a pressure setting of 40 psi (27.6 kN/m<sup>2</sup>) to pack the ablative material into the honeycomb cells. Vibrate the assembly by alternating direction until the "head" of material remaining above the core is approximately  $\frac{1}{2}$  inch.
- 4.2.10 Place assembly into autoclave and subject to a 10-minute dwell at 50 psi (34.5 kN/m<sup>2</sup>) after a pressurization rate of 5 to 10 psi (3.45 to 6.9 kN/m<sup>2</sup>) per minute.
- 4.2.11 After completion of the pressure cycle, remove the assembly from the autoclave and remove the vacuum bag and bleeder ply and respread the material "head" evenly to a uniform depth of approximately  $\frac{1}{2}$  inch.